AEDC-TR-66-17

[redacted]

(U) SIMULATED ALTITUDE TESTING OF THE APOLLO SERVICE MODULE PROPULSION SYSTEM (REPORT II, PHASE II DEVELOPMENT TEST)

Per A.F. Letter Dt'd. 27 June, 73.

G. H. Schulz and J. F. DeFord
ARO, Inc.

February 1966

~~In addition to security requirements which must be met, this document is subject to special export controls and each transmittal to foreign governments or foreign nationals may be made only with prior approval of National Aeronautics and Space Administration — Manned Spacecraft Center, Houston, Texas.~~ (EP-2)

ROCKET TEST FACILITY
ARNOLD ENGINEERING DEVELOPMENT CENTER
AIR FORCE SYSTEMS COMMAND
ARNOLD AIR FORCE STATION, TENNESSEE

[redacted]

NOTICES

When U. S. Government drawings specifications, or other data are used for any purpose other than a definitely related Government procurement operation, the Government thereby incurs no responsibility nor any obligation whatsoever, and the fact that the Government may have formulated, furnished, or in any way supplied the said drawings, specifications, or other data, is not to be regarded by implication or otherwise, or in any manner licensing the holder or any other person or corporation, or conveying any rights or permission to manufacture, use, or sell any patented invention that may in any way be related thereto.

Qualified users may obtain copies of this report from the Defense Documentation Center.

This document contains information affecting the national defense of the United States within the meaning of the Espionage Laws (Title 18, U.S.C., sections 793 and 794) the transmission or revelation of which in any manner to an unauthorized person is prohibited by law.

References to named commercial products in this report are not to be considered in any sense as an endorsement of the product by the United States Air Force or the Government.

Do not return this copy. When not needed, destroy in accordance with pertinent security regulations.

[redacted]

(U) SIMULATED ALTITUDE TESTING OF THE APOLLO SERVICE MODULE PROPULSION SYSTEM (REPORT II, PHASE II DEVELOPMENT TEST)

G. H. Schulz and J. F. DeFord
ARO, Inc.

[redacted]

FOREWORD

(U) The contents of this report are the results of a test program sponsored by the National Aeronautics and Space Administration-Manned Spacecraft Center (NASA-MSC). Technical liaison was provided by the Aerojet-General Corporation (AGC), which is subcontractor for the development of the Apollo Service Propulsion System engine (AJ10-137). The prime contractor to NASA-MSC for the Apollo Service Module is North American Aviation, Space and Information Division (NAA-S&ID). The test program was requested to support the Apollo Project under System 921E.

(U) Testing was conducted by ARO, Inc. (a subsidiary of Sverdrup and Parcel, Inc.), contract operator of the Arnold Engineering Development Center (AEDC), Air Force Systems Command (AFSC), Arnold Air Force Station, Tennessee, under Contract AF40(600)-1200. The results reported herein were obtained in Propulsion Engine Test Cell (J-3) of the Rocket Test Facility (RTF) during the period between April 27 and October 1, 1965, under ARO Project No. RM1356 and the manuscript was submitted for publication on December 28, 1965.

(U) The authors wish to acknowledge invaluable collaboration in the preparation of this report by their associates in the J-3 Projects Section: C. R. Bartlett, E. S. Gall, M. W. McIlveen, C. E. Robinson, and R. B. Runyan.

(U) This report contains no classified information extracted from other classified documents.

(U) This technical report has been reviewed and is approved.

Ralph W. Everett
Major, USAF
AF Representative, RTF
DCS/Test

Jean A. Jack
Colonel, USAF
DCS/Test

UNCLASSIFIED ABSTRACT

(U) The Apollo Service Module (S/M) propulsion system, tested at Arnold Engineering Development Center (AEDC), consisted of the Aerojet-General Corporation AJ10-137 flight-type rocket engine and a North American Aviation ground test version of the Apollo S/M propellant system and was subjected to simulated altitudes above 100,000 ft during engine firing operations. This testing was conducted with the last six engine assemblies of the AEDC Phase II development program and included test firings with an accumulated duration of 3367.1 sec. The primary objectives of the test were to check out system operation, define propulsion system altitude performance, and prove engine structural endurance over ranges of propellant mixture ratio and combustion chamber pressure. Engine gimbaling operations were performed during certain firings. Ballistic performance of the six engine assemblies tested is presented in this report. Engine temperature data, the effect of ablation on the thrust vector, and a discussion of engine gimbal operation are also presented.

CONTENTS

ILLUSTRATIONS

TABLES

NOMENCLATURE

A/A^*	Area ratio
A_t	Throat area, in.^{2}
$A_{t_{calc}}$	Calculated throat area, in.^{2}
A_{t_m}	Measured throat area, in.^{2}
C_F	Thrust coefficient
C_{F_v}	Vacuum thrust coefficient
$C_{i,j}$	Calibration constants
c^*	Characteristic velocity, ft/sec
c^*_i	Characteristic velocity calculated at the beginning of a test which used a new combustion chamber, ft/sec
F_a	Axial thrust, lb_f
$F_{a_{cal}}$	Axial thrust calibrate, lb_f
F_m	Measured thrust, lb_f
$F_{P_{1cal}}$	Upper pitch force calibrate, lb_f

$F_{P_{1data}}$	Upper pitch force data, lb_f
$F_{P_{2cal}}$	Lower pitch force calibrate, lb_f
$F_{P_{2data}}$	Lower pitch force data, lb_f
$F_{R_{cal}}$	Roll force calibrate, lb_f
F_v	Vacuum thrust, lb_f
$F_{Y_{1cal}}$	Upper yaw force calibrate, lb_f
$F_{Y_{1data}}$	Upper yaw force data, lb_f
$F_{Y_{2cal}}$	Lower yaw force calibrate, lb_f
$F_{Y_{2data}}$	Lower yaw force data, lb_f
f_{corr}	Mixture ratio correction
g	Dimensional constant, 32.174 lb_m-ft/lb_f-sec^2
I_{sp}	Specific impulse, lb_f-sec/lb_m
I_{sp_v}	Vacuum specific impulse, lb_f-sec/lb_m
I_t	Total impulse, lb_f-sec
K_{fm}	Flowmeter constant, lb-H_2O/cycle
$K_{j,i}$	Balance constants
L_j	Applied load
MR	Mixture ratio, oxidizer to fuel
P_a	Test cell pressure, psia
P_c	Combustion chamber pressure, psia
P_{c_m}	Measured combustion chamber pressure, psia
P_{f_j}	Fuel injector pressure, psia
P_{ftca}	Fuel interface pressure, psia
P_{oj}	Oxidizer injector pressure, psia
P_{otca}	Oxidizer interface pressure, psia
R_i	Data load cell output, lb_f
$\dot{W}_f$	Fuel weight flow, lb_m/sec
$\dot{W}_o$	Oxidizer weight flow, lb_m/sec
$\dot{W}_t$	Total propellant weight flow, lb_m/sec
$\dot{W}_{tm}$	Measured total propellant weight flow, lb_m/sec
θ	Pitch angle, deg
ϕ	Yaw angle, deg

SECTION I
INTRODUCTION

(U) The Apollo spacecraft and Lunar Excursion Modules (LEM) are the "life supporting" modules of the "man-on-the-moon" mission. The Apollo spacecraft consists of a Command Module (three-man capsule) and an attached Service Module (S/M). The S/M houses the propulsion system which provides energy for midcourse velocity correction and injection into and ejection from lunar orbit. The Apollo S/M will remain in a lunar orbit while lunar exploration takes place with the LEM. After LEM rendezvous with the S/M and Command Modules and ejection from lunar orbit, the S/M is used for final return midcourse correction.

(U) Three phases of Apollo S/M development and qualification testing at altitude pressure conditions were planned for conduct at AEDC. Phase I, completed in April 1964, was concerned with developmental testing of the S/M rocket engine. Phase II was a systems test for extended developmental testing of the engine with a heavy-duty version of the S/M propellant tankage (F-3 fixture) and with flight-type propellant feed lines. The Phase III altitude qualification program for the Aerojet-General Corporation AJ10-137 liquid-propellant rocket engine is also to be conducted with the F-3 fixture.

(U) Presented in this report are the results obtained during the last 11 test periods of Phase II, which includes test firings with a total duration of 3367.1 sec on six different engine assemblies. Previous tests, conducted during the Phase II program, are reported in Ref. 1.

(U) The primary objective of Phase II development tests was to establish the operating characteristics and performance level of the Apollo S/M engine at simulated altitudes above 110,000 ft. Specific objectives included the following:

1. Engine ballistic performance at design operating conditions,
2. Engine ballistic performance and durability at off-design chamber pressures, mixture ratios, and propellant temperatures,
3. Effect of thrust chamber valve alternate passage selection on engine ballistic performance,
4. Gimbal system operation,
5. Minimum impulse bit operation,
6. Thrust vector determination,

7. Ablation characteristics,
8. Start and shutdown impulse characteristics, and
9. Restart capability.

SECTION II
APPARATUS

2.1 TEST ARTICLE – GENERAL

(U) The AJ10-137 rocket engine and an Apollo S/M version propellant system (tankage and plumbing, designated the F-3 fixture) constituted the test article for these AEDC tests. Six different flight-type engine assemblies, designated engines S/N 9A, 11A, 9B, 11B, 11C, and 11D, were tested during this report period. The engine configurations included one configuration without gimbal actuators.

(U) The F-3 fixture, provided by NAA/S&ID, was a heavy-duty propellant storage and supply version of the S/M propellant system. The boilerplate tanks were of spacecraft size, shape and volume; the propellant lines duplicated spacecraft size, hydrodynamics, and approximate routing; and the spacecraft propellant feed pressurization system was duplicated except for the helium pressurant supply storage. A heavy structural steel frame supported the tanks and plumbing and provided a base mount for the engine mount/thrust balance cage.

2.2 ENGINE

2.2.1 General Description

(U) The AJ10-137 engine tested during this report period is a pressure-fed, liquid-propellant rocket engine consisting of a thrust chamber assembly, a bipropellant valve assembly, and a gimbal actuator-ring mount assembly. The overall height of the engine is approximately 13 ft, and the diameter of the nozzle exit is approximately 8 ft.

(U) The design vacuum performance of the engine is 21,900-lb_f thrust at a propellant weight mixture ratio of 2.0 and a chamber pressure (measured at the injector face) of 100 psia. The engine is designed to be capable of a minimum of 50 restarts over the design operating life of 750 sec (Ref. 2). The engine burns hypergolic, storable propellants; nitrogen tetroxide (N_2O_4) is the oxidizer, and the fuel is 50-50 weight

blend of hydrazine (N_2H_4) and unsymmetrical dimethylhydrazine (UDMH).

(U) The thrust chamber assembly consists of a propellant injector, an ablatively cooled combustion chamber, and a radiation-cooled nozzle extension. The bipropellant valve is mounted on top of the injector dome. The thrust chamber assembly is mounted in a ring mount assembly and is gimbaled in two orthogonal planes by two electrically operated gimbal actuators.

(U) One of the six engines tested during this report period is shown without the nozzle extension in Fig. 1. The engine assembly components were

Test Periods	Engine S/N	Injector S/N	Propellant Valve (TCV) S/N	Combustion Chamber S/N	Nozzle Extension S/N
L	9A	047	036	077	027
M, N	11A	091	032	075	028
P, Q	9B	047	101	074	025
R, S	11B	046	101	155	028
T, U	11C	064	101	208	027
V, W	11D	064	101	211	026

2.2.2 Propellant Injector

(U) The type of injector used during these tests had doublet orifice impingement in a concentric-ring pattern and was baffled (Fig. 2) for improved combustion stability. A pulse charge was placed in the combustion chamber for test firings to investigate the capability of the engine combustion mechanism to recover from induced combustion instability. The pulse charge was a No. 8 blasting cap and 2.46 gm of C-4 explosive in a Teflon® holder which was screwed into the center of the injector face (Fig. 3). The pulse charge was located on the centerline of the combustion chamber about 6 in. downstream of the injector face. Pulse charge detonation was by combustion heat.

(U) The injector baffles were regeneratively cooled with fuel, which was routed through the baffles and back to the injection ring passages. Fuel coolant was not discharged directly from the baffles. Film cooling of the combustion chamber was provided by fuel flow from orifices in the outer fuel ring of the injector, adjacent to the injector

mounting flange. Approximately 5 percent of the engine fuel flow was injected for film cooling.

2.2.3 Combustion Chamber

(U) The combustion chamber was constructed with an ablative liner, an asbestos insulating layer, and an external structural wrap (Fig. 4a). The ablative material consisted of a silica glass fabric tape impregnated with a phenolic resin compound. The chambers were constructed so that the maximum ablative thickness was obtained at the throat section. Several layers of resin-impregnated fiber glass wrap (glass fabric and glass filament) were bonded over the asbestos. The mounting flanges for the injector and nozzle extension were attached to the chamber by bonding the flange lips to the ablative material and structural wrap. Figure 4a also details the combustion chamber dimensions.

(U) Six combustion chambers were used during these tests (see section 2.2.1). The exit cone of each chamber extended to the 6:1 area ratio. The nozzle attachment flange design was designated the modified J-flange (Fig. 4a).

(U) The two chambers used for the T, U, V, and W test periods had an extra layer of glass filament roving which extended from the throat station forward and lapped over the injector mounting flange (Fig. 4a). The combustion chamber used during the V and W test periods had 44 anchor pins installed in the ablative lining at the injector end (Figs. 4a and b). Additional glass roving was used to strengthen the joint of the ablative chamber and the injector mounting flange. The anchor pin modification was to prevent separation and dislocation of the ablative cloth layers in the chamber/injector interface area.

2.2.4 Exhaust Nozzle Extension

(U) The radiation-cooled nozzle extension was bolted to the ablative chamber at the 6:1 area ratio and extended to the 62.5:1 area ratio. The nozzle extension design used during these tests is shown in Fig. 5.

(U) This nozzle extension was fabricated with columbium to the 40:1 area ratio and titanium alloy from the 40:1 to the 62.5:1 area ratio (Fig. 5). The columbium section thickness was 0.030 in. to area ratio 20 and was 0.022 in. from area ratio 20 to the columbium-titanium joint. The titanium portion was fabricated from 0.025-in.-thick titanium alloy (5 Al and 2.5 Sn). The columbium section was

coated to prevent oxidation, and the titanium section was coated to improve emissivity and thus reduce surface temperature.

2.2.5 Thrust Chamber Propellant Valve (TCV)

(U) Two different types of propellant valves were used during these tests. The first type was actuated by fuel pressure and was used with engines 9A and 11A. The latter valve was actuated by engine-stored gaseous nitrogen (GN_2) and was used with engines 9B through 11D. Both valve types utilized electrical commands for opening and closing. The propellant valving system consisted of eight ball valves: two each in the two parallel fuel passages and two each in the two parallel oxidizer passages, as shown in Fig. 6. Each of the TCV actuators operated one fuel and one oxidizer ball valve. Each of two solenoid pilot valves operated a pair of actuators (banks A and B). Thus, either bank, A or B, or both, could fire or shut down the engine. An auxiliary system, supplying GN_2 to the actuators, was installed at AEDC to effect TCV operation for checks and to actuate the fuel-activated TCV in the event normal fuel pressure actuation malfunctioned.

(U) Orifices at the TCV inlets were provided to balance the parallel passages, so that engine operation using either bank A or B would produce the same engine ballistic performance for given propellant interface pressures (Ref. 2). Engine ballistic performance was expected to change about two percent from "single bank" to "both banks" operation for given propellant interface pressures.

2.3 NAA F-3 FIXTURE

2.3.1 General

(U) The F-3 fixture (Fig. 7) was designed to reproduce the propellant system hydrodynamics of the S/M spacecraft with necessary modifications incorporated to facilitate ground test operations. The fixture structural frame, tanks, and plumbing had overall dimensions of 100 by 153 in. laterally and 15 ft high. The fixture weighed approximately 27,500 lb. A schematic diagram of the F-3 fixture propellant and pressurization plumbing is presented in Fig. 8.

2.3.2 Propellant System

(U) The propellant tanks were of spacecraft size, shape, and volume, consisting of two 1050-gal fuel tanks and two 1310-gal oxidizer tanks, but were designed and fabricated to meet the specification of the

ASME pressure vessel code. As in the S/M spacecraft, the two propellant tanks were series connected with propellant crossover lines; the engine propellant feed lines were connected to the sump tanks, and propellant force feed pressurization was through the storage tanks. The tandem tanks and crossover line arrangement resulted in variations of propellant feed pressures with changes in propellant level, although force feed pressurization was constant.

(U) The fixture propellant feed lines were modified to accommodate AEDC flowmeters and bypass connections for flowmeter calibration. Duplication of spacecraft line pressure losses was retained by changing the fixture line balance orifices.

2.3.3 Propellant Feed Pressurization System

(U) The pneumatic pressurization system of the F-3 fixture used equivalent components and schematic configuration but did not duplicate the spacecraft system. Fixture flight-type regulators could not be remotely controlled for the frequent testing at off-design mixture ratios or chamber pressures; therefore, AEDC facility helium pressurization regulators were located in the test cell and were used instead of the fixture regulators. As in the spacecraft, the regulator discharges were manifolded with a connecting line. An array of doubly redundant check valves was located in each propellant tank pressurization line, downstream of the connecting line, to prevent mixing of hypergolic propellant vapors. A valve was provided in the connecting line to accommodate off-design mixture ratio testing.

2.3.4 Heat Shield

(U) The heat shield used for test periods M and N was an early model shield, designed for the protection of the spacecraft propellant plumbing and tankage from nozzle extension thermal radiation. A 120-deg sector of this heat shield was supplied by NAA for use during part of this testing. The NAA shield was composed of a rigid bell of corrosion resistant steel and fiber glass material and flexible boot of high-silica glass cloth and batting, as shown in Fig. 9. The bell outer edge was cut away for plumbing clearance and mounting on the lower framework of the F-3 fixture. The remaining periphery was filled with a temporary-type heat shield fabricated inplace. This consisted of a fiber glass insulation material and an aluminum foil reflector between two layers of wire mesh (Fig. 9b). In the L test period, the entire heat shield was of the fiber glass, aluminum, and wire mesh temporary-type construction.

(U) A permanent-type heat shield was fabricated at AEDC for the P through W test periods. This shield was a compromise design intended to approximate the contour of the NAA flight-type shield, but to protect the thrust system instrumentation, F-3 fixture, and installation plumbing from the thermal radiation of the nozzle extension. This shield consisted of two layers of corrosion resistant steel with high temperature silica insulation between (Fig. 9c). The conical area facing the nozzle extension was covered with white or black Teflon to provide heat dissipation by sublimation.

2.4 INSTALLATION

(U) The Apollo S/M propulsion system F-3 fixture and the AJ10-137 engine were installed in the Propulsion Engine Test Cell (J-3), a vertical test cell for testing rocket engines at pressure altitudes in excess of 100,000 ft (Fig. 10 and Ref. 3). An aluminum test cell capsule, which is 18 ft in diameter and 40 ft high, was installed over the test article to form the pressure-sealed test chamber.

(U) The engine was installed in a multicomponent force balance. This balance was mounted in the F-3 fixture by six flexure-mounted load cells for thrust vector measurement (Fig. 11). The six load cells were used to determine the six components, three forces (axial, pitch, and yaw) and three thrust moments (pitch, yaw, and roll), generated by the thrust vector.

(U) Pressure altitudes were maintained, prior to and following test engine firing, by a steam-driven ejector in the test cell exhaust duct in series with the facility exhaust compressors and during the steady-state portion of the test by a supersonic engine exhaust diffuser (Fig. 10b). Ejector steam was supplied by the AEDC stationary boiler plant, supplemented by a steam-gas mixture from a rocket-type combustion steam generator. Facility systems included ground-level propellant storage; helium for test article propellant tank pressurization; gaseous nitrogen for test article pressure/leak checking, purging, and valve operation; F-3 fixture helium pressurization controls, operable from the J-3 control room; and electrical power in both 28 v dc and 100 v, 60 cps, ac. Equipment for test article operation, located in the J-3 control room, included the gimbal system checkout and controls consoles and the engine firing control and combustion stability monitor (CSM) console.

2.5 INSTRUMENTATION

(U) Instrumentation was provided to measure engine thrust (including axial and side forces); chamber pressure; propellant system

pressures, temperatures, and flow rates; nozzle extension and combustion chamber case temperatures; test cell pressures and wall temperatures; gimbal system electrical signals; and various vibrations and accelerations. Schematic diagrams of relative locations of the test article and test cell instrumentation are shown in Figs. 10b and 12.

2.5.1 Force Measuring System

2.5.1.1 Axial Force

(U) Axial force (F_a) was measured with a dual-bridge, strain-gage-type load cell of 50,000-lb_f rated capacity. In-place calibration was accomplished with a hydraulic actuator axial loading system containing a calibration load cell (Fig. 10b and Ref. 4). The calibration load cell was periodically laboratory calibrated with traceability to the National Bureau of Standards (NBS).

2.5.1.2 Side and Roll Forces

(U) Two yaw forces, two pitch forces, and one roll force were measured with strain-gage-type load cells of 500-lb_f rated capacity. These forces complete the complement of the six-component system for engine thrust vector determination. In-place loading calibration with NBS traceability was provided for these load cells also.

2.5.2 Pressures

2.5.2.1 Combustion Chamber Pressure

(U) Chamber pressure was measured using two strain-gage-type pressure transducers. One transducer was close-coupled to optimize response to pressure transients; the other transducer was provided with the capability for in-place applied-pressure calibration (Fig. 13). The calibration transducer was a precision reluctance type, which was laboratory calibrated with NBS traceability.

2.5.2.2 Cell Pressure

(U) Test cell pressure was measured with two capacitance-type precision pressure transducers located outside the cell capsule in a self-contained, controlled-temperature environment. These transducers were laboratory calibrated periodically with a precision mercury manometer. In-place calibrations were made by electrical voltage substitutions only.

(U) Test cell pressure was also measured with two auxiliary strain-gage-type transducers. These were situated in the test cell behind the F-3 fixture support structure to minimize exposure to thermal radiation.

2.5.2.3 Propellant Pressures

(U) Propellant pressures in the F-3 fixture lines, engine lines, thrust chamber valve, and injector manifolds were measured with strain-gage-type pressure transducers.

2.5.3 Temperatures

2.5.3.1 Engine Assembly Temperatures

(U) Exhaust nozzle extension, combustion chamber, and injector surface temperatures were measured with Chromel®-Alumel® thermocouples. Combustion chamber case temperature thermocouples were welded or bonded to the structure surface as appropriate for the base material.

2.5.3.2 Propellant Temperatures

(U) Propellant temperatures in the F-3 fixture tanks and engine line inlets were measured with copper-constantan thermocouple immersion probes. Propellant temperatures in the F-3 fixture propellant tanks were measured with resistance temperature transducer (RTT) immersion probes.

2.5.3.3 Test Cell Wall Temperature

(U) Cell wall interior surface temperatures were sensed with copper-constantan thermocouples welded to the cell capsule wall surface.

2.5.4 Propellant Flow Rates

(U) Propellant flow rates were measured with one flowmeter in each F-3 fixture propellant feed line, upstream of the engine interface. The flowmeters are rotating permanent magnet, turbine-type, axial flow, volumetric flow sensors with two induction coil signal generators.

2.5.5 Engine Vibration and Acceleration

(U) Engine injector, combustion chamber, and mount structure vibration were measured in three perpendicular planes with piezoelectric-type accelerometers (Fig. 12). Any engine vibration caused by

combustion instability was sensed by one of the accelerometers mounted on the engine injector (Fig. 12). The accelerometer output signal was analyzed by the AGC combustion stability monitor (CSM) to automatically initiate engine shutdown in the event of rough combustion (defined as engine acceleration exceeding 60 g's peak-to-peak at a frequency above 600 cps for longer than 0.040 sec).

2.5.6 Gimbal System Electrical Signals

(U) Electrical voltage and current signals from the gimbal control and actuation systems were tapped to indicate gimbal actuator position, actuator position change rate, actuator drive motor voltage and current, and actuator clutch currents.

2.5.7 Data Conditioning and Recording

(U) A continuous recording of analog data on magnetic tape was recorded from analog instrument signals by (1) analog-to-frequency converters and (2) magnetic tape, frequency-modulated (FM) recording with a saturation-level pulse technique. Instrument signals produced in a proportionate frequency form were amplified for continuous FM recording on magnetic tape. Magnetic tape recording in digital form used a recorder system that both produces and tape-records an analog signal in a binary-coded decimal form. Various instrument analog signals were (1) amplified and converted to a common range of analog base-level and amplitude, (2) commutated for sequential scanning, and (3) converted to the binary code for magnetic tape recordings.

(U) Light-beam oscillographs were used for continuous graphic recordings of analog and proportionate frequency signals. Proportionate frequency signals of the propellant flowmeters were recorded on the oscillograph with a divided frequency to improve record readability.

(U) Direct-inking, strip chart recorders were used for immediate access, continuous, graphic recordings. Analog signals produced pen deflections with a null-balance potentiometer mechanism. Proportionate frequency signals were converted to analog for strip-chart recording.

2.5.8 Visual Coverage

(U) Two closed-circuit television systems permitted visual monitoring of the test article during testing operations. Permanent visual documentation of engine test firings was provided by color

motion pictures with 16-mm cameras located in the test cell. An oscilloscope enabled visual observation of the CSM accelerometer signal during testing operations. Various engine and F-3 fixture parameters were recorded on strip-chart recorders with visual indicators in addition to the direct-inking feature to provide control room indications of test article operation, performance, and environment during testing operations.

SECTION III
PROCEDURE

3.1 PRE-TEST OPERATIONS

(U) Prior to each test period, the following functions were performed at sea-level pressure:

1. The F-3 fixture was loaded with propellants,
2. Flowmeters were in-place calibrated using the J-3 flowmeter calibration system (Ref. 1),
3. Propellant samples were taken to determine the specific gravity and particulate contamination count of foreign matter in the propellants,
4. Propellant tanks were pressurized,
5. Instrumentation systems were calibrated,
6. A functional/sequence check of all systems was made,
7. An in-place calibration of the six-component thrust system was made (Ref. 4 provides a detailed explanation of the calibration procedures), and
8. Axial thrust and chamber and cell pressures were in-place calibrated.

(U) After the above procedures were completed, the test cell pressure was reduced to approximately 0.4 psia with the facility exhaust compressors for altitude calibrations and steps 5, 6, and 8 above were repeated.

(U) After completion of instrumentation altitude calibrations, the steam ejector was used to reduce the test cell pressure to about 0.2 psia. All pre-fire operations, 60 sec prior to firing, and all immediate post-fire operations were automatically sequenced. These

operations included instrumentation and camera starts, engine firing, engine shutdown, instrumentation and camera stops, and steam generator firing and shutdown. Steam augmentation by operation of the steam generator further reduced the test cell pressure to a level between 0.05 and 0.1 psia prior to ignition of the test engine. Simulated altitudes were maintained during engine coast periods by the facility exhaust compressors.

(U) After the final firing of a test period, the following functions were performed:

1. The steam ejector was shut down and the cell pressure maintained at about 0.4 psia by the facility exhaust compressors,
2. Pre-test steps 5 and 8 were repeated for post-test altitude calibration,
3. The F-3 fixture propellant tanks were drained and depressurized,
4. The engine propellant valves were opened for approximately an hour to aspirate the propellant lines (occasionally F-3 tanks also),
5. The propellant valves were closed and the test cell pressure was raised to one atmosphere, and
6. Pre-test steps 5, 7, and 8 were performed for post-test, sea-level calibration.

(U) Installation of instrumentation on the test engines and engine rebuilding were accomplished by AGC and ARO technicians in an engine assembly room where contamination particle size was maintained below 500 microns. Engine rebuilding was accomplished in accord with procedures supplied by AGC.

3.2 PERFORMANCE DATA ACQUISITION AND REDUCTION

3.2.1 General

(U) Engine performance data were acquired as shown in Table I. Digital computers were used to recover data from magnetic tape records, produce data printouts in engineering units, and perform computations to produce engine performance information as follows:

1. Rocket engine ballistic performance (vacuum thrust, thrust coefficient, specific impulse, and characteristic velocity),
2. Total impulse of start and shutdown transients,

3. Total impulse of minimum impulse bit operation, and
4. Thrust vector determination.

(U) The equations used for engine performance calculations were according to general standard practice, except for adaptations in usage, which were made to account for area changes of the ablative combustion chamber throat. Performance calculations were based on combustion chamber pressure measured at the injector. No correction was made for total pressure loss due to heat addition. Steady-state performance calculations were made from measured data which were averaged over 2-sec time periods.

3.2.2 Ballistic Performance

(U) Because of the nonuniform variations of the effective nozzle throat area during a firing and the physical impossibility of measuring the throat area between firings, characteristic velocity and nozzle throat area were calculated during firing series using the following assumptions:

1. Characteristic velocity, corrected to a mixture ratio of 2.0, is constant for a given injector and is independent of chamber geometry,
2. Characteristic velocity is a function of mixture ratio and chamber pressure only. (However, because of a paucity of experimental data, c* was assumed to vary linearly with chamber pressure), and
3. The slope of the c* versus MR curve conforms to previous experimental data.

(U) Characteristic velocity (c^*_i) for a given injector was calculated using (1) the engine data between 2 and 4 sec of the initial firing on a new chamber, (2) the pre-test measured nozzle throat area, and (3) the relationship: $c^*_i = P_{cm} A_{t_m} g/\dot{W}_t$. The c* for a mixture ratio (MR) of 2.0 was derived using a curve slope factor (shown below) supplied by the AGC (which was based on data from tests with the known throat area of a steel combustion chamber):

$$f_{corr} = 5592.0 / [5277.91 + 691.846\,(MR) - 267.12\,(MR^2)]$$

$$c^*_i\,(\text{at MR} = 2) = (c^*_i)\,(f_{corr})$$

This c^*_i for MR = 2 was retained as the standard for the given injector, to be used for subsequent data reduction. The c* for any other MR, during subsequent firing, was derived by reversing the process and applying the MR slope factor (f_{corr}) to the standard c^*_i for MR = 2.

(U) The throat area of the nozzle for subsequent firing was calculated using the c* derived above, the measured chamber pressure, measured propellant flow rates, and the relationship: $A_{t_{calc}} = c^* \dot{W}_{t_m} / g P_{c_m}$. This calculated nozzle throat area was used with axial thrust corrected to vacuum conditions and measured chamber pressure to determine the vacuum thrust coefficient.

3.2.3 Total Impulse of Start and Shutdown Transients

(U) The total impulse (lb/sec) of the start transient covered the time period from FS-1 to 100 percent of steady-state combustion chamber pressure. The impulse integral was derived using calculated thrust based on chamber pressure; that is,

$$I_t = C_F A_t \int_o^t P_c dt$$

Intermediate impulse values were also derived for levels of chamber pressure at intervals of 10 percent up to the steady-state level. The total impulse of the shutdown transient covered the time period from 100 to 1 percent of steady-state combustion chamber pressure. Vacuum thrust, computed from measured thrust, was not used because system dynamics invalidate thrust data during the starting and shutdown transients. In addition, at chamber pressures below about 60 psia, during the shutdown transient, the nozzle no longer flows full with the existing chamber-to-cell pressure ratio.

(U) Measured combustion chamber pressure was reduced at 0.005-sec intervals (200 intervals/sec) from the continuous magnetic tape recording of close-coupled transducer data. The combustion chamber pressure was used with calculated steady-state vacuum thrust coefficient and calculated nozzle throat area to compute vacuum thrust. The values of C_{F_V} and A_t, derived at the steady-state operation nearest the transient of interest, were assumed to be constant throughout the transient. The assumption of constant C_{F_V}, during the transients, implies that the nozzle throat is choked throughout the entire transient. Any discrepancies inherent in this assumption occur within a relatively small time period at very low chamber pressure only and are not, therefore, sufficient to detract from the significance of the results.

(U) A digital computer program determined the time of occurrence, the thrust-rise-rate, and the integrated total impulse at the specific percentage levels of chamber pressure during the start and shutdown transients. The 100-percent chamber pressure basis is that derived from pressure measured during the steady-state data period nearest the transient of interest.

3.2.4 Total Impulse of Minimum Impulse Bit (MIB) Operation

(U) The method used for calculating the total impulse integrals (lb-sec) of the MIB firings was like that used for the start and shutdown transients. In MIB firings, the impulse was totaled for the entire firing from FS-1 through the thrust decay to one percent of engine nominal chamber pressure. As in the transient impulse calculations, thrust was computed from combustion chamber pressure measured at 5-msec intervals. Since the MIB firings were too short to establish steady-state engine performance levels, the vacuum thrust coefficient (C_{F_V}) and exit nozzle throat area (A_t) used were obtained from the nearest previous engine firing which produced steady-state data. The same assumptions of constant C_{F_V} and A_t throughout the MIB firing were retained.

3.2.5 Thrust Vector Determination

(U) The multicomponent force measurement system is shown schematically in Fig. 11. These load cells were used to measure the six components of force: forward and aft pitch, forward and aft yaw, roll, and axial. The force balance system employed the premise of a linear repeatable mechanical interaction for a given force application. That is, for a given force application (L), the force (R) measured in any load cell could be obtained from the following relationship:

$$R_i = C_{i,j} L_j$$

where $C_{i,j}$ represented the calibration constants based on the slope of the interaction. Because there were six data and six calibrate load cells, both i (which represented the data load cell being observed) and j (which represented the load applicator being used) varied from 1 to 6, and $C_{i,j}$ was a six by six matrix.

(U) To obtain true forces from the thrust system, an equation of the following form was required,

$$L_j = K_{j,i} R_i$$

where $K_{j,i}$ represents the balance constants and was the inverse of the calibration constant matrix ($C_{i,j}$). The true forces were obtained by multiplying the force measured by the inversion of the calibration constants. A complete explanation of the force system and the method of determining balance constants is given in Ref. 4.

(U) Once the forces were determined at the six load cells, the equations of static equilibrium were employed to resolve these forces into a thrust vector at the engine gimbal plane (plane of engine throat).

This thrust vector is presented in the form of the angle, from vertical, in the pitch and yaw planes and the offset from the centerline of the inner thrust cage at the point of intersection of the thrust vector with the gimbal plane.

SECTION IV
RESULTS AND DISCUSSION

4.1 GENERAL

(U) The primary objective of these tests was to establish the operating characteristics and performance level of the Apollo S/M propulsion system at simulated altitudes above 110,000 ft. Specific objectives were to determine:

1. Engine performance at design operating conditions,
2. Engine performance at off-design chamber pressures, mixture ratios, and propellant temperatures,
3. Engine ballistic performance with single and both bank thrust chamber propellant valve operation,
4. Thrust vector determination,
5. Combustion chamber ablation characteristics,
6. Start and shutdown impulse characteristics,
7. Gimbal system operation,
8. Minimum impulse bit operation, and
9. Restart capability.

(U) One hundred and eighteen test firings with an accumulated duration of 3367.1 sec were conducted using six engine assemblies to meet these test objectives and complete the Phase II testing program. A brief description of each test period (covered by this report) is presented in Appendix I, and a summary of test number, dates, objectives, and durations is listed in Table I. In addition to the objectives stated above, the test article temperature during firings and extended coast periods at simulated high altitudes is presented, and rocket engine durability is discussed. During this report period, testing was conducted with both cold propellants (35°F) and hot propellants (140°F). Test cell wall temperatures were established and maintained at the same temperature as the propellants for these tests. The final testing

of this program was conducted to identify the cause of inadequate durability of the combustion chamber.

4.2 ENGINE PERFORMANCE

4.2.1 General

(U) The ballistic performance of the Apollo S/M Engine was determined for six engine assemblies by conducting 90 test firings over a mixture ratio range from 1.62 to 2.43, and a chamber pressure range from 80 to 125 psia. The effect of extreme propellant temperatures on engine performance was investigated during test periods N and P by conditioning the propellants to temperatures of 140 and 35°F, respectively.

(U) Three basic parameters were used to describe engine performance: specific impulse corrected to vacuum conditions (I_{sp_V}) was used to define the overall engine performance; characteristic velocity (c*), computed using injector face pressure, indicated the combustion chamber performance; and thrust coefficient, corrected to vacuum conditions, indicated the nozzle performance. The calculation of I_{sp_V} used measured data only and incorporated no assumptions, whereas c* and C_{F_V} did (Section 3.2.2); therefore I_{sp} should be considered the most accurate of these calculations.

4.2.2 Overall Engine Performance

(U) (C) Vacuum Specific Impulse (I_{sp_V}) data obtained from steady-state operations at the design chamber pressure are presented in Table II and in Fig. 14. All steady-state data obtained between 7 and 40 sec after FS-1 in these tests were used to construct (by digital computer) a second-order, least-squares curve applicable to each engine. The results of this analysis indicated the precision of the data aquisition and the repeatability of the engine operation and provided a mathematical expression for the overall engine performance. Data from engine S/N 11C were not included because of a measurement error in thrust (approximately 0.35 percent high), suspected to have been caused by mechanical interference in the thrust measurement system. To expedite the test schedule, side load calibrations were not made for this period of firings; therefore, it was not possible to determine if mechanical trouble actually existed. Data from engine S/N 11D are not presented in the above analysis because of the limited amount of data obtained at design conditions; however, these data are included in

Table II. A summary of the engine performance information for this analysis is as follows:

Engine S/N	9A	11A	11A*	9B**	11B
Number of Test Periods (at design chamber pressure)	1	1	1	1	1
Number of Test Firings (P_c = 102 psia)	6	7	7	7	7
Number of Data Sample	57	65	49	39	41
One Standard Deviation of Data about Second-Order Least-Squares Curve, percent	0.050	0.049	0.082	0.076	0.049
I_{sp_v} at MR = 2.0	310.7	311.1	311.2	311.9	311.6

The least-squares fit computer program produced the second-order equations of I_{sp_v} for the engine assemblies as follows:

Engine S/N	Performance Equation
9A	$I_{sp_v} = 265.037 + 64.1802(MR) - 20.6777(MR)^2$
11A	$I_{sp_v} = 278.751 + 51.5109(MR) - 17.6644(MR)^2$
11A*	$I_{sp_v} = 327.991 - 5.9234(MR) - 1.23750(MR)^2$
9B**	$I_{sp_v} = 220.207 + 110.298(MR) - 32.234(MR)^2$
11B	$I_{sp_v} = 189.178 + 138.907(MR) - 38.8466(MR)^2$

(U) The data presented in Fig. 14 indicated that engine efficiency continually increased as mixture ratio was reduced and did not reach an apparent maximum for any of the engines within the mixture ratio range investigated (1.62 to 2.43).

(U) These data also indicated that the performance derived from the different engine assemblies was very repeatable. The slopes of the

*Propellant Temperature = 140°F
**Propellant Temperature = 35°F

data in Fig. 14 for the different engines are essentially the same, except for engine S/N 11A, test series N, which was conducted at a propellant temperature of 140°F. The cause of the change in slope for this test could not be positively determined. If all the data in Fig. 14 are grouped together (with the exception of the data from test series N), the one curve, which represented the overall performance for all the engines tested, resulted in a congregate I_{sp_v} at a mixture ratio of 2.00 of 311.3 lb_f-sec/lb_m, with a one standard deviation of 0.142 percent.

(U) Extremely low propellant temperatures (35°F) had essentially no effect on engine performance. Extremely high propellant temperatures (140°F) seemingly affected the slope of the I_{sp_v} versus MR (Fig. 14), but this could not be definitely attributed to engine performance. Because of the high vapor pressure of N_2O_4 at 140°F (74 psia), in-place flowmeter calibrations could not be obtained at this temperature. Oxidizer flowmeter calibrations were conducted with a maximum oxidizer temperature of 100°F, and flowmeter characteristics for 140°F oxidizer were produced by extrapolation. Therefore, it is possible that the slope of the oxidizer flowmeter constant versus frequency could have changed without indication at the higher oxidizer temperature. The decreasing slope of the I_{sp_v} versus MR curve at lower mixture ratios was most apparent by test N-78, in which the oxidizer flow rate was the lowest of the N tests. It is, therefore, possible that the change in slope in Fig. 14 was caused by a change in the oxidizer flowmeter constant instead of an actual degradation of engine performance.

(U) (C) Twenty-six test firings were conducted at off-design chamber pressures from 80 to 125 psia. These data (presented in Table II and Fig. 15) show that overall engine performance increased with increasing chamber pressure. The congregate I_{sp_v} values for the four engine assemblies tested at off-design chamber pressure were 312.6 lb_f-sec/lb_m at a P_c of 125 psia and 308.8 lb_f-sec/lb_m at a P_c of 80 psia. An increase in chamber pressure from design conditions (P_c = 102 to 125 psia) increased the engine performance by approximately 0.5 percent, but this increased chamber pressure was extremely detrimental to the engine durability, as discussed in Section 4.3.3.

(U) It was noted that during the longer duration firings (over 50 sec) an increase in I_{sp_v} occurred, thus indicating increasing engine efficiency with time which could not be attributed to mixture ratio changes. This performance increase is thought to be caused by improved nozzle thrust coefficient from contour changes of the nozzle extension under load at high temperature and is discussed further in Section 4.2.4.

4.2.3 Combustion Chamber Performance

(U) (C) Characteristic velocity (c*), an indicator of combustion chamber efficiency, was calculated by the method presented in Section 3.2.2. The method of calculation derives a representative c* early in the first firing (from 2 to 4 sec) of a new chamber by the $P_c/\dot{W}_t$ relation and the pre-fire measured throat area. Because of the unknown changes in nozzle throat area, which occur with an ablative chamber, the only reliable experimental c* is that calculated by this method. The c* initial values for the six engine assemblies and four injectors tested are presented in Fig. 16 and summarized as follows:

Engine S/N	9A	11A	9B	11B	11C	11D
Injector S/N	47	91	47	46	64	64
c* at MR = 2.00 ft/sec	5704	5729	5675	5712	5705	5698

These values, as stated previously, were based on chamber pressure measured at the injector face and did not account for possible differences in chamber pressure loss with the different injectors. As shown above, the combustion chamber performance for the six engine assemblies was repeatable with a one standard deviation of ±0.31 percent (±17.7 ft/sec). The two injectors S/N 47 and 64 were utilized in two engine assemblies each; the differences in c* at MR = 2.0 were 0.3 and 0.1 percent, respectively.

(U) There appeared to be no effect on c* of chamber pressure changes in the performance measured with these six engines using the prototype baffled injectors.

4.2.4 Nozzle Performance

(U) (C) Nozzle performance, as determined from thrust coefficient corrected to vacuum conditions, was obtained for four flight-type nozzle extensions. A summary of nozzle performance at design conditions is presented in Fig. 17 and summarized as follows:

Engine S/N	9A	11A(M)	11A(N)	9B	11B
Nozzle Extension S/N	27	28	25	28	26
C_{F_V} at MR = 2.0	1.754	1.748	1.747	1.768	1.756

(U) The calculated value of C_{F_V} increased with increasing chamber pressure, as shown in Fig. 18 and as follows:

Engine S/N	P_c, psia	C_{F_V} at MR = 2.0
9B	80 125	1.753 1.777
11B	80 125	1.740 1.762
11D	125	1.766

(U) This calculated increase in nozzle performance must be evaluated with care and could be misleading. These factors may be considered:

a. A change in the actual loss in combustion chamber total pressure between the injector face and the nozzle throat would affect the validity of comparing calculated values of C_{F_V} at different pressures. The calculated value of C_{F_V} would change by an amount inversely proportional to the change in the total pressure loss.

b. A change in the nozzle extension physical contour sufficient to affect the thrust coefficient at the higher pressures may also be a possible explanation for all or part of the increase noted during these tests.

(U) Figure 19, test U-136, shows that, during a longer test firing, C_{F_V} increased as the firing progressed. The increase during the 300 sec of test U-136 was 0.32 percent. This increase was concluded to be caused by recontouring of the nozzle extension under load at high temperature. It should be noted that the measured thrust returned to zero after shutdown, indicating no adverse effect of temperature on the load measuring system. Not more than 0.18 percent of this increase may be attributed to a change of the nozzle from thermal expansion.

4.2.5 Effect of Propellant Valve Bank Selection on Engine Ballistic Performance

(U) During engine operation, flow through the propellant valve assembly may be routed through TCV bank A only, through TCV bank B only, or through both banks simultaneously, as discussed in Section 2.2.5. The operating parameters changed significantly when both valve banks were used (Fig. 20a) because of the change in flow resistance through

the thrust chamber valve (Fig. 20b). However, a review of the performance indicated that, within the precision of the data (σ = 0.14 percent), all of the selections resulted in essentially the same engine combustion performance; the ratio of $P_c/\dot{W}_t$ or F_v/P_c remained essentially constant for a given mixture ratio regardless of the TCV bank selection used.

4.2.6 Start and Shutdown Transient Characteristics

(U) The total impulse (lb-sec) of several starting and shutdown transients was calculated to document the quality and repeatability of the total impulse for the non-steady-state portions of engine firings.

(U) Typical start transients are shown in Fig. 21. The time requirements for thrust buildup and the general repeatability of the time of ignition are shown in Fig. 21a. The start transient total impulse repeatability is shown by the dispersion of the termini of the impulse history curves in Fig. 21b. A summary of start transient impulse data is given in Table IIIa.

(U) Typical shutdown transients are shown in Fig. 22. The thrust decline repeatability is shown in Fig. 22a. A summary of the shutdown transient impulse data is presented in Table IIIb.

(U) The magnitude of the total start or shutdown impulse was a function of (1) the engine chamber pressure and MR operation levels, (2) the TCV bank selection, and (3) the TCV timing (opening or closing times), which was altered for the different engines tested with the pneumatically actuated TCV (engine S/N 9B and subsequent). In general, the initial valve operations of the earlier test periods with the pneumatic TCV were sluggish and resulted in a larger start impulse. This was undoubtedly because the valve was new and dry. In later test periods with engines S/N 11C and 11D, the valve was not as sluggish.

(U) The repeatability of starting transient impulse was strongly dependent on the TCV timing which produced starting impulses within ±2 percent in slow operation (tests No. P-87 through P-90), and produced starting impulses within about ±10 percent in fast operation, although the actual spread in impulse lb-sec was about three times greater in slow operation. The initial operation sluggishness also appeared in the shutdown, but the percentage effect on the transient impulse repeatability was less. The effect of TCV timing on the shutdown impulse was much less than on starting impulse. The shutdown impulse was primarily a function of chamber pressure.

4.2.7 Minimum Impulse Bit Operation

(U) No attempts were made during these tests to establish the minimum impulse bit, per se, as had been done in previous testing (Ref. 1). However, the total impulse was computed, using measured chamber pressure, for the several firings of about 0.95-sec duration which were made during this testing. These impulse values are presented in Table IV and Fig. 23. The figure also shows typical combustion chamber pressure transients experienced during two of these firings which were with a design chamber pressure of 125 psia.

(U) The impulse value groups of the test period in Fig. 23b show the strong influence of TCV timing. The "rise time" data in Table III show that the TCV bank with a 0.25-sec shorter rise time consistently produced about a 5 percent higher impulse. Further variation in impulse was understandably introduced by the variation of chamber pressure. The reason for the wide variation in the impulse values of the S period is not known. The narrow bandwidth of the two data groups and the absence of intermediate values indicate that the TCV bank designations were erroneous, and the two groups were probably produced by the different valve banks. However, the impulse values for this wide band of data were still repeatable within ±9 percent of a median.

4.3 OPERATIONAL PERFORMANCE AND RELIABILITY

4.3.1 Propellant Injector Performance

(U) Tests were made to determine the capability of the combustion mechanism to recover from induced instability. A small explosive charge (No. 8 blasting cap and 2.46 gm of C-4 explosive) was installed in the forward center of the combustion chamber for the initial firings of the L, M, P, R, T, and V test periods. The installation and location of the charge were the same as described for the earlier testing reported in Ref. 1. The heat of engine combustion fired the pulse charge at about 1 sec after engine ignition. Combustion stability recovery was satisfactory for all tests during which the explosive charge was used.

4.3.2 Exit Nozzle Extension

(U) Nozzle extension durability during this testing was satisfactory. It may be noted that all nozzle extensions used during these tests, except S/N 025, were used for two engine test series.

4.3.3 TCA Structural Reliability

(U) The test series of engine S/N 9A was discontinued after the first test period (L). The firing time had totaled some 602 sec, of which the final firing was 500 sec. When the nozzle extension was removed to repair a puncture, engine inspection revealed deterioration of the ablative combustion chamber in the region of the nozzle extension mounting flange. Bonding separation of the ablative lining material from the metal flange had occurred. Numerous small delaminations were apparent in the ablative material at the chamber/nozzle seal surface (Fig. 24).

(U) Post-test inspection of engine 11A disclosed a cracked weld at the injector face junction inside the central cylindrical baffle (Fig. 25). The crack was not sufficiently severe to impair baffle durability, but the effect on engine performance was noticeable as shown in the data for test No. N-85 (Fig. 26). This injector was returned to AGC for retrofit with a new design weld which had been developed to prevent this type of cracking. No further difficulties of this nature were experienced in subsequent tests.

(U) The combustion chamber of engine 11A endured the complete firing schedule of 758 sec at design chamber pressure without apparent major damage. Although it was not regarded seriously at the time, some delamination of the ablative material layers at the injector seal area had occurred by the end of this testing series (Fig. 27).

(U) The test series of engines S/N 9B and 11B were terminated short of completion by failure of the combustion chamber at the injector mounting flange. Engine 9B had experienced about 408 sec of firing time, of which the last 223 sec were with 125-psia combustion chamber pressure. Engine 11B had experienced about 332 sec of firing time, of which the last 149 sec were with 125-psia combustion chamber pressure. The details of the failure mode were not apparent from these two tests because the tests had proceeded through chamber separation from the injector mounting flange (Figs. 28a, b, and c). However, it was generally concluded that the structural bond was failing between the chamber structural glass wrap and the metal injector mounting flange. Post-test inspections of the chambers revealed delaminations of the foremost layers of ablative material. At this point, these delaminations were suspected of contributing to, or perhaps even initiating, the flange bond failures. The delaminations would permit hot gas circulation behind the chamber/injector seal to overheat and deteriorate the mounting flange bond.

(U) Engine 11C had a modified combustion chamber with additional structural glass roving wrap and redesigned injector seal (Section 2.2.3 and Fig. 4a). Extra temperature measuring thermocouples were added to the injector and chamber flanges for the 11C and 11D engine series to gain a keener insight into the flange local temperatures. The more complete temperature information was also used for a control room warning of incipient failure. Engine 11C test series was discontinued 5 sec short of completion because injector flange and chamber flange temperatures were exceeding 400°F and rising rapidly (Fig. 29). The engine had experienced a total firing time of about 766 sec, of which the final firings had included 200 sec with 125-psia chamber pressure and 355 sec with 110-psia chamber pressure. Post-test inspection disclosed delamination of the forward chamber ablative material and damage of the new metal seal ring (Fig. 30). This chamber design exhibited a notable improvement in durability over those tested previously, in that firing durations were extended and rather high flange temperatures were experienced without incurring a chamber and flange separation. However, it was ventured that the post-test chamber condition indicated that a chamber burnthrough was probably imminent.

(U) The engine 11D test series was conducted with a chamber design like that of engine 11C, but with the addition of the anchor pins (Fig. 4) to immobilize the forward layers of ablative material (Section 2.2.3). The pins were installed only in portions of the chamber circumference in order to evaluate their relative efficiency for durability improvement. A firing sequence was selected which duplicated AGC tests at sea-level conditions and simulated the initial planned sequence of forthcoming engine qualification tests. This test series was discontinued short of completion because injector and chamber flange temperatures were excessive. Figure 31 is a plot of the injector and chamber flange temperature. The engine had a total firing time of about 501 sec, of which the final 278 sec had been at 125-psia chamber pressure. Post-test examination revealed the same fore-end delamination and showed that the anchor pins had not markedly improved chamber durability (Fig. 32). A further result of this firing series was the flame damage of the injector which was apparently caused by deterioration of the chamber/injector seal.

(U) It was concluded that the Phase II combustion chamber design was amply durable for the design engine life of 760 sec with engine operation at design chamber pressure. However, the Phase II chamber design could not dependably endure 125-psia chamber pressure operation at altitude pressure test conditions. Other engine components were satisfactorily durable.

4.3.4 Thrust Chamber Valve

(U) The prototype pneumatically actuated TCV S/N 101 was used for the last four engine test series without significant difficulties. The obsolete, fuel pressure-actuated TCV was used with engines S/N 9A and 11A without significant difficulty.

4.3.5 Engine Restart

(U) Engine restart capability was demonstrated by all 118 engine firings during this testing, which were made without an irregular ignition. It should be noted that these tests also included operations with high and low temperature propellants (approximately 140 and 35°F).

4.4 ENGINE TEMPERATURE CHARACTERISTICS

4.4.1 Nozzle Extension Temperature

(U) Figures 33a through e present the temperature history for the longest firing duration tests of engines S/N 9A, 11A, 9B, 11B, and 11C, respectively. Equilibrium temperatures were at about the same level for all engines tested and were reached after about 80 sec of operation.

(U) Figures 34a and b show the nozzle temperature profiles during tests with various mixture ratios. Figure 34a shows that mixture ratio variation in the test range between 1.6 and 2.2 had little effect on the nozzle extension temperatures. In Fig. 34b, the equilibrium temperature data for engine S/N 11A indicated that the higher mixture ratio produced higher temperatures. However, the intermediate MR data were too varied to definitely support the trend.

(U) A comparison of nozzle extension temperatures versus combustion chamber pressure could not be made, since many of these tests were too short in duration to provide equilibrium temperature. However, previous testing in this program had shown nozzle extension temperatures to have been approximately proportional to chamber pressure (Ref. 1).

(U) The temperatures at 160 sec after FS-1 for the four nozzle extensions tested are presented in Fig. 34b. This summary includes test No. N-78, during which the test cell temperature and propellants temperature were conditioned to about 140°F. Although station temperature data differed by as much as 250°F, the general appearance of the

data indicates sensing errors have increased data spread; therefore, station temperature from test to test is concluded to be more repeatable than shown. The high propellant temperatures of test No. N-78 did not result in any detectable change in the indicated temperatures of the nozzle extension. Comparison of temperatures with a wider range of propellant temperature was not made because P test period firings, with low-temperature propellants (about 35°F), were too short in duration to provide equilibrium nozzle extension temperatures.

(U) A significantly higher temperature consistently occurred on the titanium side of the columbium-titanium joint of the nozzle extension, as shown in Fig. 34b, apparently caused by the lower emissivity of the titanium material.

4.4.2 Combustion Chamber Temperature

(U) It was difficult to derive any but gross conclusions from the chamber temperature data. The temperature-time history was greatly dependent on the firing history for that chamber. The number and length of firings and duration of coast preceding a test influenced the chamber temperatures by the heat capacity of the chamber and the test cell installation components. Furthermore, the temperature measuring thermocouples were not entirely reliable, which introduced an additional measure of uncertainty into analysis and comparisons.

(U) Thermal equilibrium on the chamber outer surface was not attained during any of these test firings because of the low thermal conductivity of the chamber ablative material. Figure 35a shows the temperatures during and following a 500-sec firing. The peak temperatures were experienced during the post-fire coast, considerably after engine shutdown, as a result of heat soak-through from the firing. The outer surface rapid temperature rise and fall, during and immediately following the firing, were too fast to have been the result of conduction through the chamber ablative and insulation bulk. These were concluded to have been the result of (1) thermal radiation from the nozzle extension and (2) conduction through the metallic flanges. This conclusion was supported by the subsequent temperature rise by thermal conduction through the ablative and insulating layers from the heated inner surface. It was expected that the highest temperature peak would occur near the chamber/nozzle throat. However, the highest temperature, in the coast following the firing, occurred near the forward end of the chamber, some inches from the injector mounting flange. This heat concentration was undoubtedly symptomatic of the chamber durability problem encountered in later tests (see Section 4.3.3).

(U) The maximum temperature reached on the outer surface at the chamber throat during the various long duration firings was generally the same, as shown in Figs. 35a through d and summarized as follows:

Engine S/N	Test Duration, sec	Peak Temperature, °F	Peak Temperature Time after FS-2, min
9A	500	325 (est.)	45 (est.)
11C	300	377	35
11A	250	270	38
11D	234	250	44

These data also indicated that the length of firing had little effect on the time for the peak throat temperatures to occur (via conduction).

(U) The high and low cell wall and propellant conditioning temperatures, of about 140 and 35°F in the N and P test periods, had no significant effect on the temperatures experienced by the combustion chamber, as shown in Figs. 36a and b. Although the test firing durations of the cold tests were too short to provide definitive temperature data, the temperature rise rate appeared about the same as for the hot cell and propellant tests.

(U) Combustion chamber outer surface and flange temperatures, measured during tests for chamber durability proof, are presented with the discussion of durability in Section 4.3.3.

4.5 THRUST VECTOR DETERMINATION

(U) A six-component force balance was used to measure the thrust vector and its excursion with time during steady-state, nongimbaling operations of the Apollo S/M Engine (Ref.. 4). Engine S/N 9A was fired for a total firing time of 602 sec with no gimbaling (Tests No. L-55 to L-60). The thrust vector during these six firings was determined and is presented in Figs. 37, 38, and 39.

(U) The initial firing of engine S/N 9A established the initial angular offset from vertical (Fig. 37). This initial offset was 0.36 deg in the pitch plane and -0.62 deg in the yaw plane. Vector excursion was measured from these initial angular values. The excursion of the thrust vector for the first five 20-sec firings was insignificant in both the pitch and yaw planes, indicating that the deposition of ablative material slough in the chamber throat was uniform during these initial short

firings. The 500-sec firing (L-60) resulted in angular variations, the extremes of which spanned 0.44 deg in pitch and 0.30 deg in yaw. The gradually larger angle changes indicate the nonuniformity of chamber ablation and throat deposition. The relatively sudden change of the pitch component at about 490 sec indicates an abrupt change or localized loss of the throat deposit.

(U) To completely define the thrust vector generated by the engine, a position location, in addition to the vector angle, is required. The vector position was determined as component distances from the balance centerline in the nozzle/chamber throat plane and is presented in Fig. 38. The initial position, determined from the first firing of engine S/N 9A, was -0.236 in. from the balance centerline in the pitch plane and -0.075 in. from the balance centerline in the yaw plane. The thrust vector position change covered a span of 0.15 in. in the pitch plane and 0.35 in. in the yaw plane. The excursion of the vector position in the throat plane, during the L test firings, is presented in Fig. 39. The progressive variation of vector position indicated the shifting of the effective centroid of the throat and/or variant distortion of the nozzle extension.

(U) Thrust vector presentations are not made for engines S/N 11A, 9B, 11B, 11C, and 11D because insufficient duration in nongimbaling, steady-state operations preclude definitive analysis.

4.6 GIMBAL SYSTEM OPERATION

(U) Gimbaling operations were conducted during 60 of the 118 firings made in this testing (Table I). Gimbal operations were omitted (1) in the L series to accommodate thrust vector data acquisition, (2) in the firings of less than 10 sec duration, and (3) in firings which were introduced into the test schedule with too short a notice for revision of the AGC gimbal programming. The gimbal amplitude was limited to 1.5 deg during these operations to preclude spilling the nozzle exhaust over the inlet edge of the exhaust diffuser and into the test cell (see Fig. 10b). The gimbal operations included ramp, step, and sine function command signals of various frequencies to document gimbal system mechanical and electrical dynamics. A description of these operations and examples of oscillograph data are given in Ref. 1. These gimbal operations of the engine, complete with nozzle extension at altitude pressure conditions, were performed to provide data for definition of the engine mount/gimbal system vibration characteristics (such as system spring rate, effective mass, and damping). Analysis of the gimbal data was done by AGC and NAA.

(U) The engine gimbal operations were conducted satisfactorily. Engine gimbal actuators exhibited satisfactory durability within the range investigated during these tests.

4.7 COMBUSTION CHAMBER ABLATION CHARACTERISTICS

(U) Other than the chamber seal areas, as discussed previously, the chamber durability was satisfactory. Figure 28a shows the relatively shallow char depth produced in engine 9B by 408 sec of firing time, of which 223 sec were at 125-psia chamber pressure (125 percent of design chamber pressure). Figures 27, 28, 40, and 41 typify the chamber ablation produced in this testing. In general, the chambers showed fairly uniform ablation. The slight localized ablation shown in the figures was oriented such that the more prominent streaks were aligned with injector radial baffles. The wake of the baffles apparently somewhat disrupt the chamber fuel film cooling. The lesser streaks were oriented midway between baffles and may have been caused by the existence of an acoustic node or concentration effect on the cooling fuel film.

SECTION V
SUMMARY OF RESULTS

(U) Significant results obtained during this part of the Apollo S/M Engine Phase II test program are summarized as follows:

(U) 1. The congregate I_{sp_v} of the engines tested was 311.3 lb_f-sec/lb_m at design chamber pressure and MR (100 psia and 2.00) with a one standard deviation of 0.14 percent.

(U) 2. Off-design I_{sp_v} of these engines was:

   a. 312.6 lb_f-sec/lb_m at 125-psia P_c and 308.8 lb_f-sec/lb_m at 80-psia P_c with 2.0 MR.

   b. 301.8 lb_f-sec/lb_m at 2.36 MR to 314.7 lb_f-sec/lb_m at 1.63 MR at 100-psia P_c without an apparent maximum having been reached.

(U) 3. Variation of propellants temperature between 35 and 140°F had no apparent effect on engine operation or ballistic performance.

(U) 4. There was no apparent effect of chamber pressure on c* over the range from 80 to 125 percent of design chamber pressure.

(U) 5. Thrust coefficient increased in longer duration firings and in high chamber pressure tests, and the increase was attributed to nozzle extension contour changes from thermal and pressure loading effects.

(U) 6. The ablative combustion chamber design was adequately durable for operation at design chamber pressure, but the chamber ablative lining at the injector seal area could not dependably endure operation at 125 percent of design chamber pressure at altitude testing conditions.

(U) 7. Thrust vector variations during an engine test series with locked position covered a span of 0.44 deg and 0.15 in. in the pitch plane and 0.30 deg and 0.35 in. in the yaw plane.

(U) 8. Engine restart capability was demonstrated in the 118 firings made successfully in this testing at high and low chamber pressure, mixture ratio, and propellant temperatures.

(U) 9. Engine operation on either or both TCV banks had no apparent effect on engine ballistic performance.

(U) 10. Operations and durability of the pneumatically operated TCV and gimbal system were satisfactory.

(U) 11. The repeatability of start and shutdown transient impulse and minimum bit impulse was strongly affected by TCV timing. Fast TCV action reduced the variation in total impulse but increased the percentage of variation in total impulse.

(U) 12. Aside from localized deterioration in the injector seal area, chamber ablation had the appearance of being fairly uniform without any severe furrowing.

APPENDIX
SUMMARY OF TESTS

L-Period (L-55 through L-60)

(U) Objectives of this series were to determine rocket engine performance at various mixture ratios (O/F) and to prove endurance during extended steady-state operation. A temporary-type heat shield was installed for this test period. The explosive pulse charge was installed on the injector face for test L-55.

(U) Propulsion system operation was normal for these tests. Stability recovery from the explosive pulse was satisfactory. During test L-60, at 389 sec, the 1/4-in. fuel, high-point bleed line ruptured. At approximately 400 sec, the fuel storage tank level transducer line broke. These failures released fuel, causing the cell pressure to rise from 0.08 to 0.15 psia and a small, low-pressure fire which resulted in instrumentation cable damage. Post-test inspection revealed that the nozzle extension had sustained a small puncture of about 1/4 by 1-1/2 in. in size, believed to have been caused by the bursting fuel transducer line. The external surface of the combustion chamber had superficial charring in the vicinity of the broken fuel transducer line. The internal surface of the ablative combustion chamber had three excessive ablation streaks which extended from the injector face to the nozzle extension mounting flange. These streaks were in line with radial baffles of the injector. Separation of laminations of the ablative lining cloth material was revealed at the combustion chamber-nozzle extension flange. Three nozzle extension mounting bolt nuts were fused (because of localized high temperature at the flange) and had to be broken to remove the nozzle extension.

(U) Gimbal actuators were installed, but the engine was held in the null position for this series.

M-Period (M-61 through M-77)

(U) Test objectives were to perform simulated acceptance and pre-launch tests: document engine performance with gimbal tests at various mixture ratios (O/F), document engine TCV bank balance at high O/F mixture ratios, and perform gimbaling during extended operation at high mixture ratios (O/F).

(U) Heat shielding for nozzle extension thermal radiation was employed using the NAA flight-type segment and an AEDC temporary-type shield. The explosive pulse charge was installed on the injector face

for test M-61. Gimbaling was accomplished during tests M-61 through M-66 and M-77.

(U) Combustion stability recovery from the charge pulse was satisfactory. Propulsion system operation was normal, and all tests were conducted without incident, except for some deterioration of the AEDC heat shield. Post-test inspection revealed that the aluminum foil and fiber glass of the AEDC heat shield melted near the nozzle extension upper portion. The metal attachment flange (to the nozzle extension) melted on the NAA heat shield segment.

N-Period (N-78 through N-85)

(U) Test objectives were to determine engine performance and to make gimbaling operations during a simulated mission duty cycle with propellants and cell environment at high temperatures. The NAA heat shield segment and an AEDC temporary-type heat shield were used. The NAA heat shield flexible boot was suspended in position without being attached to the chamber-nozzle extension flange. The engine was gimbaled during all tests except test N-84.

(U) Propulsion system operation was normal, and all tests were conducted without incident. Post-test inspection revealed two scorched spots on the combustion chamber exterior immediately above the exit flange adjacent to the propellant line interfaces. Cracks were found on the injector face inside the center circular baffle in the weld that attaches the baffle to the injector face.

P-Period (P-86 through P-92)

(U) The objective of this series was to determine engine performance with the propellant and test cell environments at low temperatures and during engine gimbal operations. The explosive pulse charge was installed on the injector face for test P-86. The engine was gimbaled during all tests in this period.

(U) This was the first series in which a nitrogen-pressure-actuated TCV was used. The nozzle extension was installed with a small AGC heat shield attached to the combustion chamber-nozzle extension mounting flange to protect the flange from nozzle extension thermal radiation.

(U) Stability recovery from the charge pulse was satisfactory. Propulsion system operation was normal for all tests. The pneumatically actuated TCV functioned satisfactorily. Difficulties with instrumentation were caused by water condensation in the test cell from the cold test cell walls and propellant tanks.

Q-Period (Q-93 through Q-104)

(U) Test series objective was to evaluate engine performance at low and high combustion chamber pressures and engine durability during extended operation at high chamber pressure.

(U) The AEDC permanent-type heat shield was used for this series. The engine was gimbaled during all tests of 10 sec or longer duration.

(U) This test period was terminated by combustion chamber failure during test Q-104 after 191 sec of the planned 500-sec test at 125 percent of design chamber pressure. The failure was judged to have been caused by a poor structural bond between the ablative combustion chamber and the metal injector mounting flange.

(U) During post-test inspection, the torque on all injector mounting bolts was found to be substandard.

R-Period (R-105 through R-119) and S-Period (S-120 through S-123)

(U) The test objectives for these two test periods were to evaluate engine performance at low and high chamber pressures and to prove engine durability. An explosive pulse charge was installed for test R-105. Combustion stability recovery was satisfactory. The engine was gimbaled during tests R-112, R-113, S-122, and S-123. The AEDC permanent-type heat shield was used for these two test periods.

(U) Combustion stability recovery from the charge pulse was satisfactory. Propulsion system operation was normal until test S-123. Test S-123 was terminated after about 118 sec of a scheduled 500-sec test because of a failure at the structural bond joint of the chamber fiber glass material and the metal injector mounting flange.

T-Period (T-124 through T-132)

(U) Test objectives were to obtain combustion chamber and injector temperature data and engine performance using a new design combustion chamber (described in Section 2.2.3). The injector had an improved design weld joint on the inside base of the central circular baffle. An explosive pulse charge was installed on the injector face for test T-124. The AEDC permanent-type heat shield with black Teflon facing was used for this test. The engine was gimbaled during tests T-124 through T-129.

(U) Combustion stability recovery from the charge pulse was satisfactory. Rocket engine operation was normal.

U-Period (U-133 through U-137)

(U) This testing was a continuation of the engine test series started in the T-period. The engine was gimbaled during tests U-135, U-136, and U-137.

(U) Engine operation was satisfactory, except that the final planned 60-sec firing was terminated 5 sec early because injector/chamber flange temperatures exceeded the AGC-established limit of 400°F. Post-test examination of the combustion chamber revealed deterioration of the ablative material in the injector interface area.

V-Period (V-138 through V-141)

(U) Test objectives were to obtain combustion chamber and injector temperature data and to prove chamber durability during high and low chamber pressure operation as required for engine qualification testing. An explosive pulse charge was installed on the injector for test V-138. The combustion chamber was the modified design as tested in the T and U periods with the addition of the ablative lining anchor pins. The engine was gimbaled during all V tests.

(U) Combustion stability recovery from the charge pulse was satisfactory. Test V-138 was terminated at about 7 sec, instead of the planned 15 sec, because an instrumentation malfunction erroneously indicated unsatisfactory facility performance. Engine operation and performance were satisfactory. Post-test inspection of the combustion chamber in the test cell (with the nozzle extension removed) indicated satisfactory condition for test series continuation.

W-Period (W-142 through W-144)

(U) This testing was a continuation of the engine series started with the V period. The engine was gimbaled during tests W-143 and W-144.

(U) The test was terminated during W-144 when the injector/chamber flange temperatures exceeded the AGC-established limit of 400°F. The engine had been fired seven times with a total time of about 500 sec, of which about 278 sec were at 125-psia chamber pressure.

(U) Post-test inspections revealed inadequate durability of the chamber ablative lining and seal at the injector end; the ablative material anchor pins were not sufficiently effective to improve durability significantly where they were used. Deterioration of the ablative chamber also resulted in flame-erosion damage of the injector.

REFERENCES

1. Schulz, G. H. and DeFord, J. F. (U) "Simulated Altitude Testing of the Apollo Service Module Propulsion System (Report I, Phase II Development Test)." AEDC-TR-65-233, January 1966. (Confidential)

2. North American Aviation, Inc., Space and Information Systems Division. Procurement Specification MC90A. (U) "Apollo Spacecraft Service Module Propulsion System Rocket Engine." November 15, 1962, Revised March 8, 1963. (Confidential)

3. Test Facilities Handbook (5th Edition). "Rocket Test Facility, Vol. 2." Arnold Engineering Development Center, July 1963.

4. Robinson, C. E. and Runyan, R. B. "Thrust Vector Determination for the Apollo Service Propulsion Engine using a Six-Component Force Balance." AEDC-TR-65-250 (AD475564), December 1965.

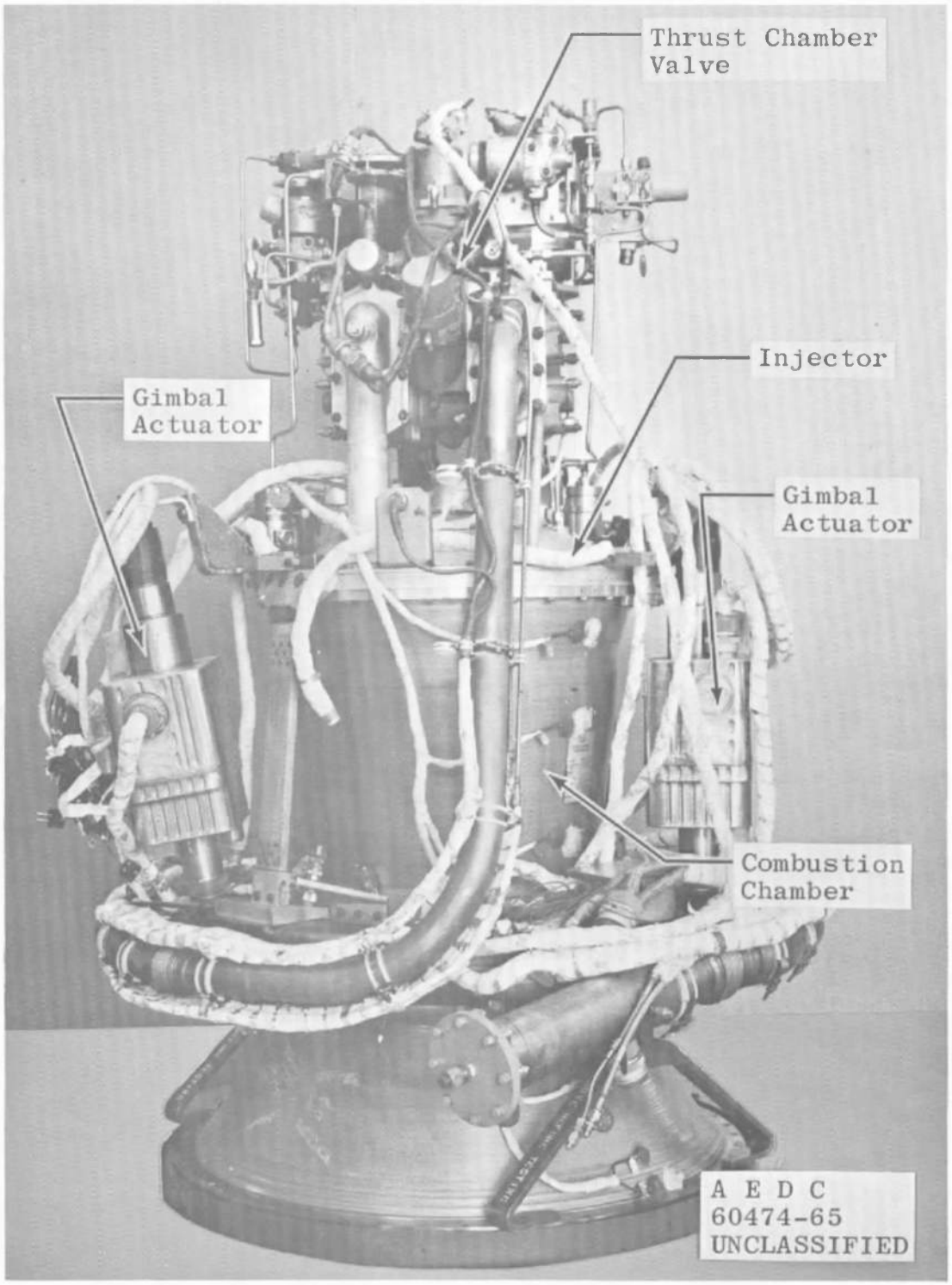

Fig. 1 AJ10-137 Rocket Engine without Nozzle Extension

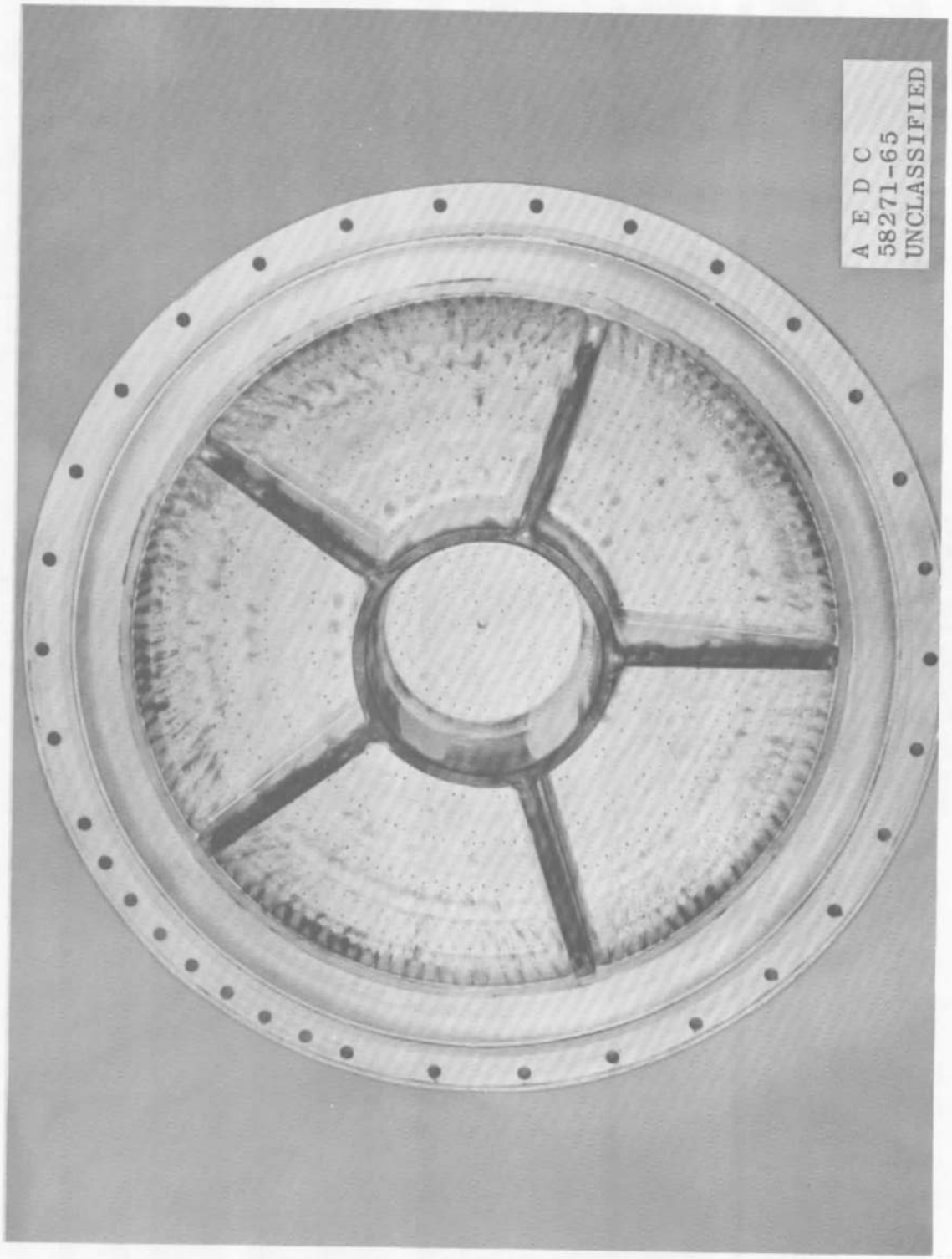

Fig. 2 Baffled Injector Configuration

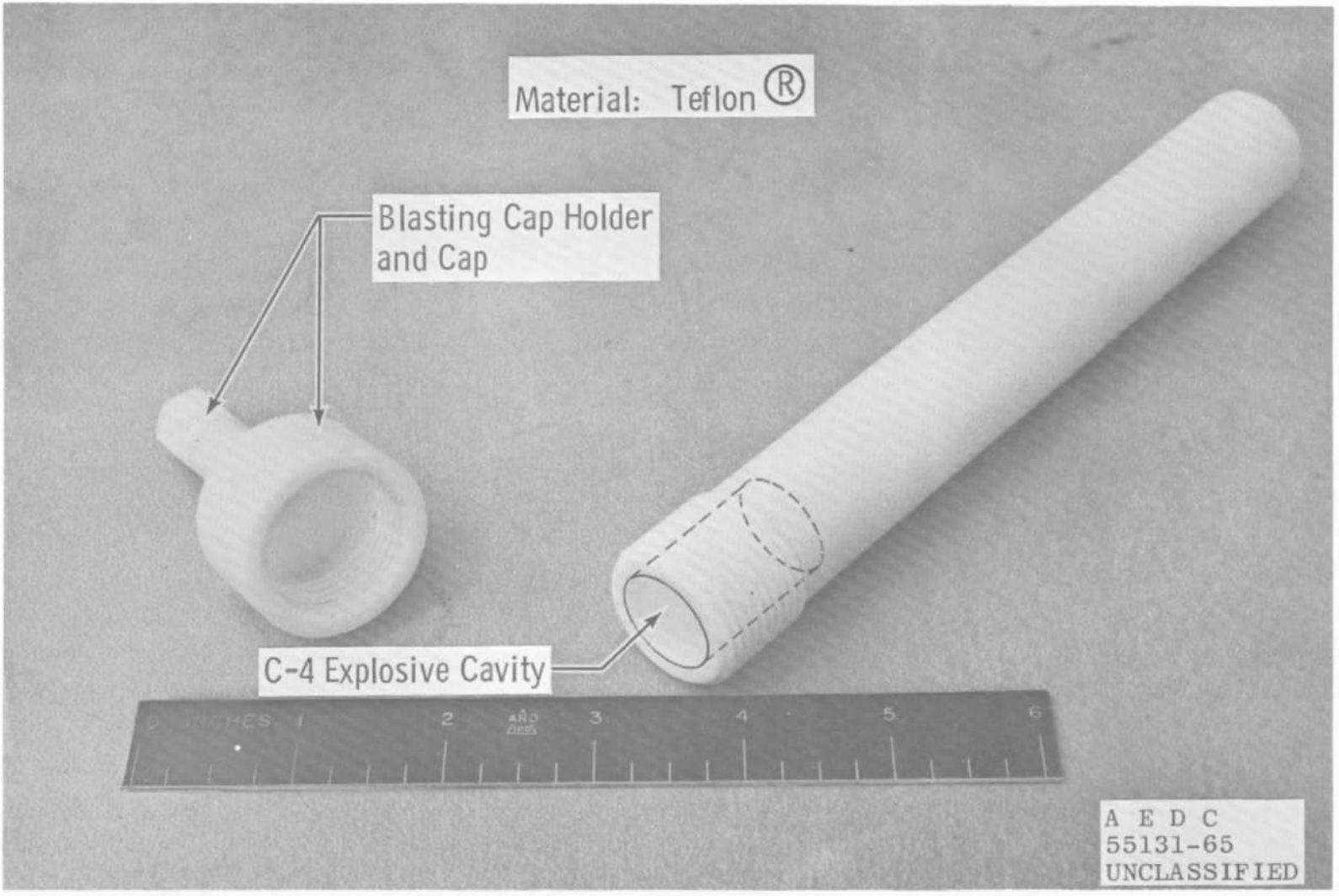

a. Holder Disassembled

Fig. 3 Pulse Charge Container

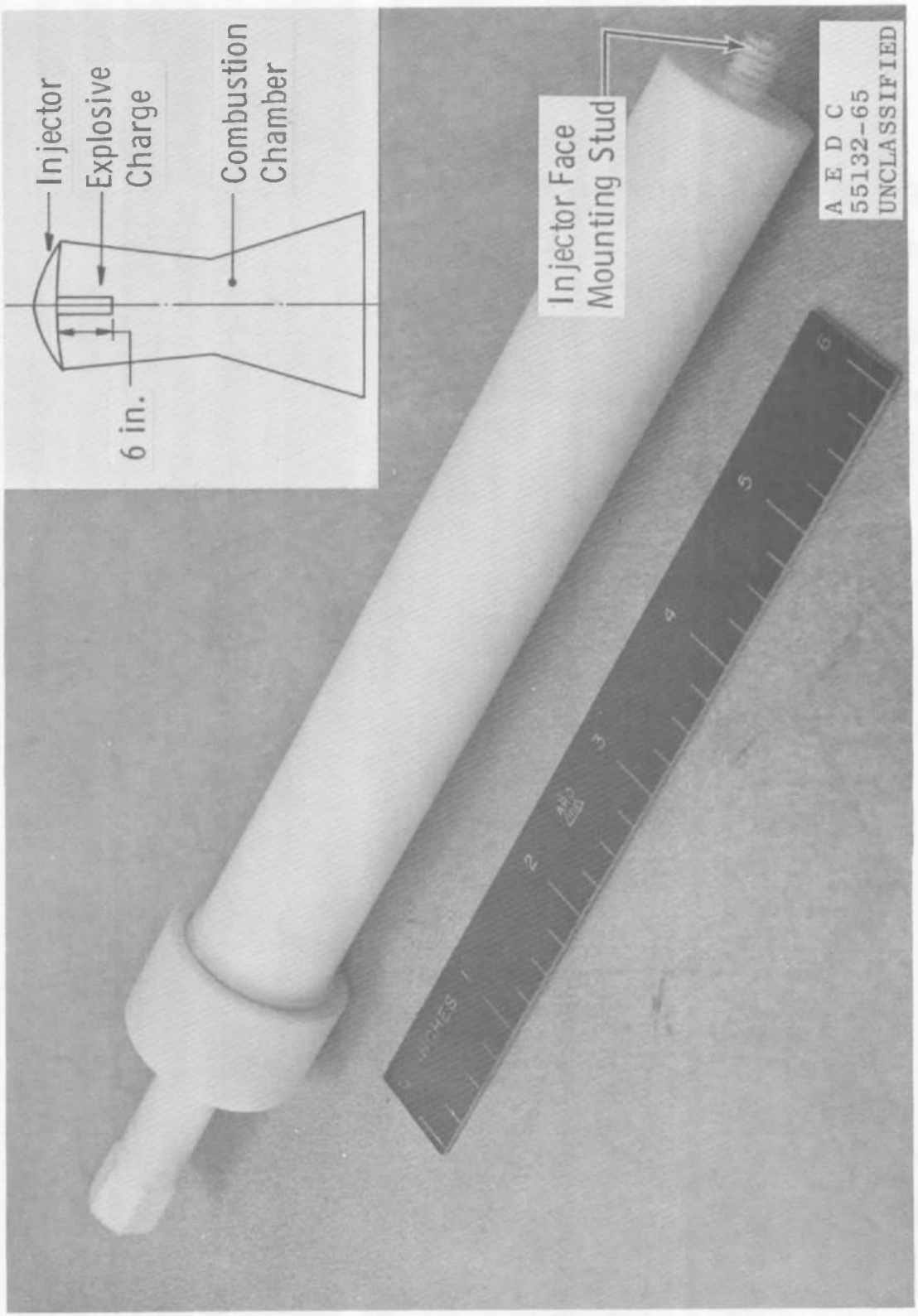

b. Holder Assembled

Fig. 3 Concluded

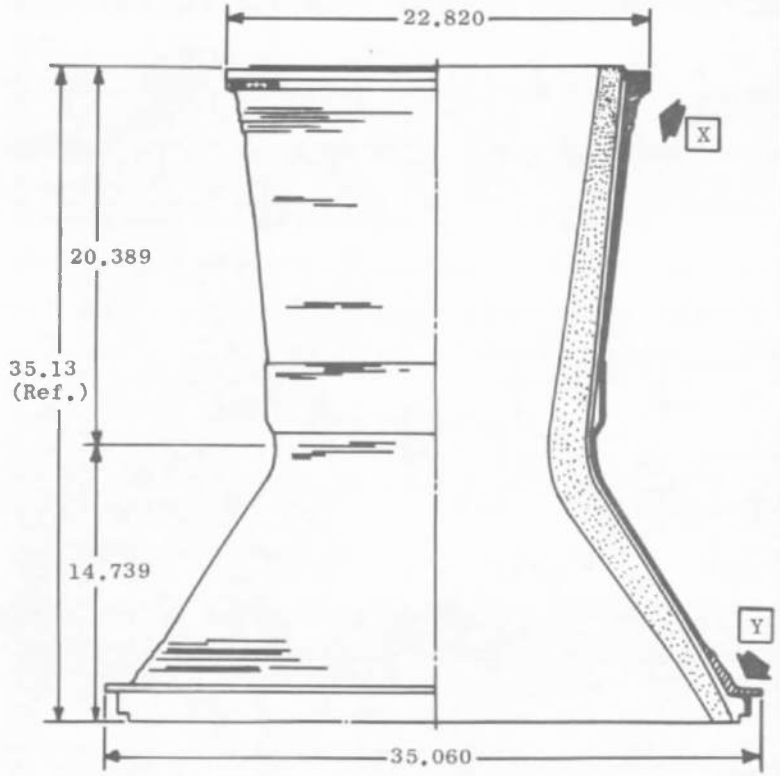

All Dimensions in Inches

a. Dimensions and Details

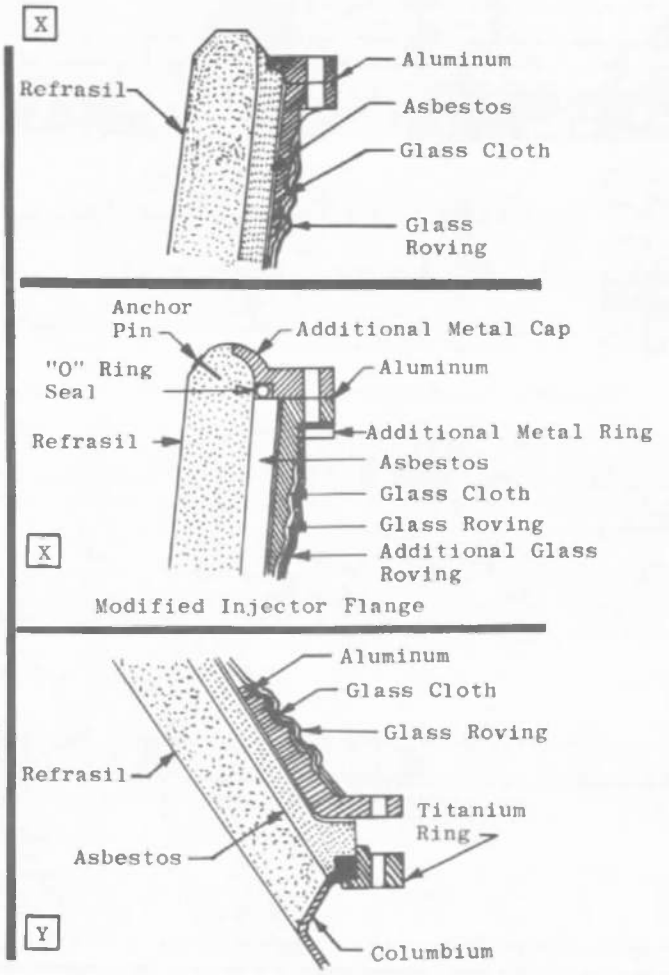

Fig. 4 AJ10-137 Ablative Thrust Chamber

UNCLASSIFIED

UNCLASSIFIED

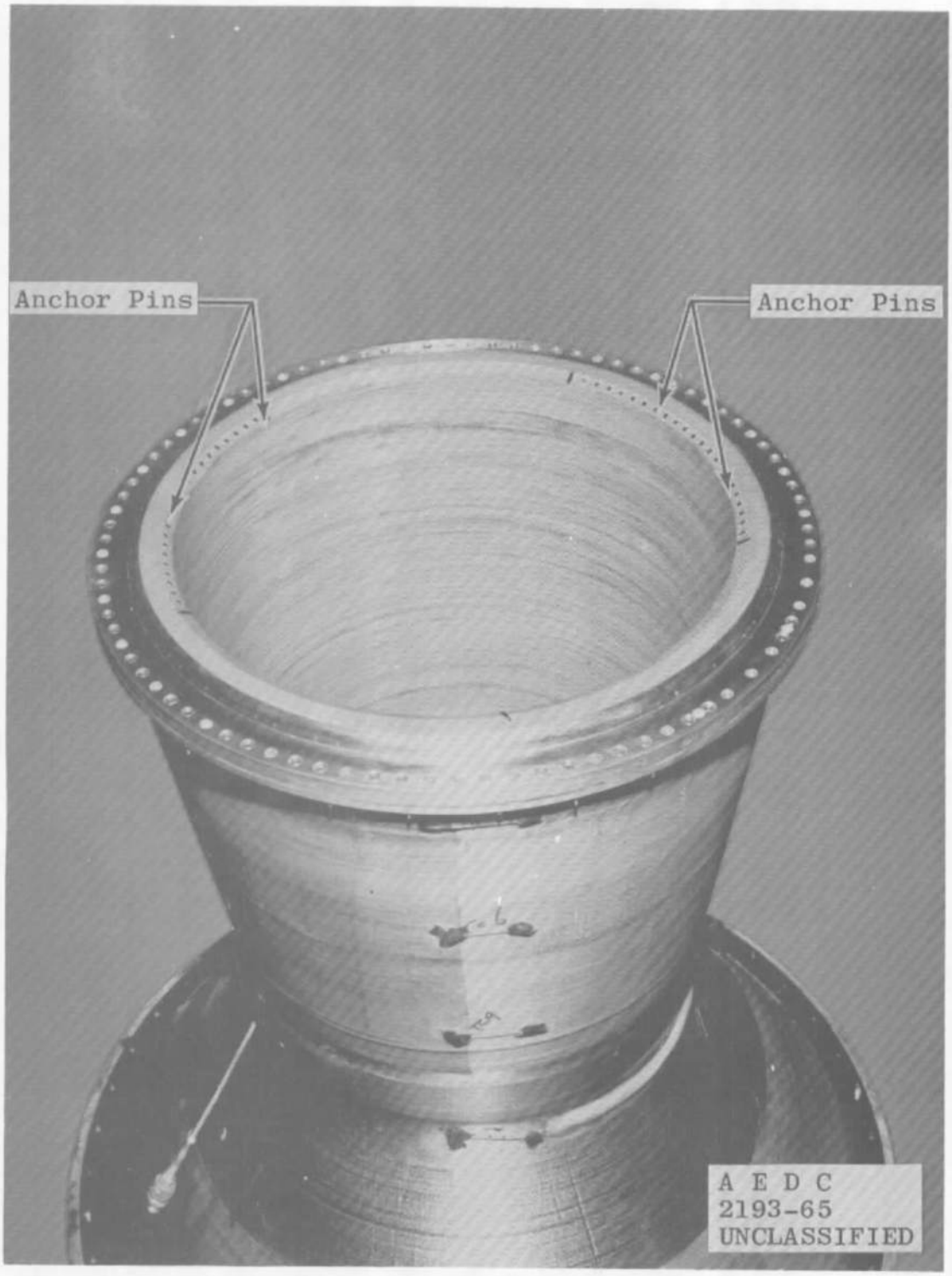

b. Engine S/N 11D, Chamber Modifications

Fig. 4 Concluded

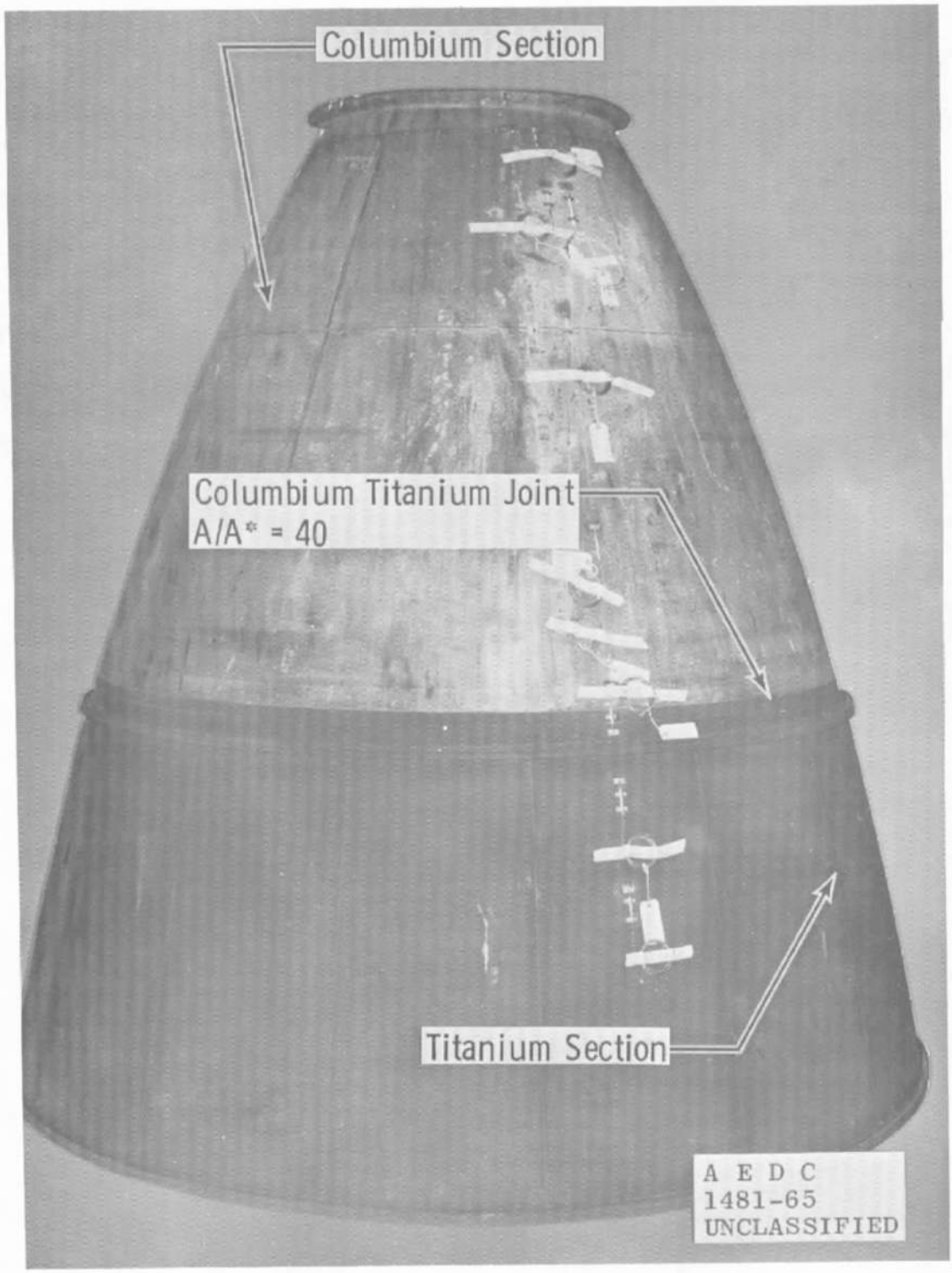

Fig. 5 Exit Nozzle Extension

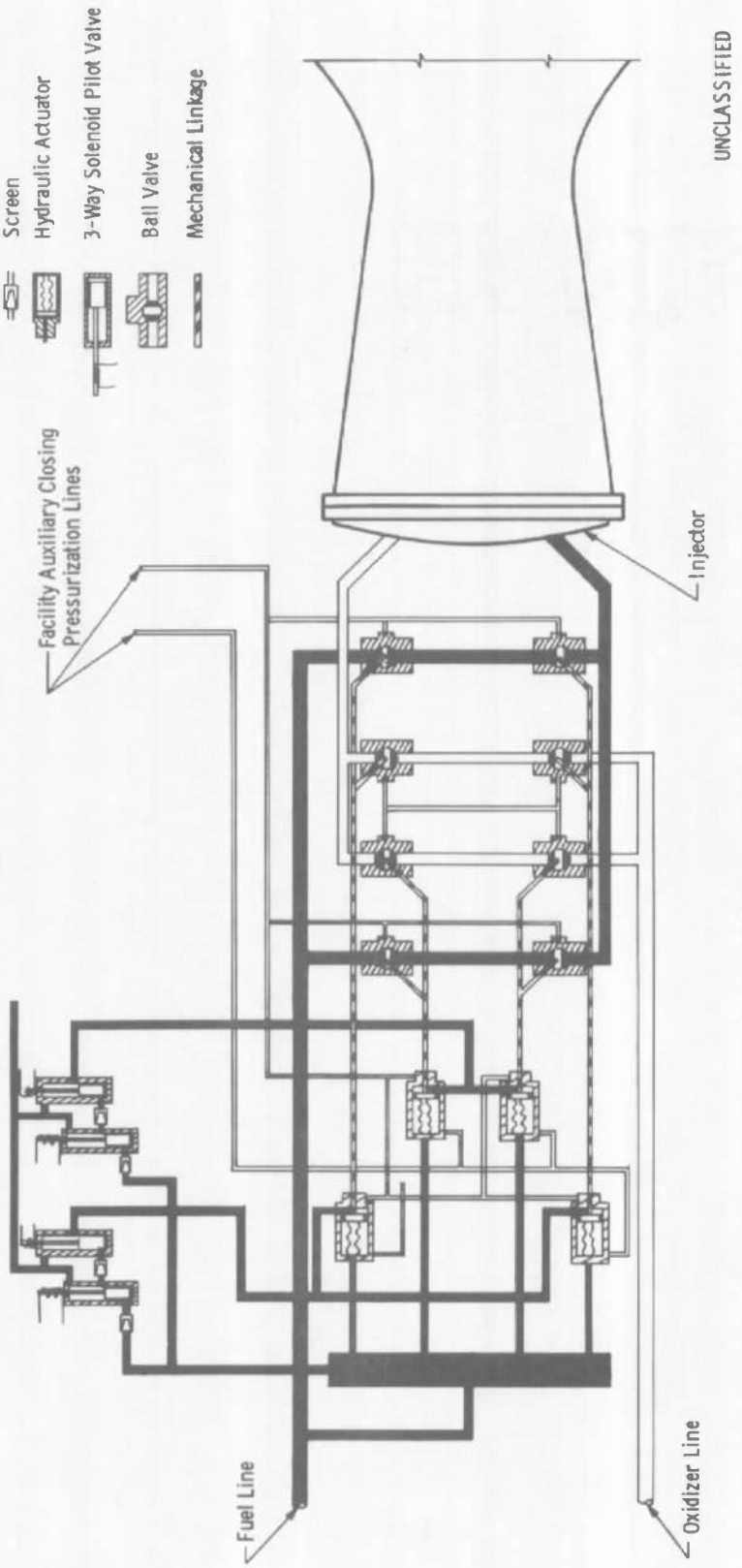

a. Fuel-Pressure Actuated Configuration

Fig. 6 Schematic Diagram of Apollo Thrust Chamber Valves

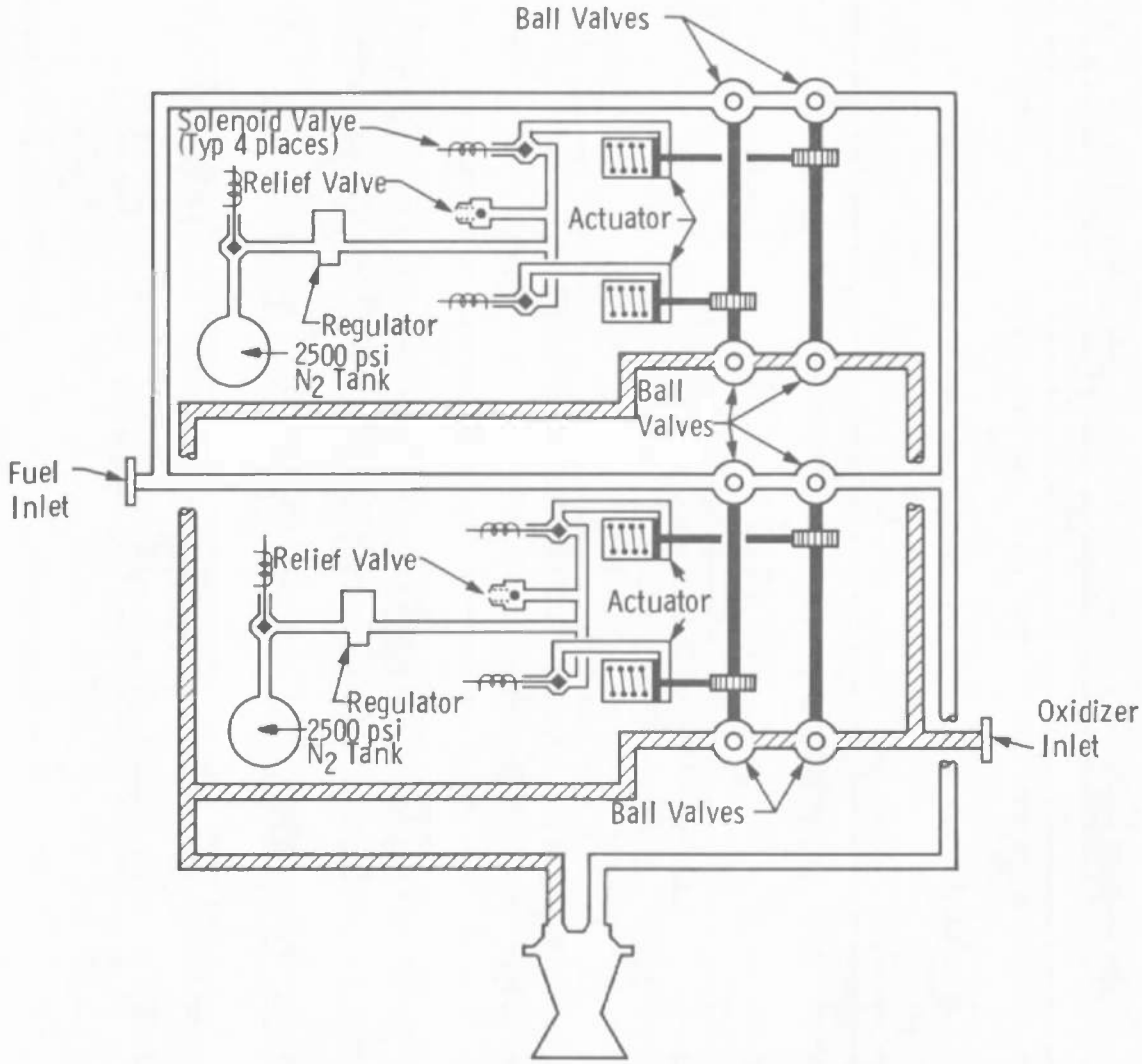

b. Pneumatic-Pressure Actuated Configuration UNCLASSIFIED

Fig. 6 Concluded

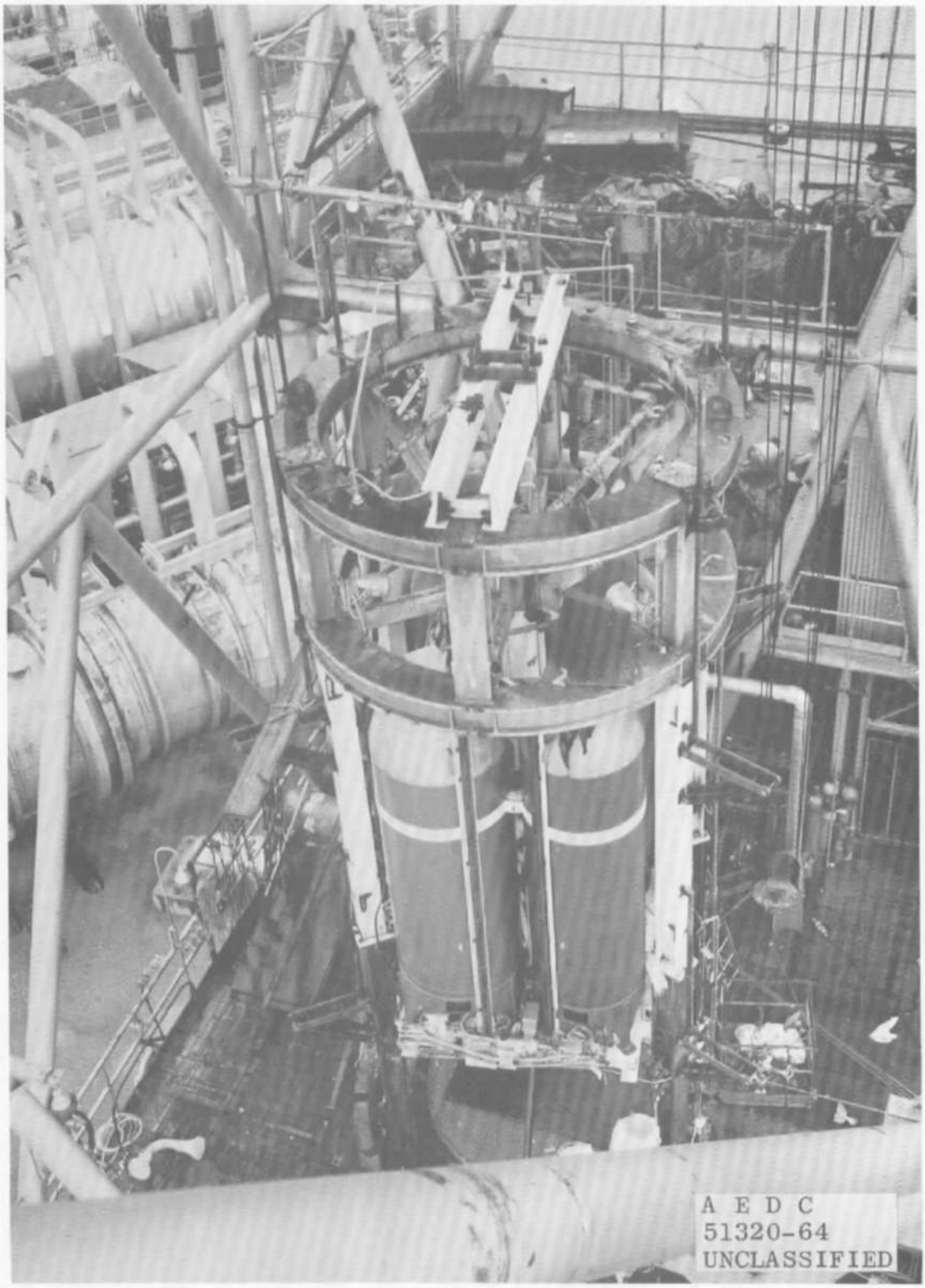

Fig. 7 F-3 Fixture Cell Installation

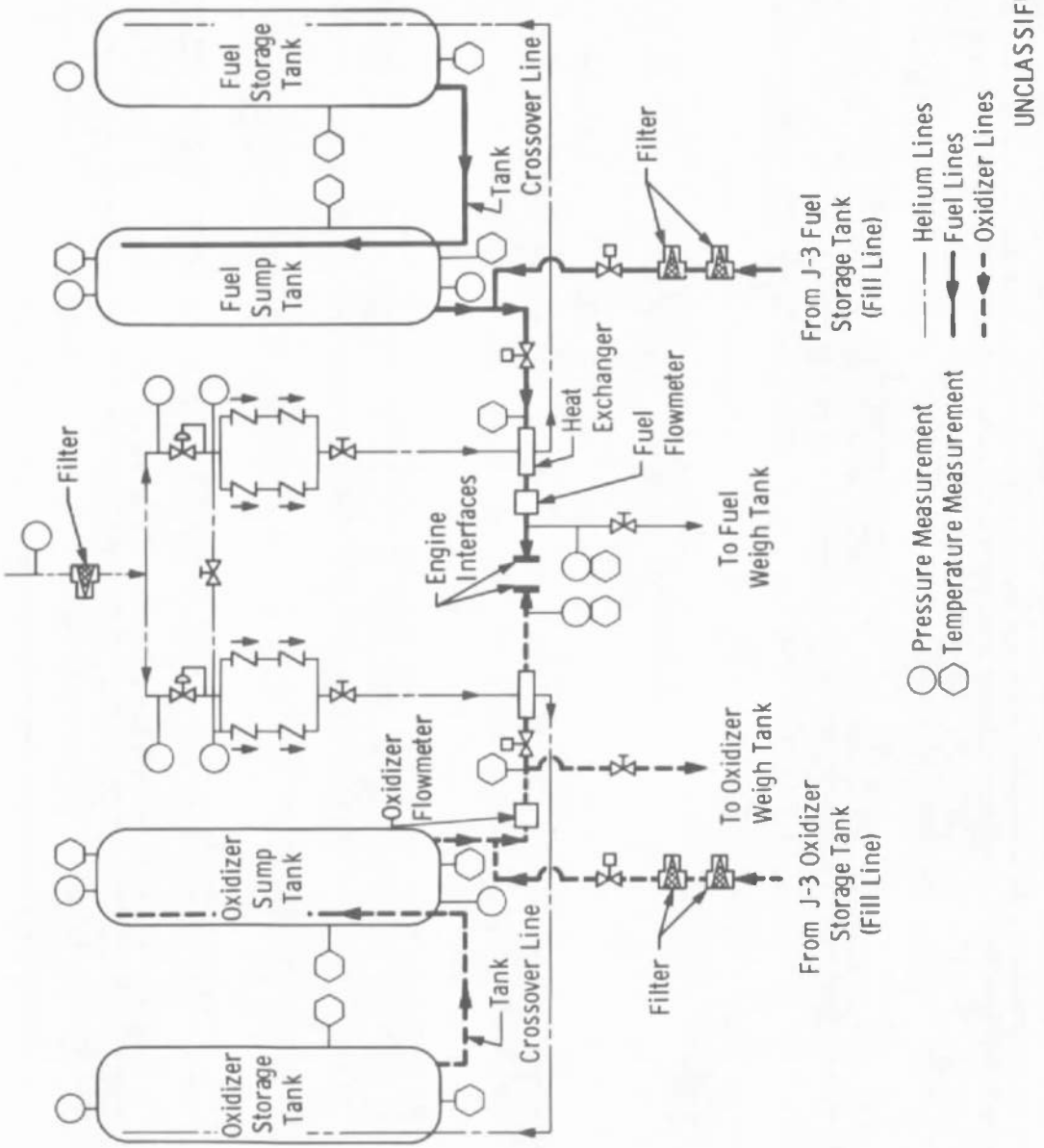

Fig. 8 NAA F-3 Fixture System Schematic

a. NAA Flight-Type Shield Segment

Fig. 9 Heat Shield Configurations

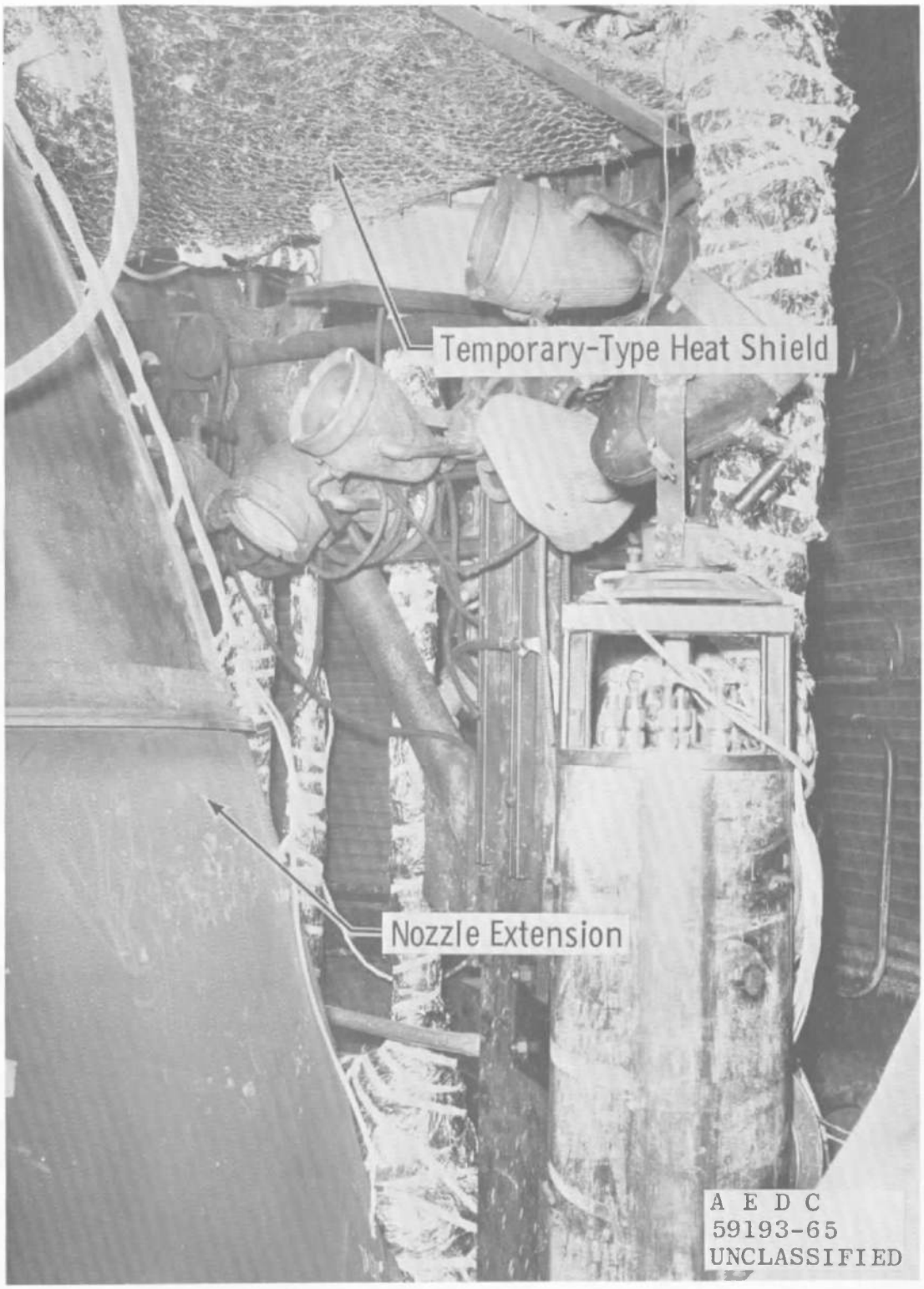

b. Temporary-Type Shield

Fig. 9 Continued

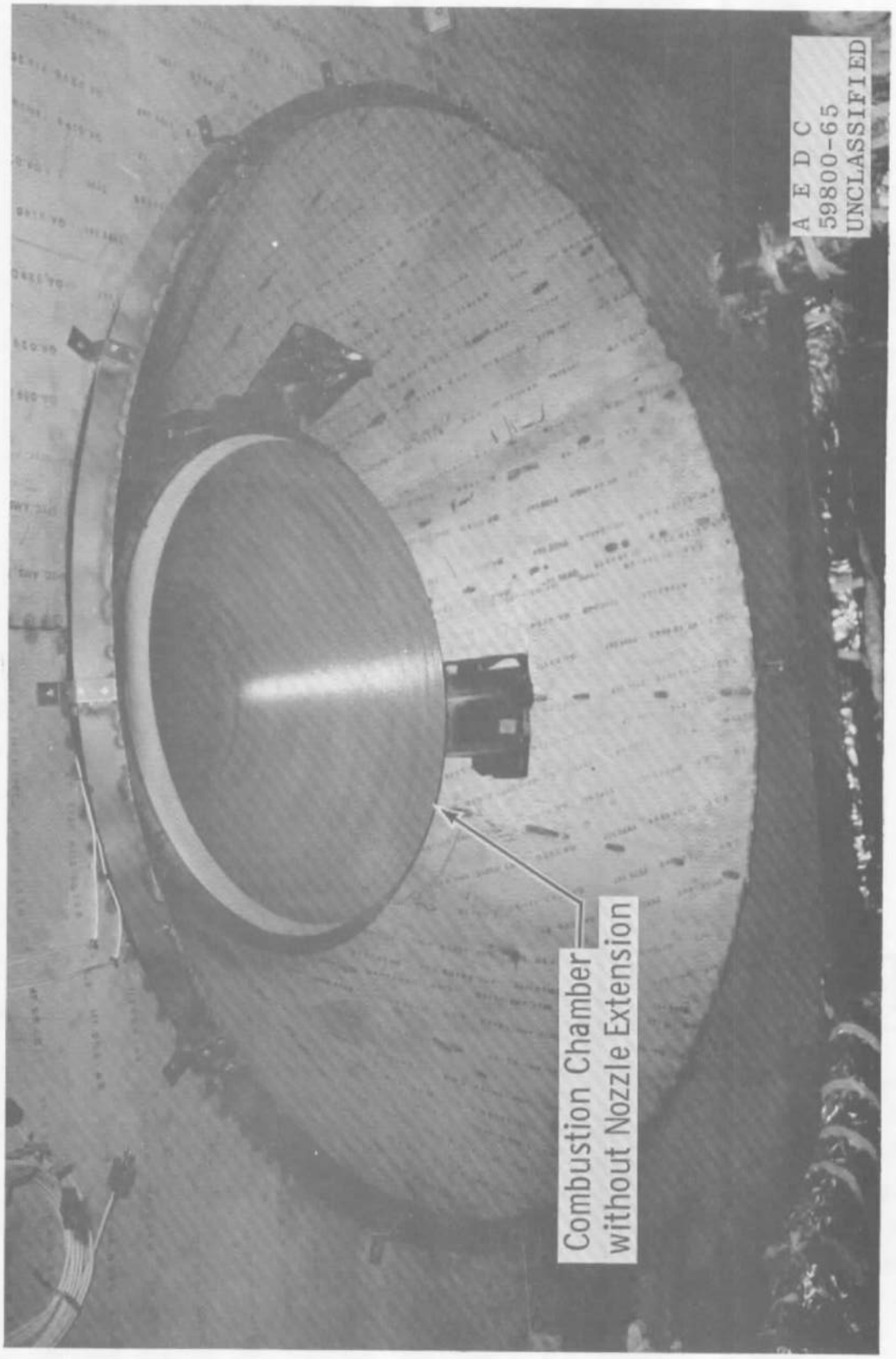

c. Permanent-Type Shield

Fig. 9 (Concluded)

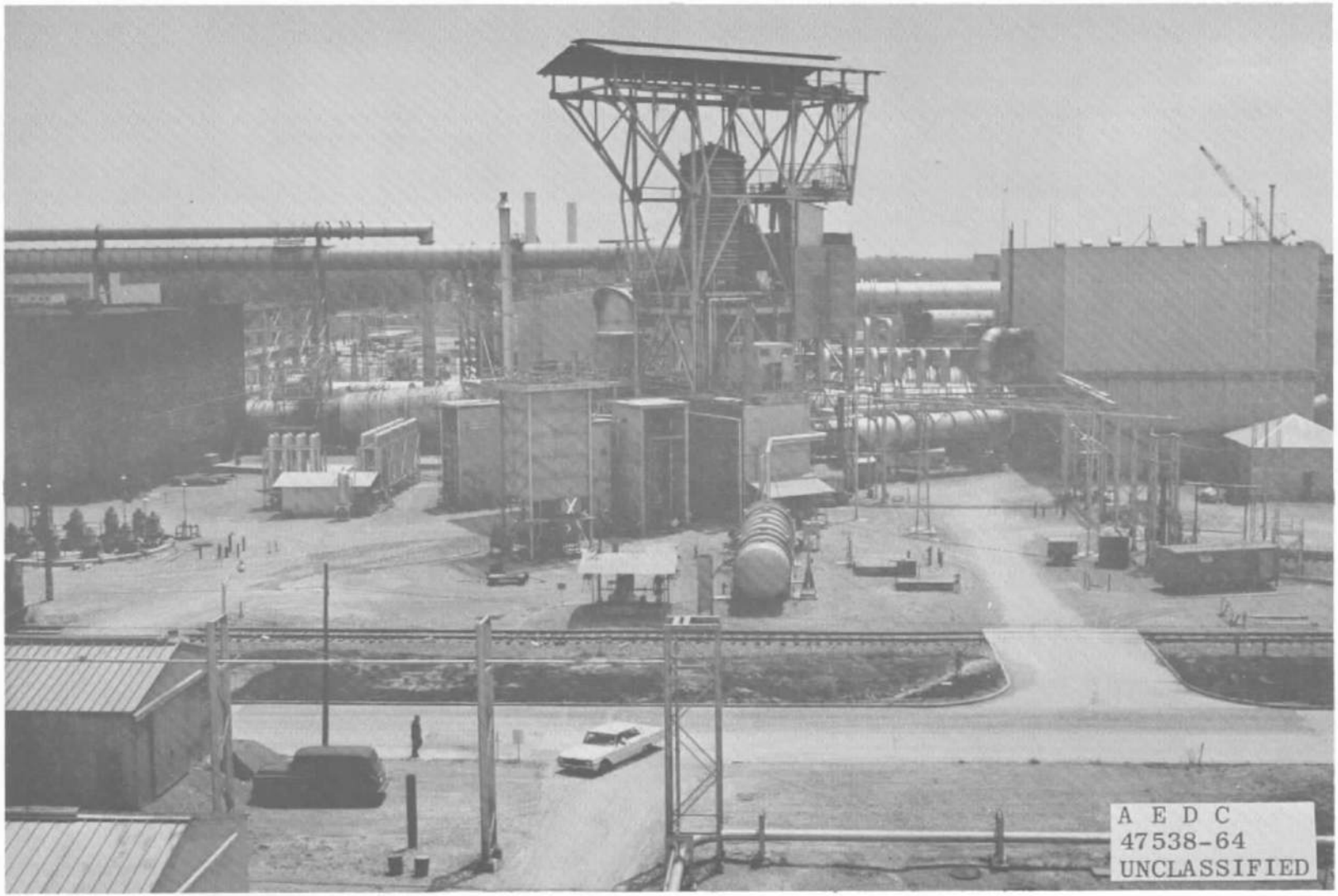

a. J-3 Complex

Fig. 10 Propulsion Engine Test Cell (J-3)

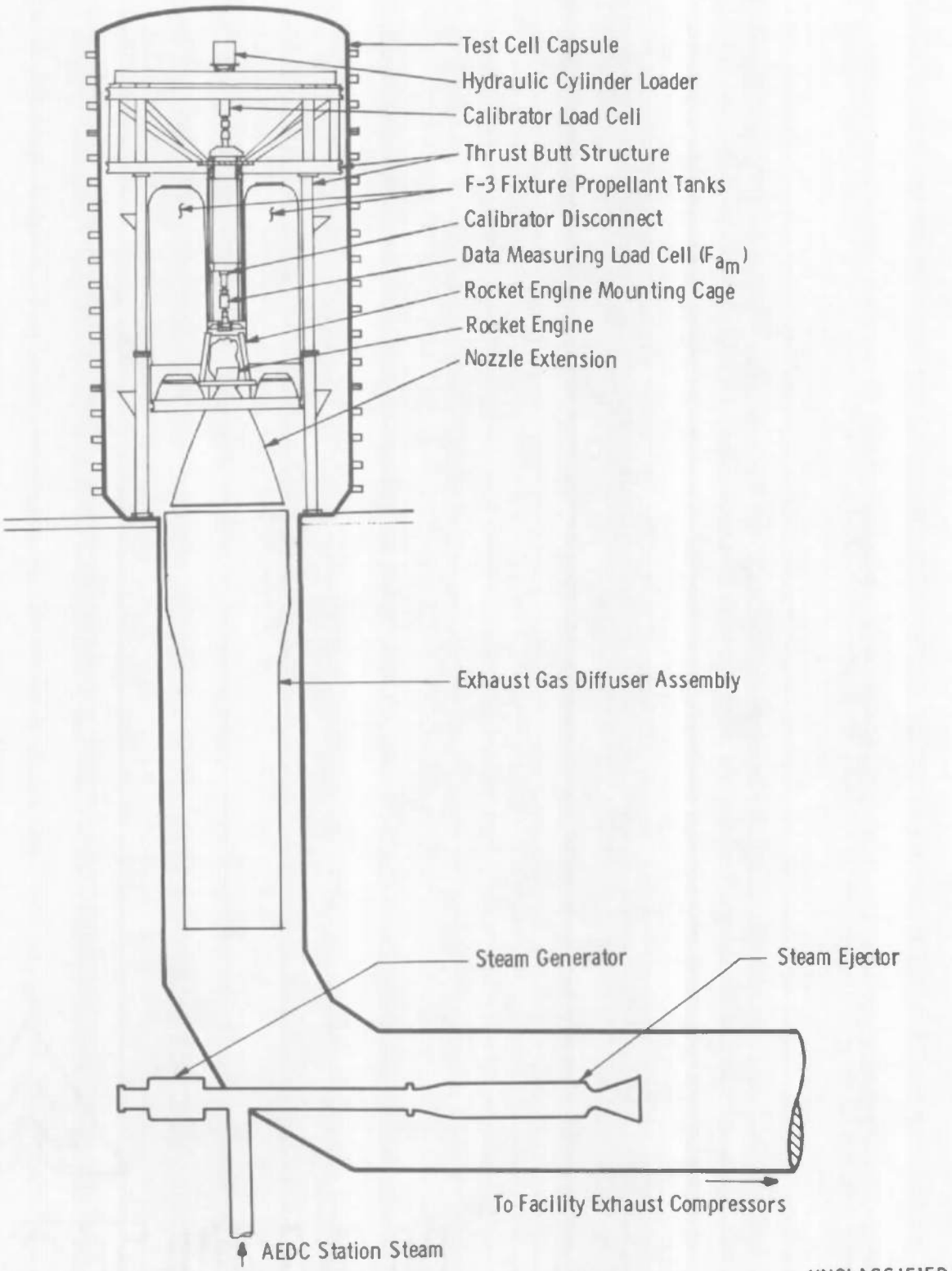

b. Side View, Test Article Installation

Fig. 10 Concluded

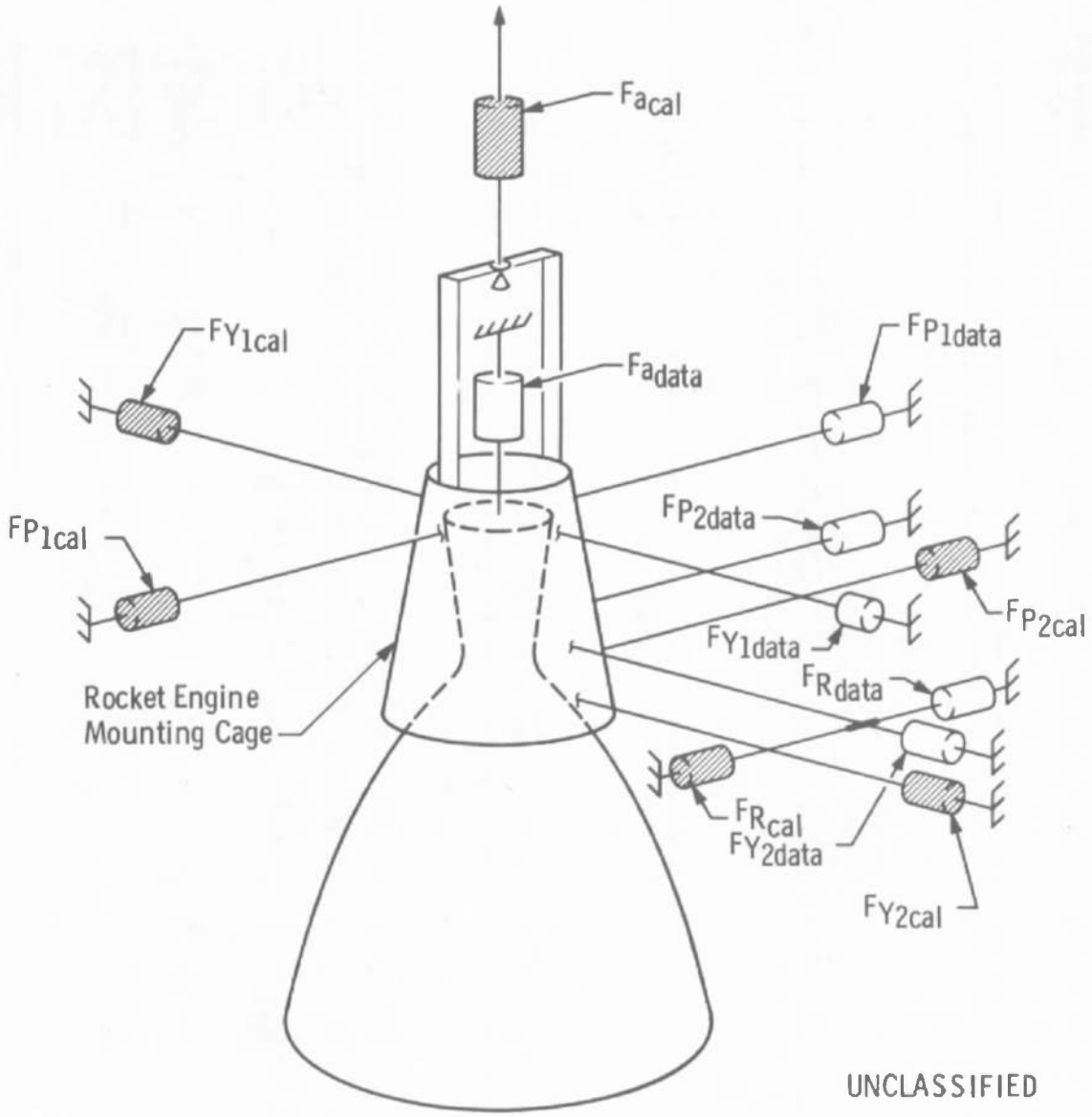

Fig. 11 Schematic of Six-Component Thrust System

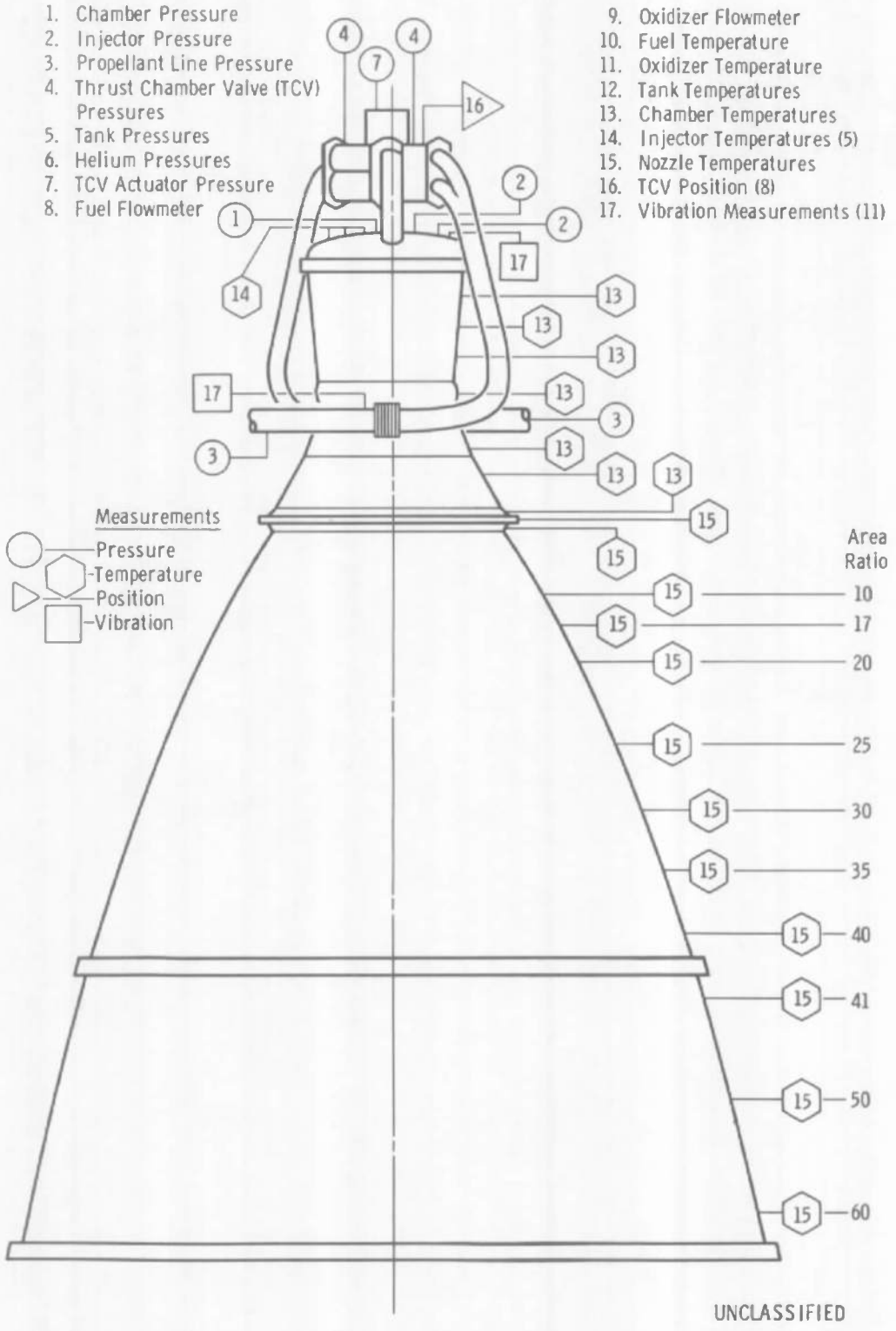

Fig. 12 Engine and Nozzle Extension Instrumentation Locations

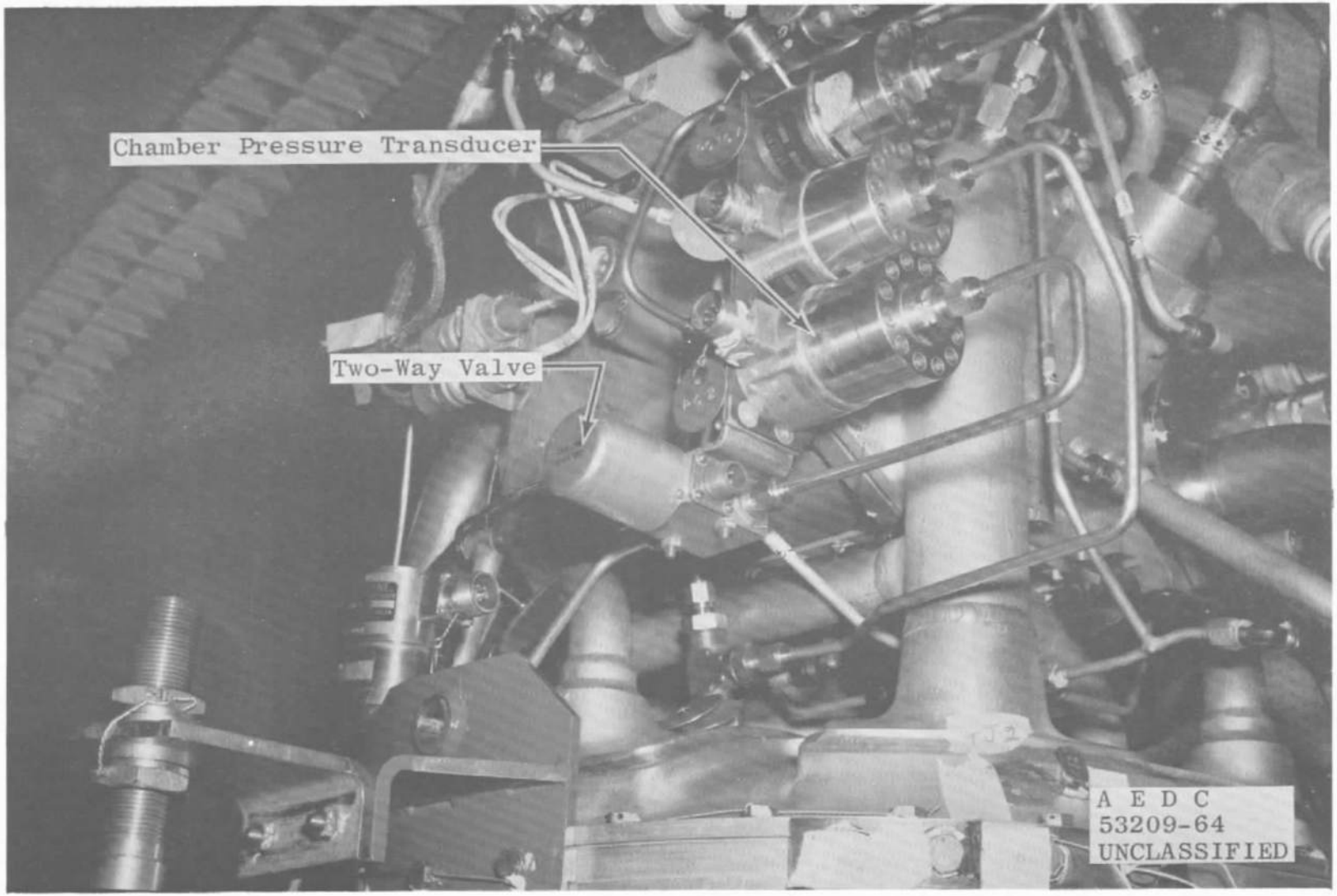

a. Chamber Pressure Transducer (In-Place Calibrated)

Fig. 13 Engine Instrumentation

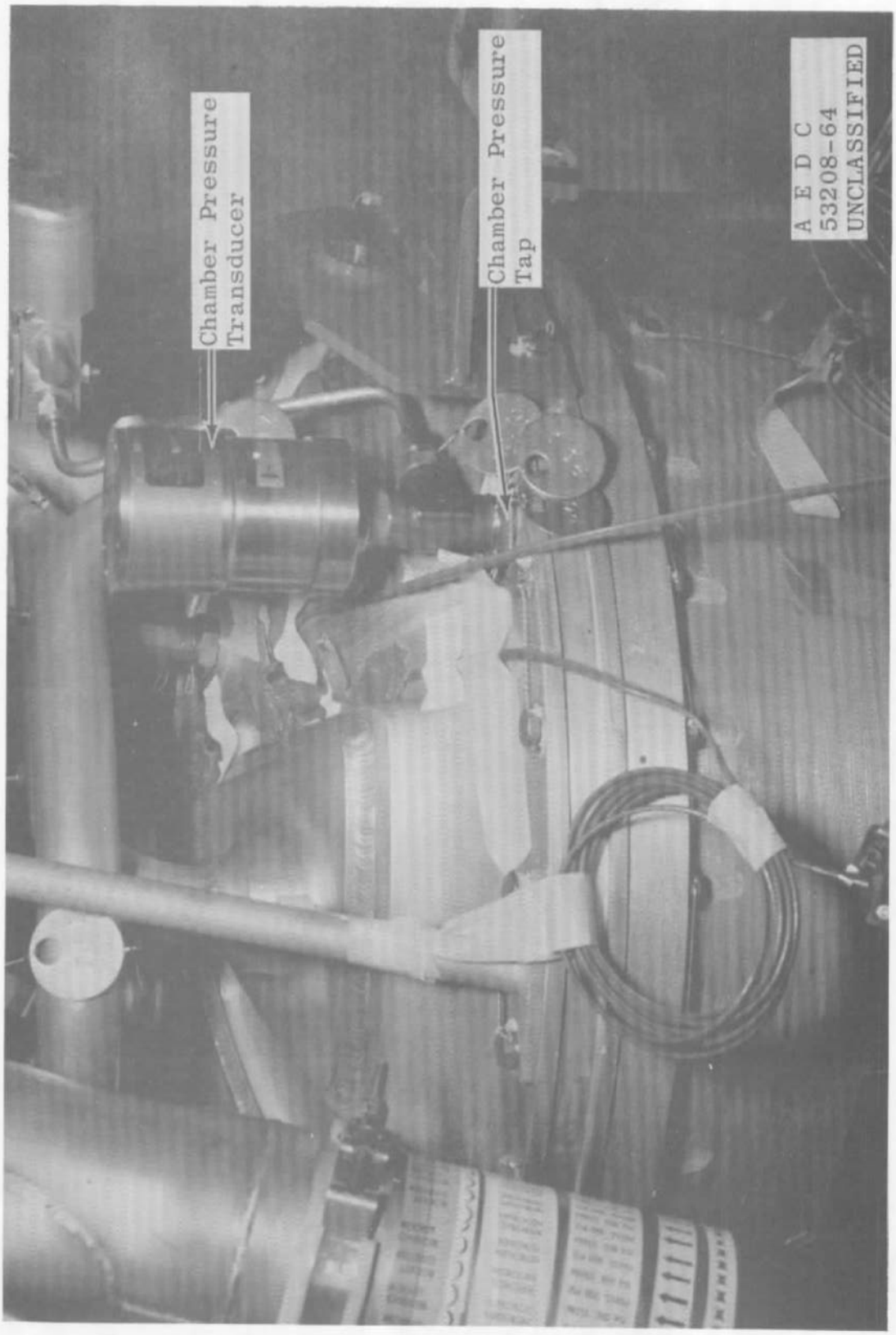

b. Chamber Pressure Transducer (Close-Coupled)

Fig. 13 (Concluded)

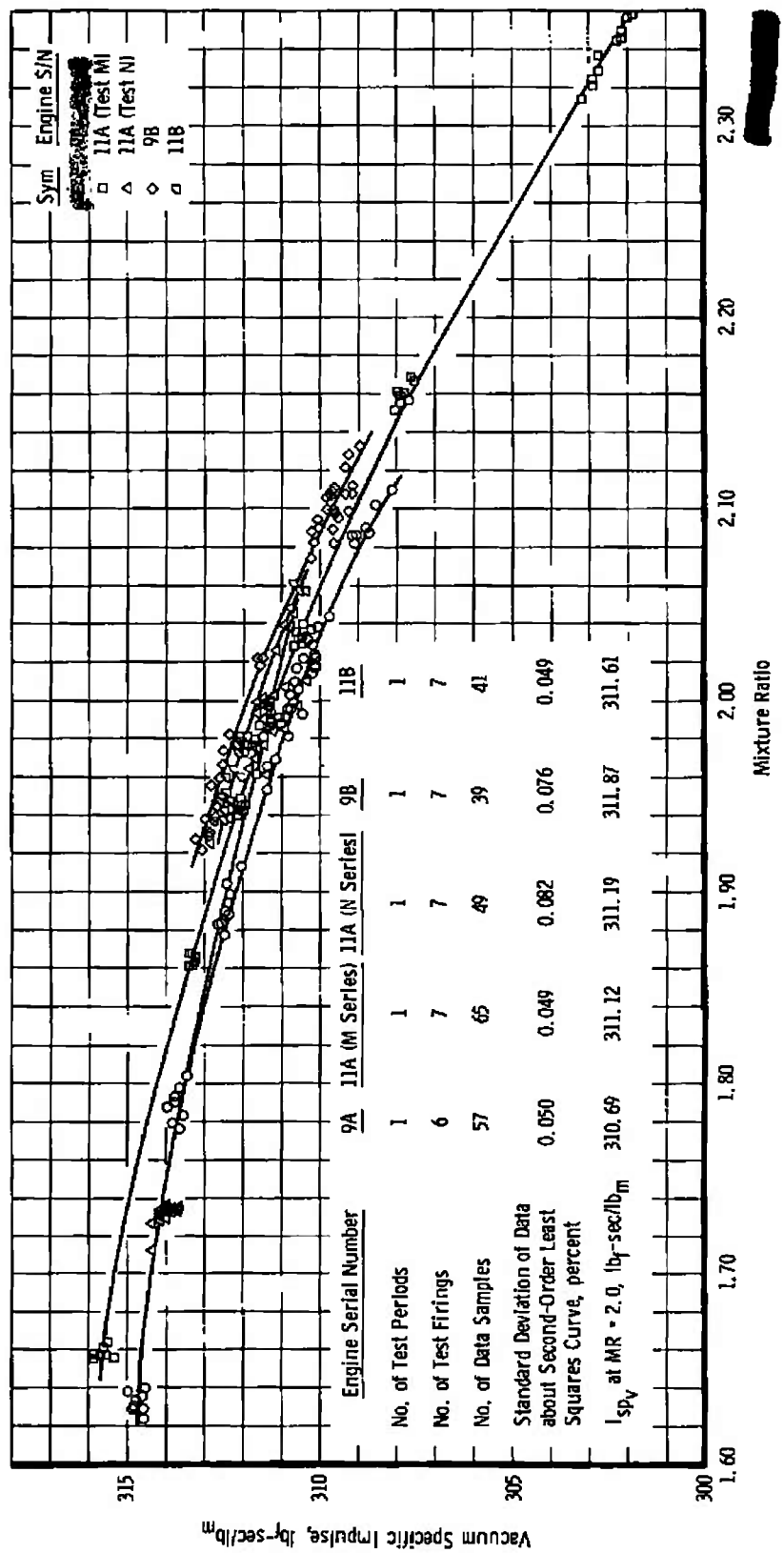

Fig. 14 Engine Performance at Design Chamber Pressure

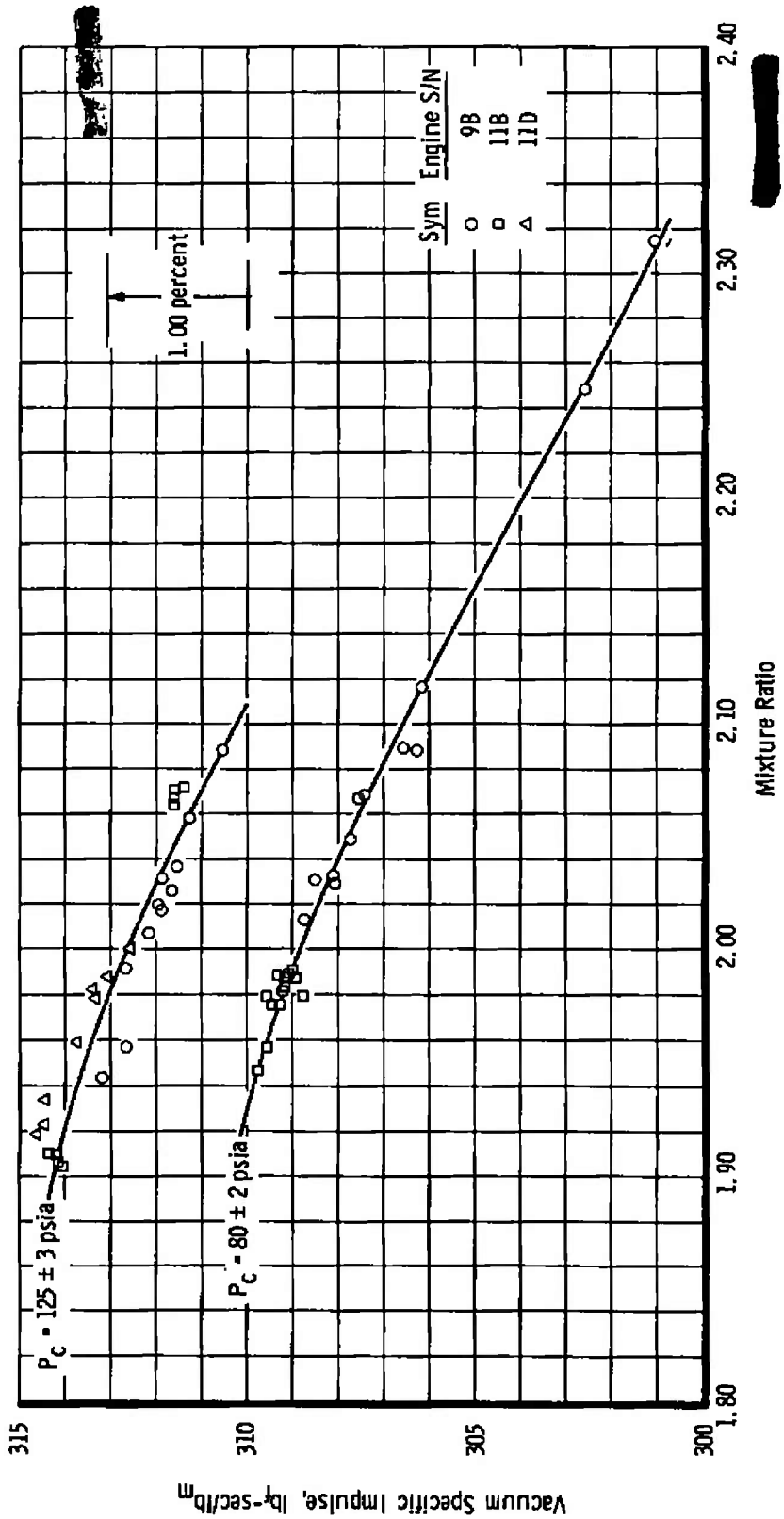

Fig. 15 Engine Performance at Off-Design Chamber Pressures

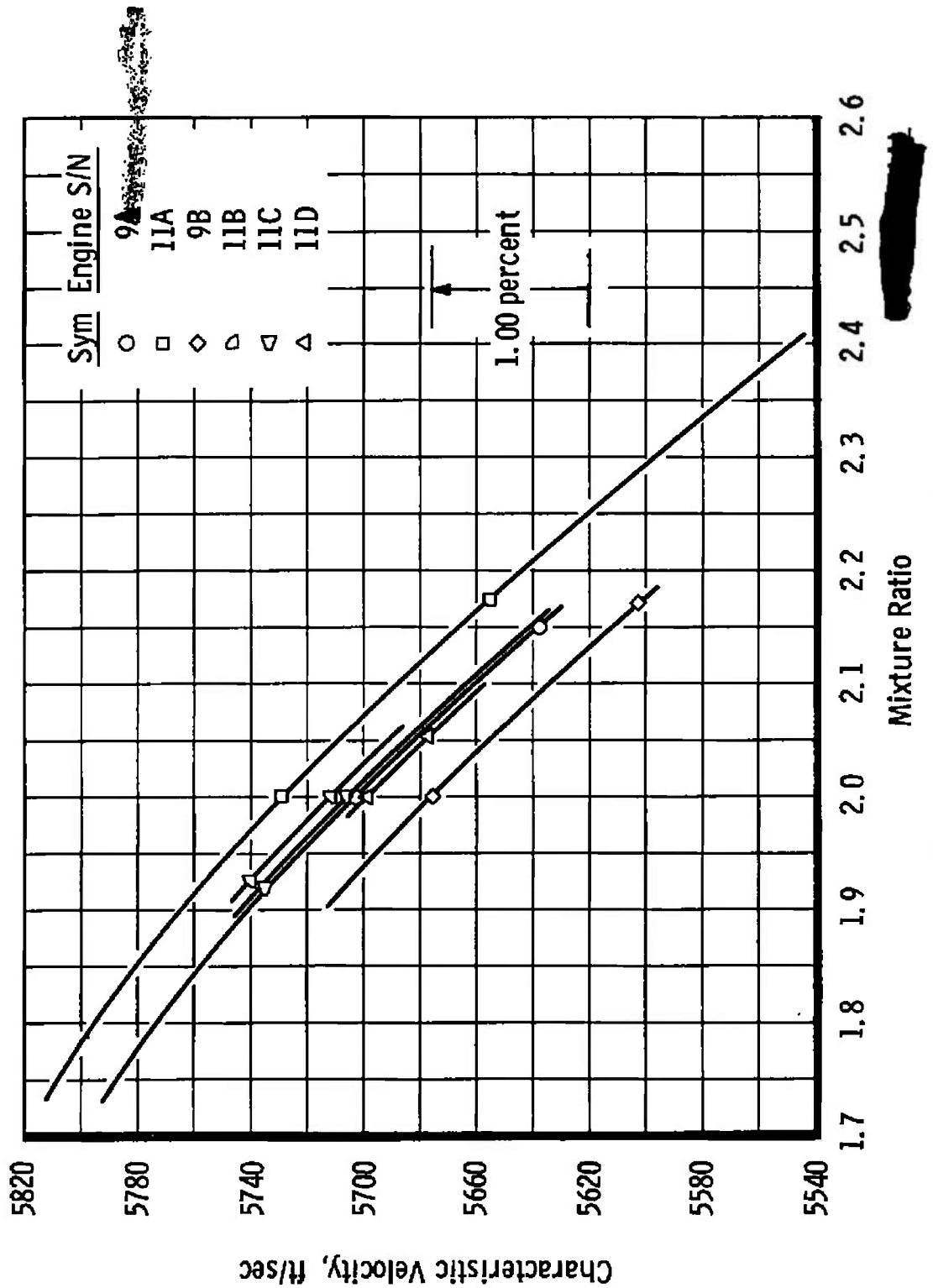

Fig. 16 Characteristic Velocity–Mixture Ratio Relation

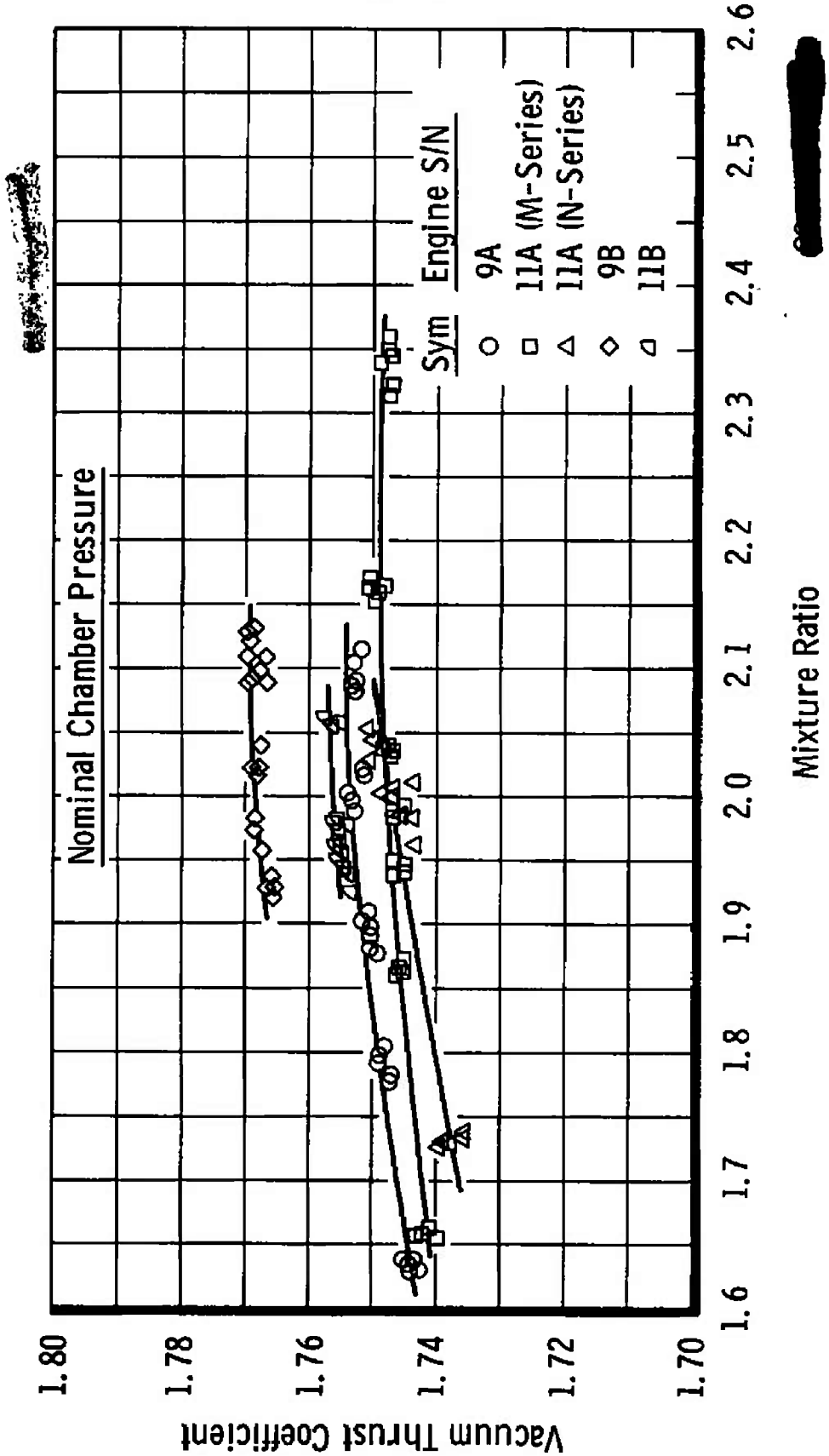

Fig. 17 Nozzle Performance at Design Chamber Pressure

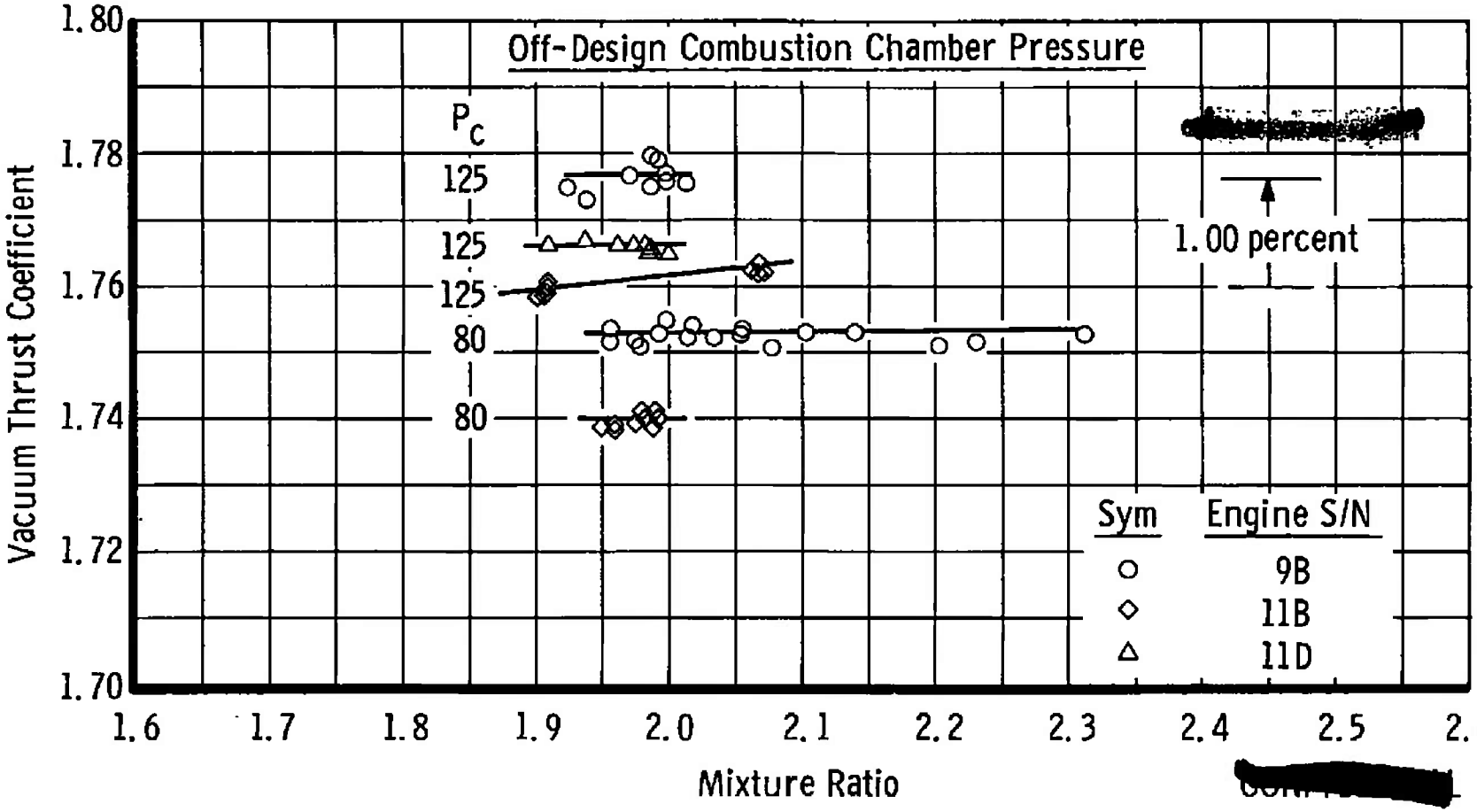

Fig. 18 Nozzle Performance at Off-Design Chamber Pressure

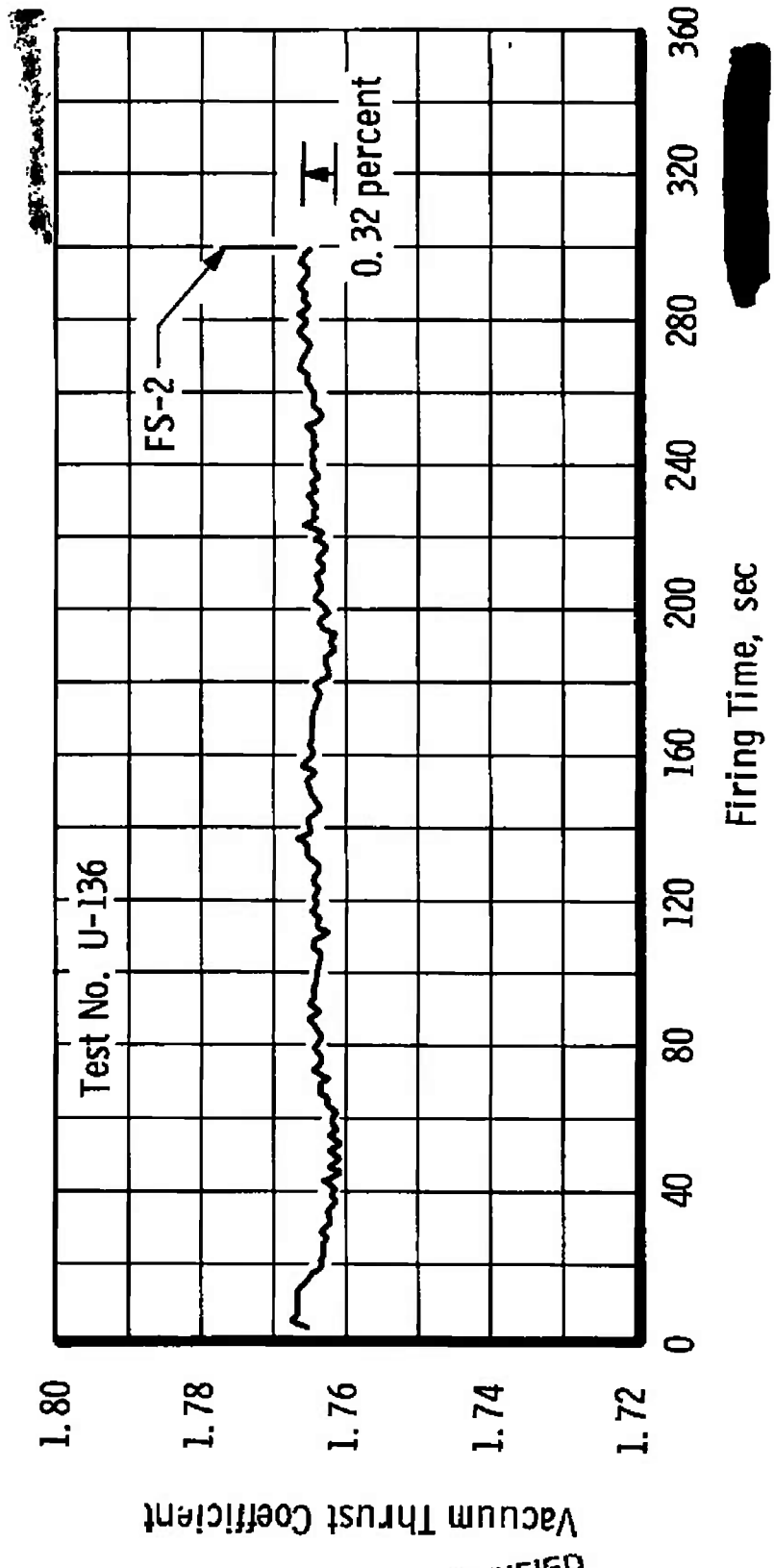

Fig. 19 Vacuum Thrust Coefficient-Time History

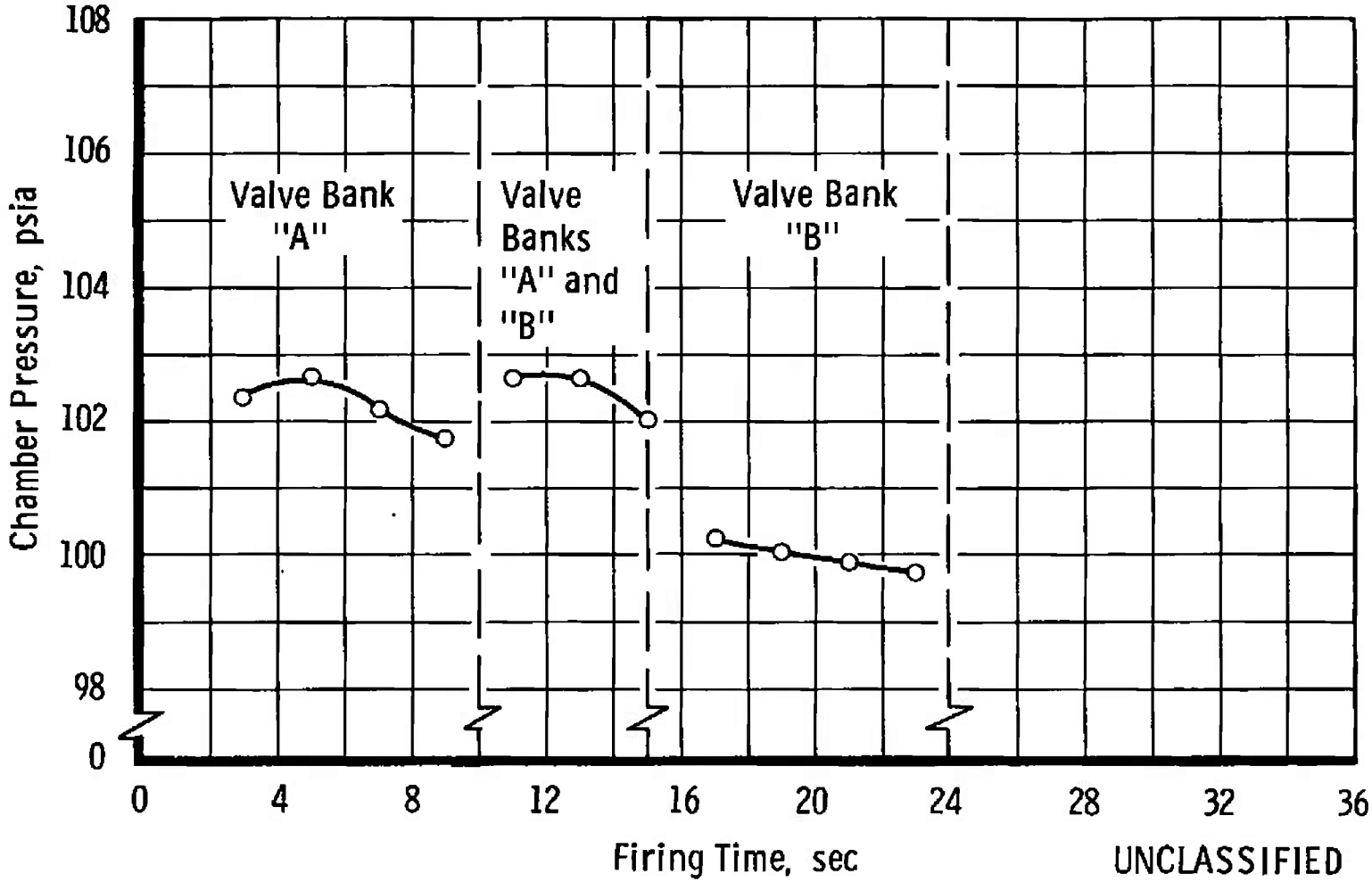

a. Chamber Pressure Effect

Fig. 20 Effect of Valve Bank Selection on Engine Operation

UNCLASSIFIED

b. Flow Resistance through the Thrust Chamber Valve

Fig. 20 Concluded

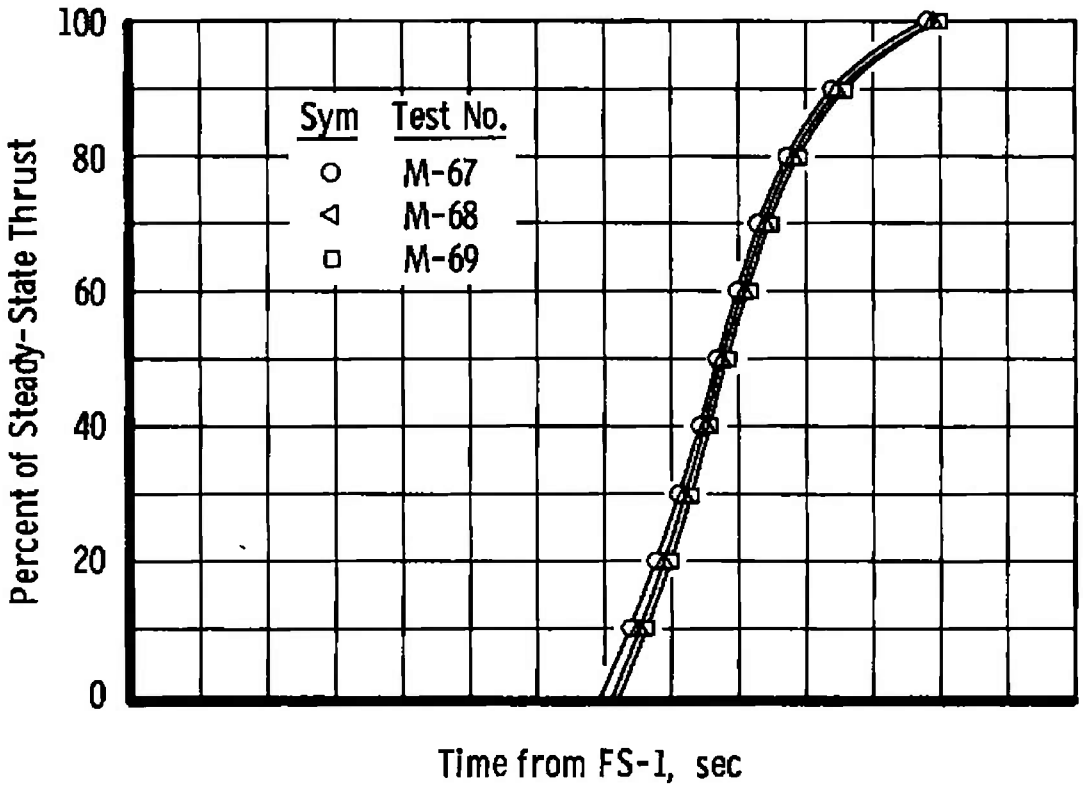

a. Starting Thrust Buildup

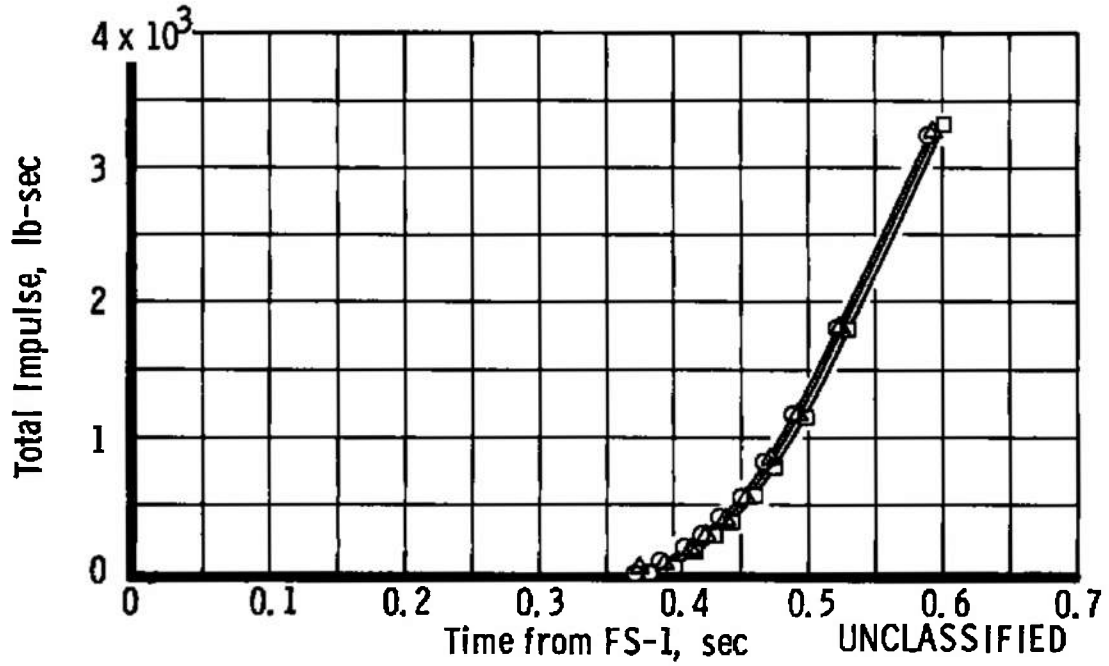

b. Start Transient Impulse

Fig. 21 Ignition Transient Characteristics

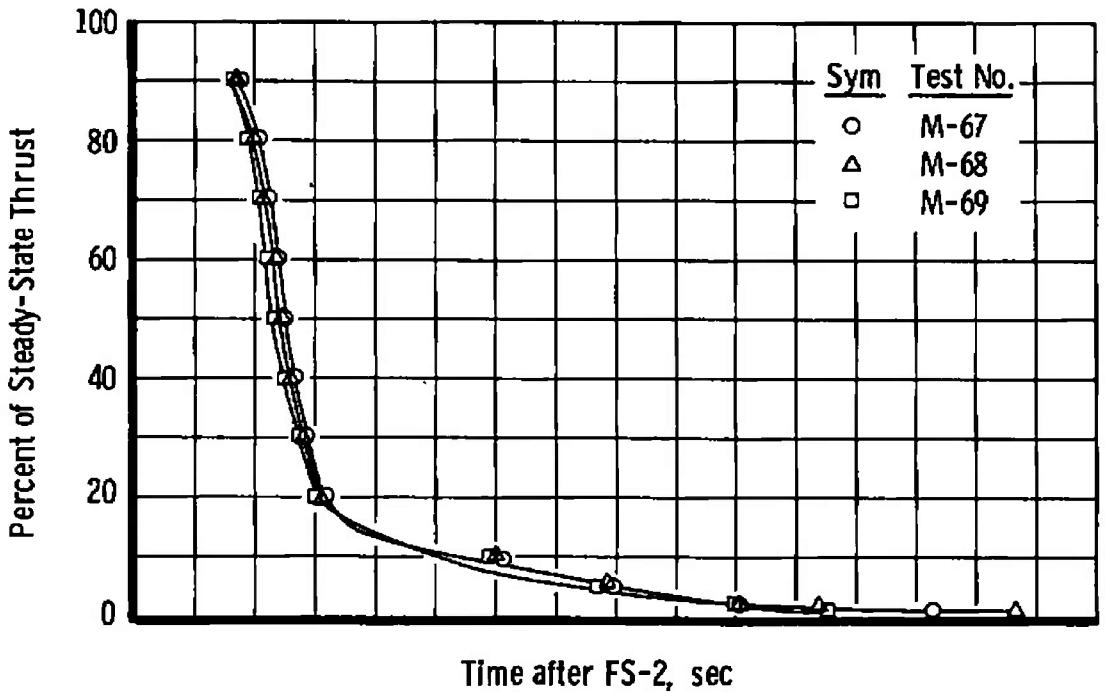

a. Shutdown Thrust Tailoff

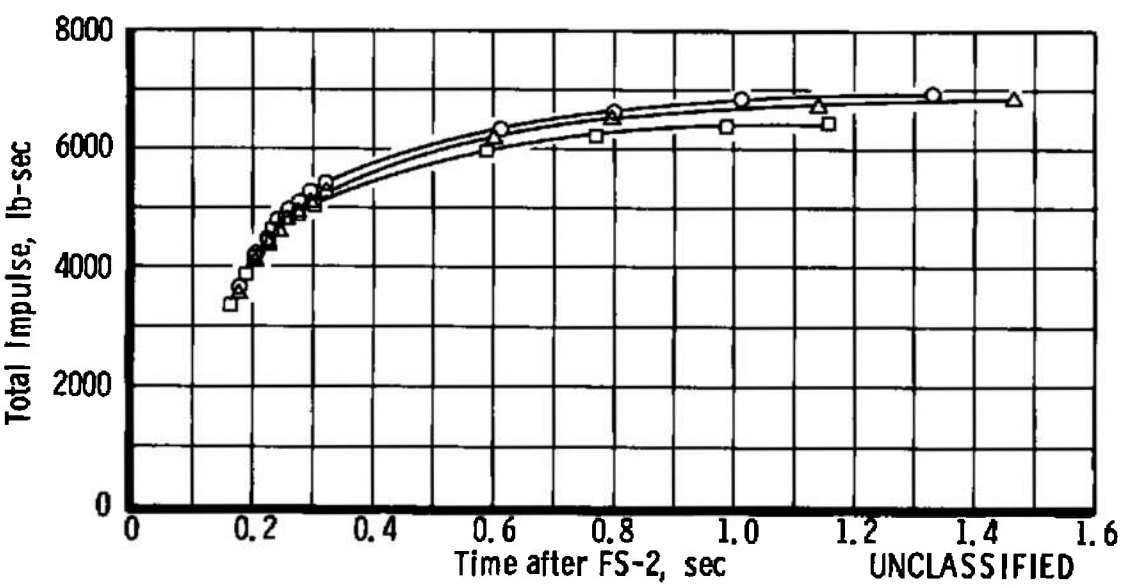

b. Shutdown Transient Impulse

Fig. 22 Shutdown Transient Characteristics

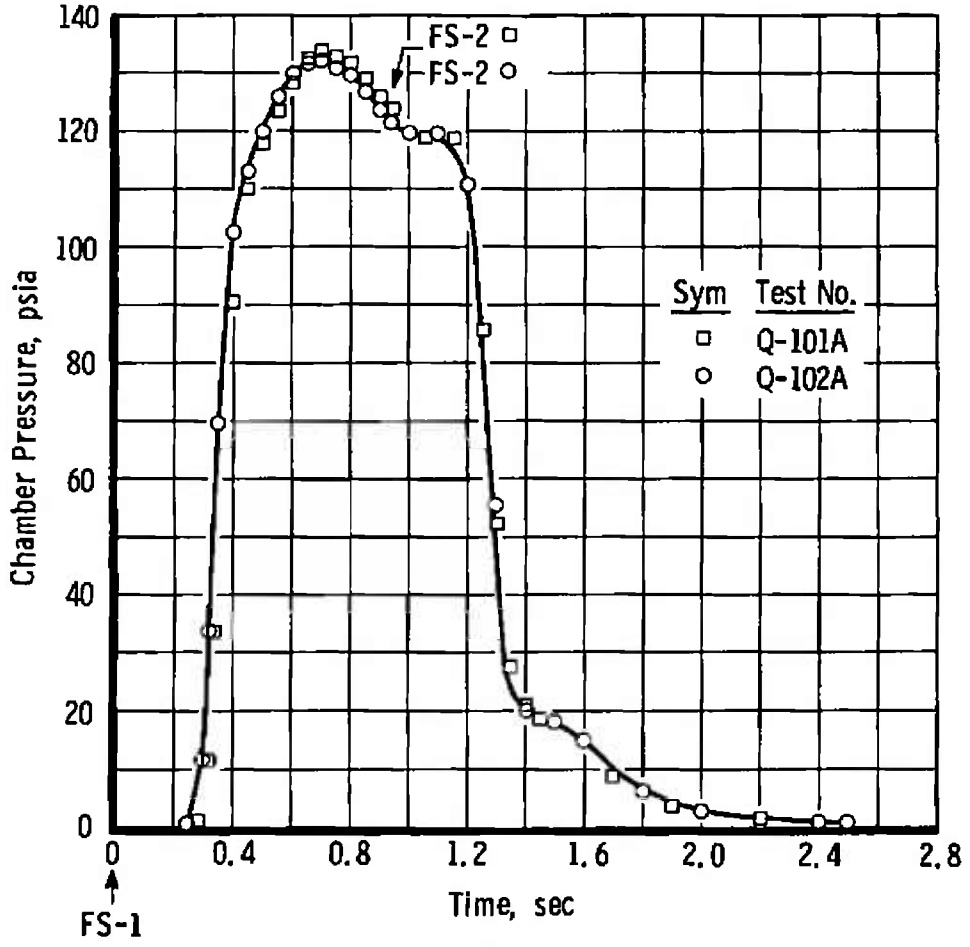

a. Chamber Pressure Transient

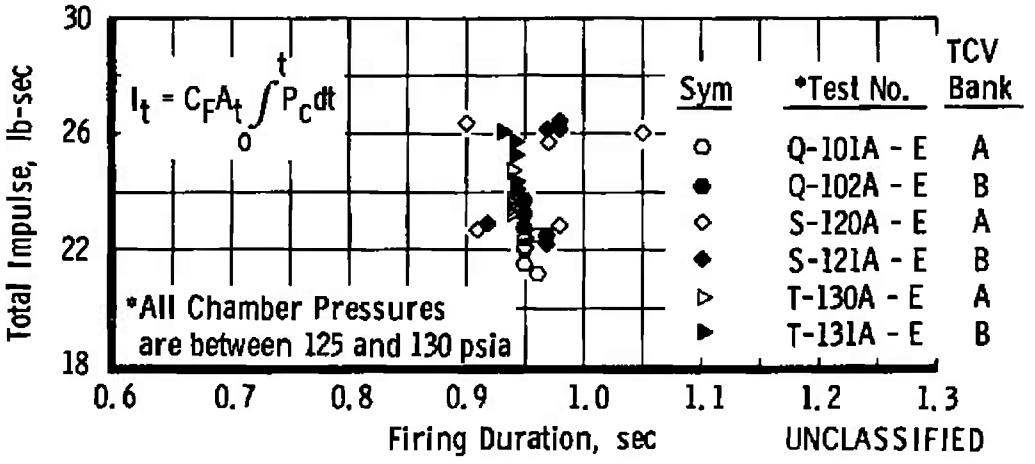

b. Integrated Total Impulse

Fig. 23 Minimum Impulse Bit Operation

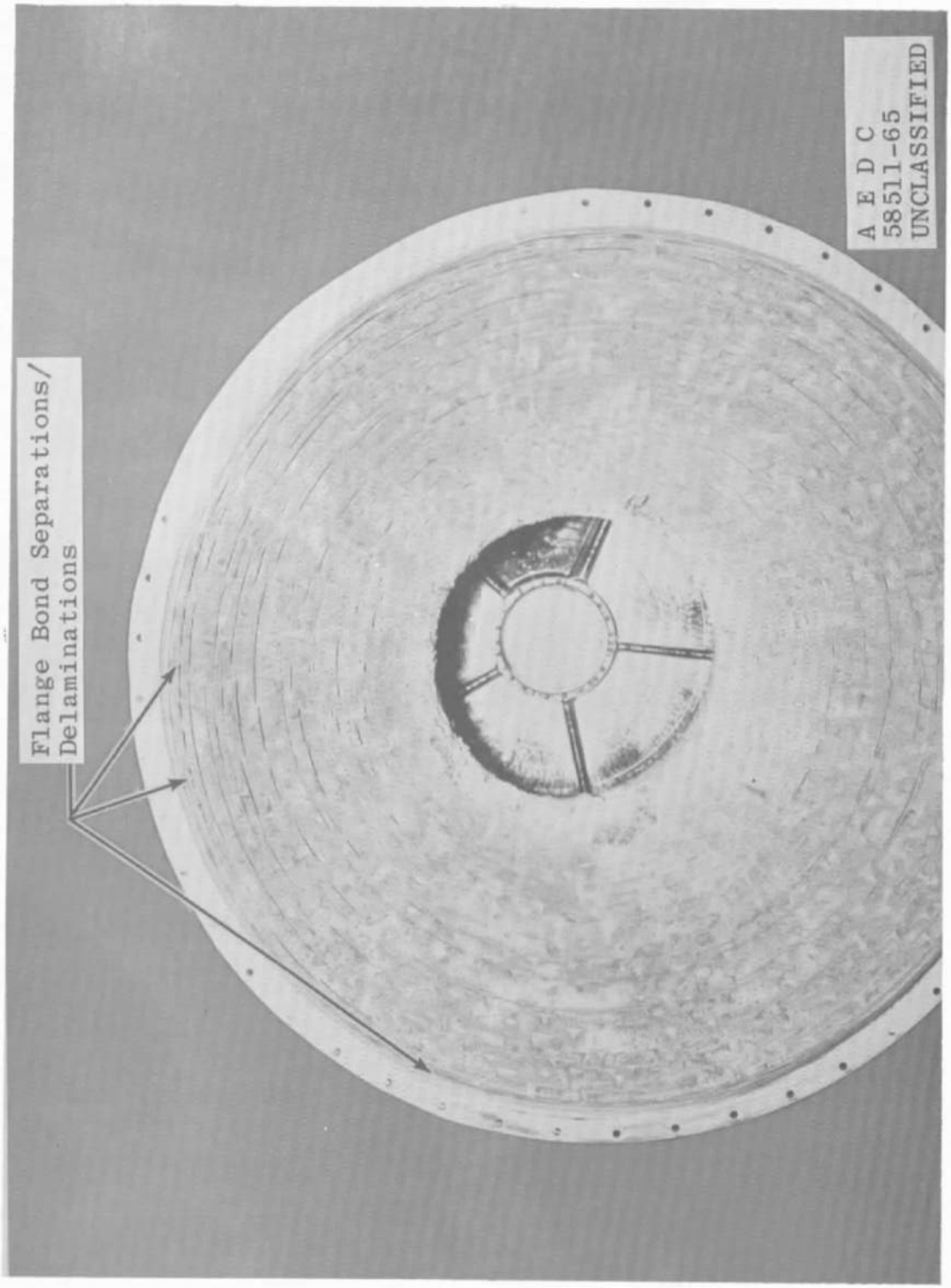

Fig. 24 Engine S/N 9A Chamber, Post-Fire

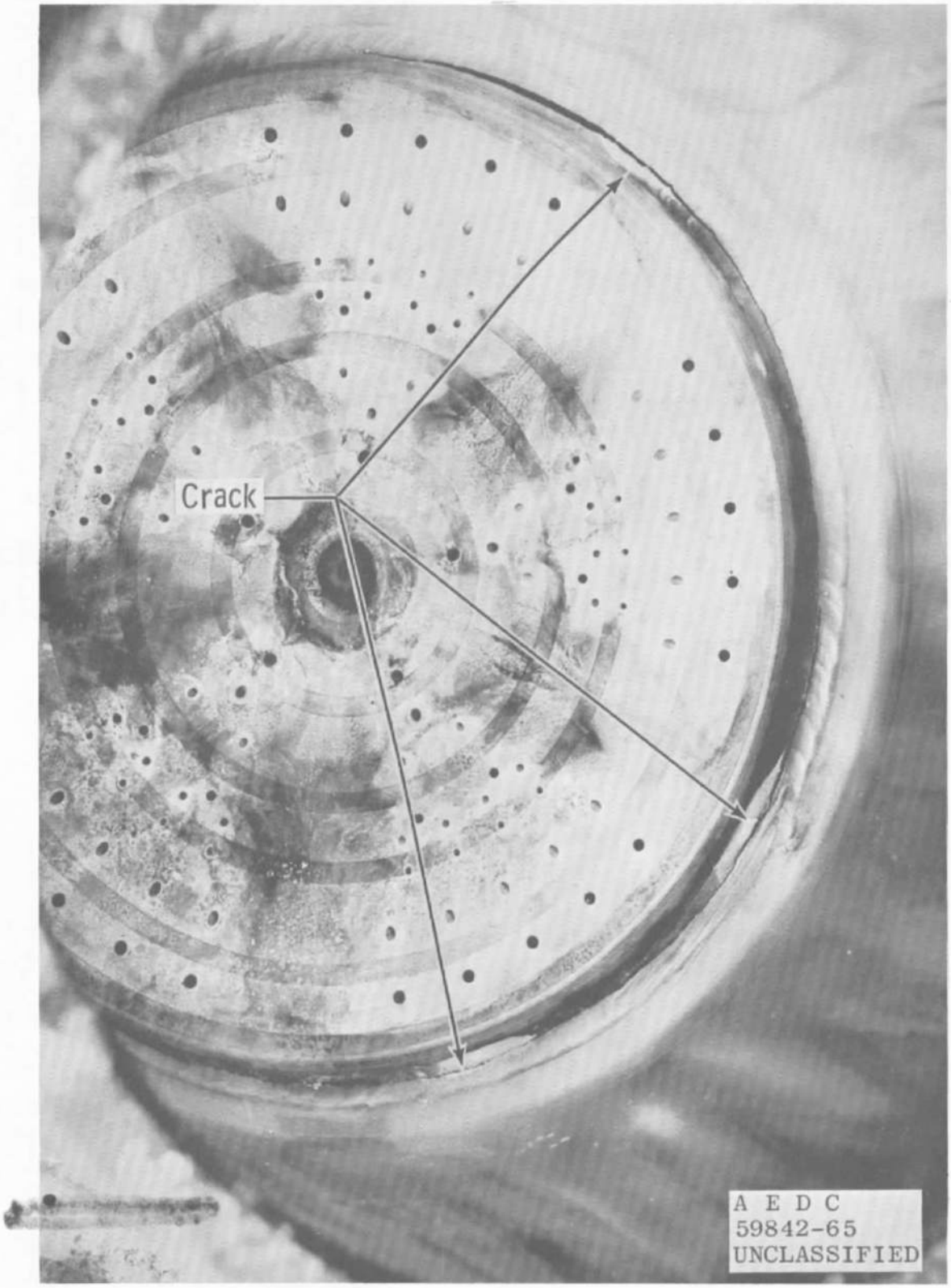

Fig. 25 Engine S/N 11A Injector, Post-Fire

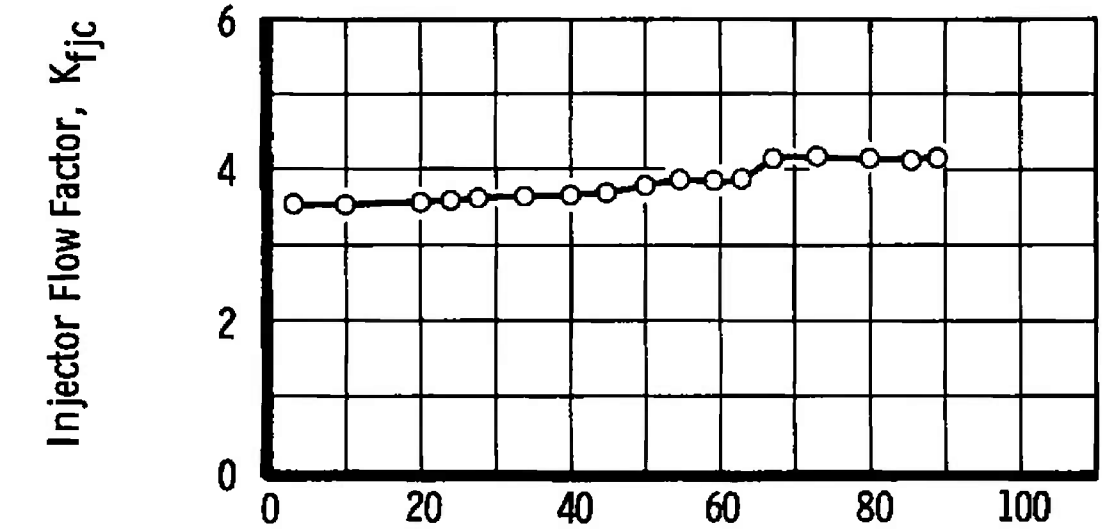

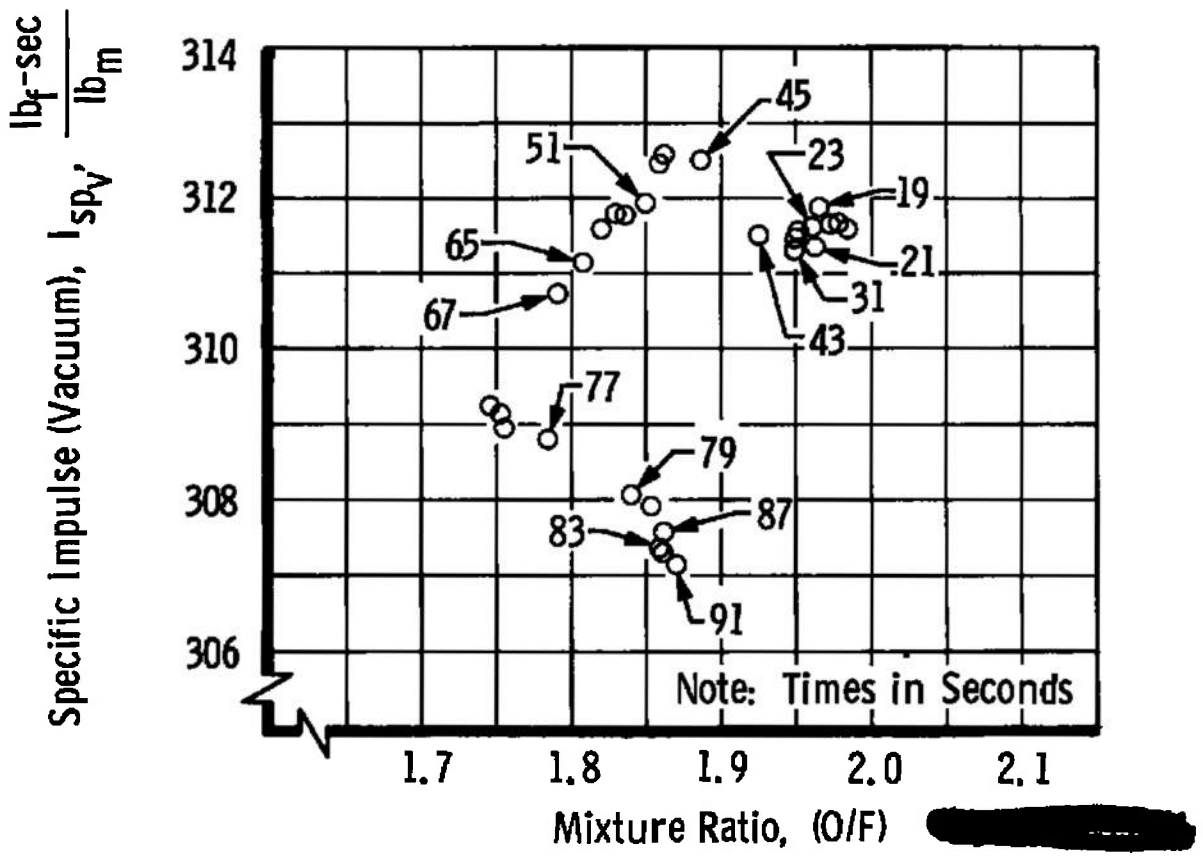

Fig. 26 Effect of Injector Crack on Engine Performance during Test N-85

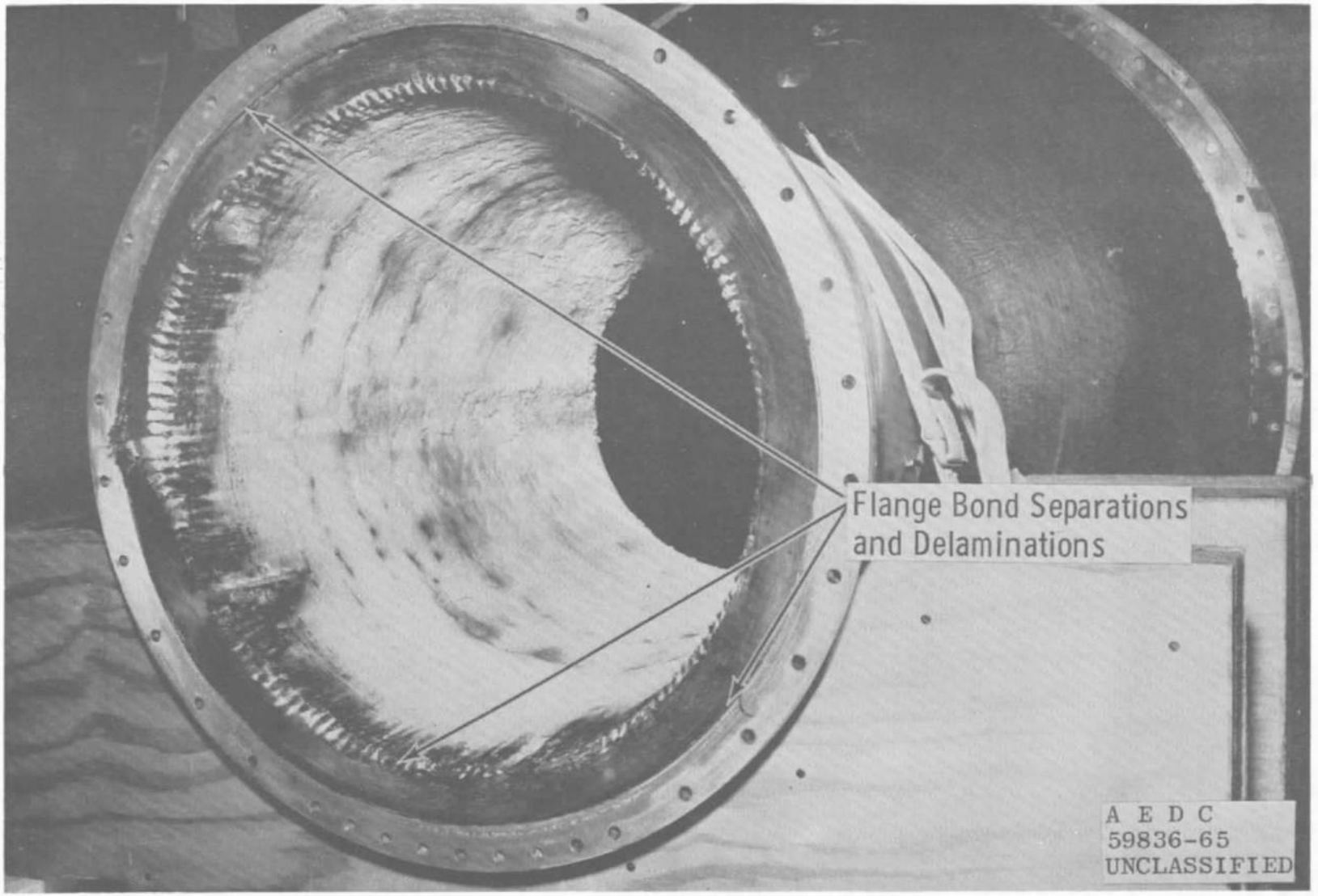

Fig. 27 Engine S/N 11A Chamber, Post-Fire

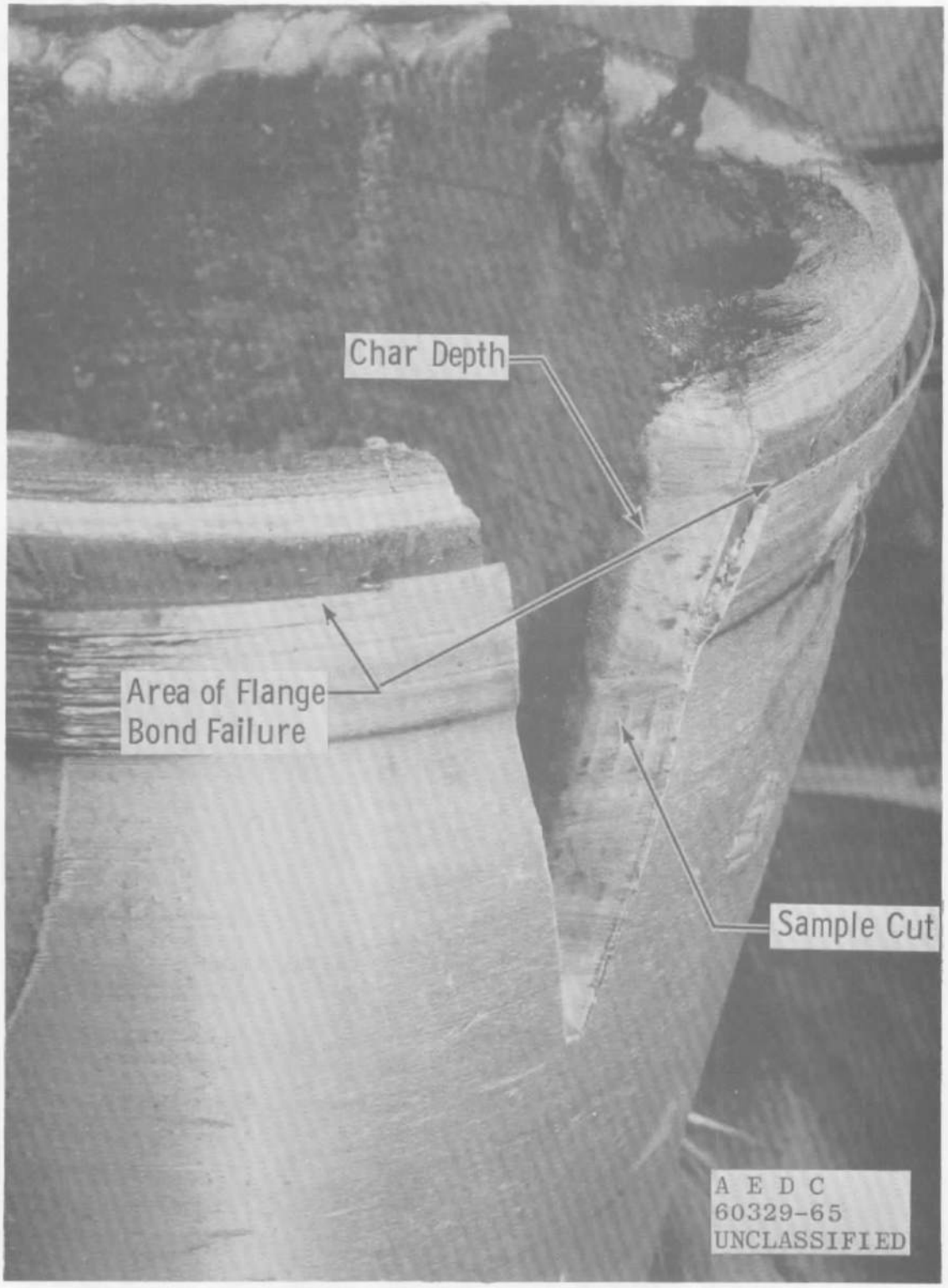

a. Engine S/N 9B Chamber

Fig. 28 Post-Fire Engine Condition

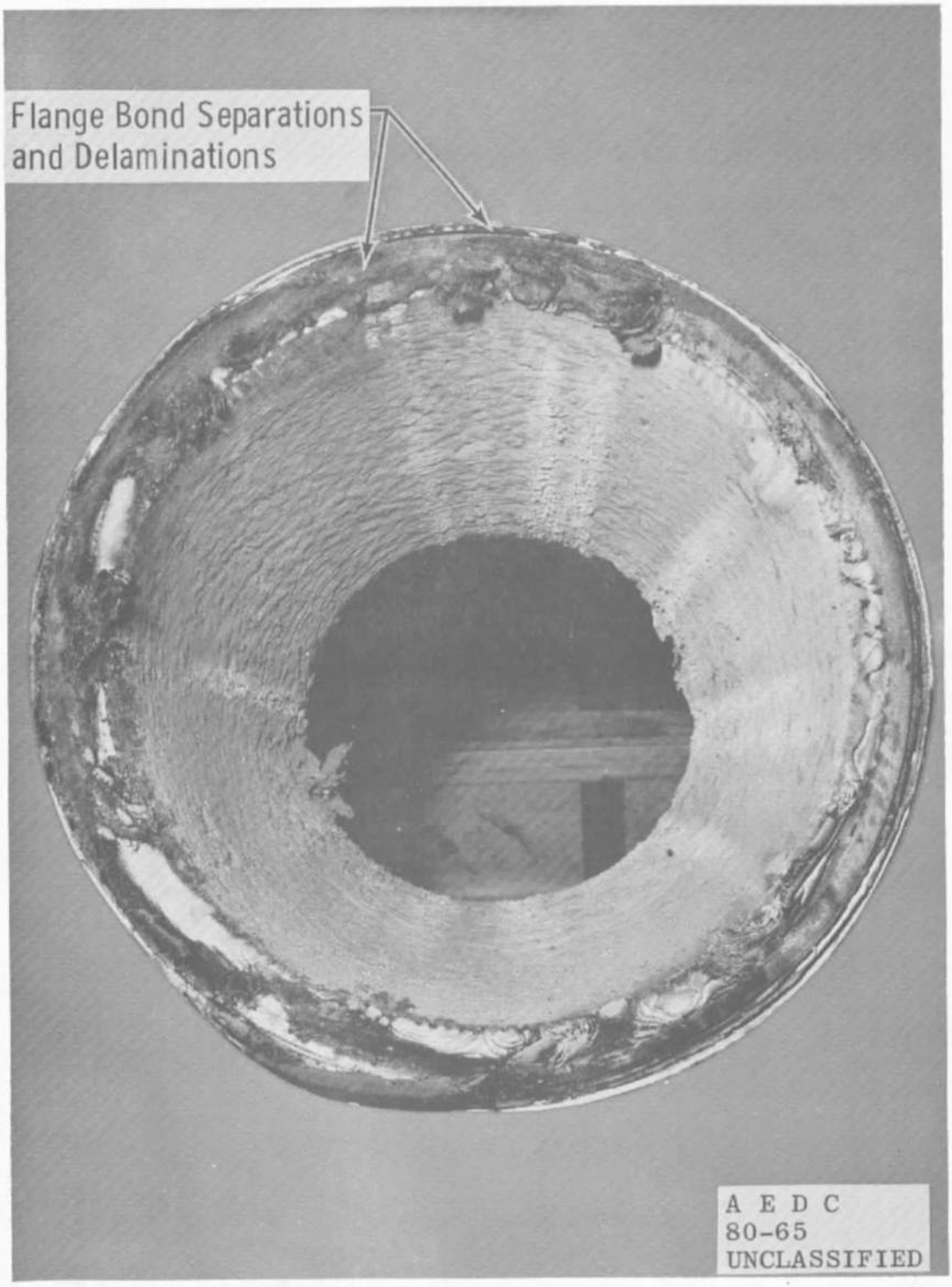

b. Engine S/N 11B Chamber

Fig. 28 Continued

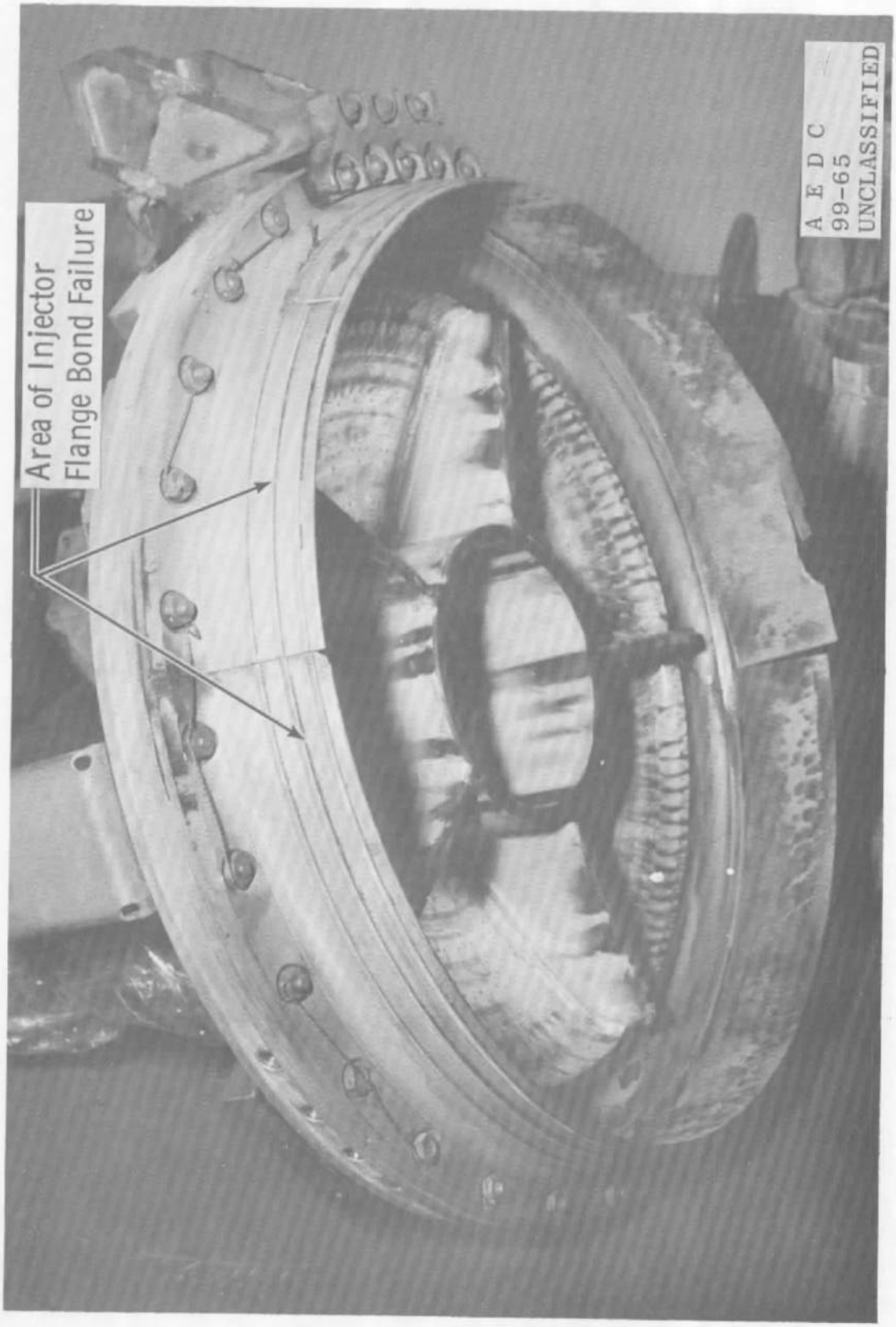

c. Engine S/N 11B Injector

Fig. 28 Concluded

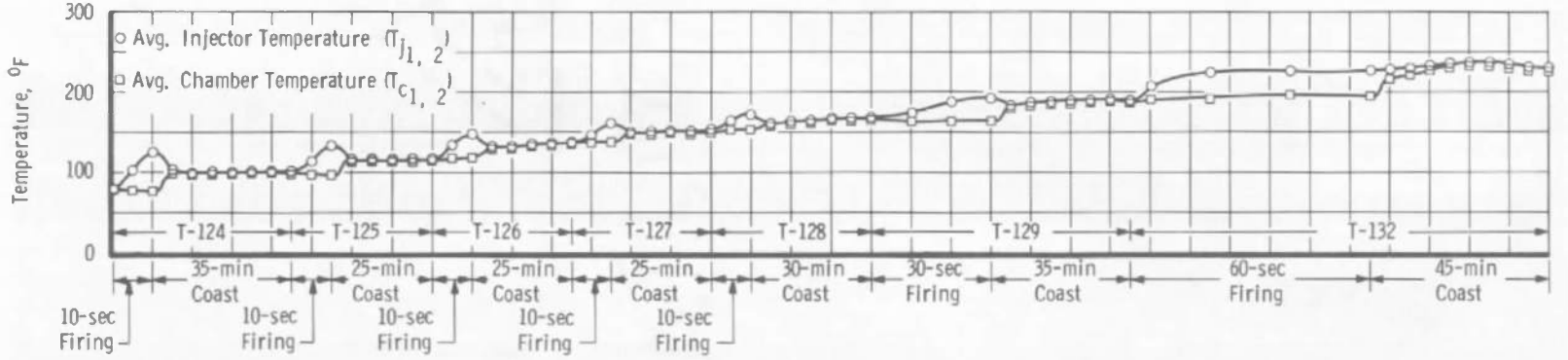

a. Initial Firings

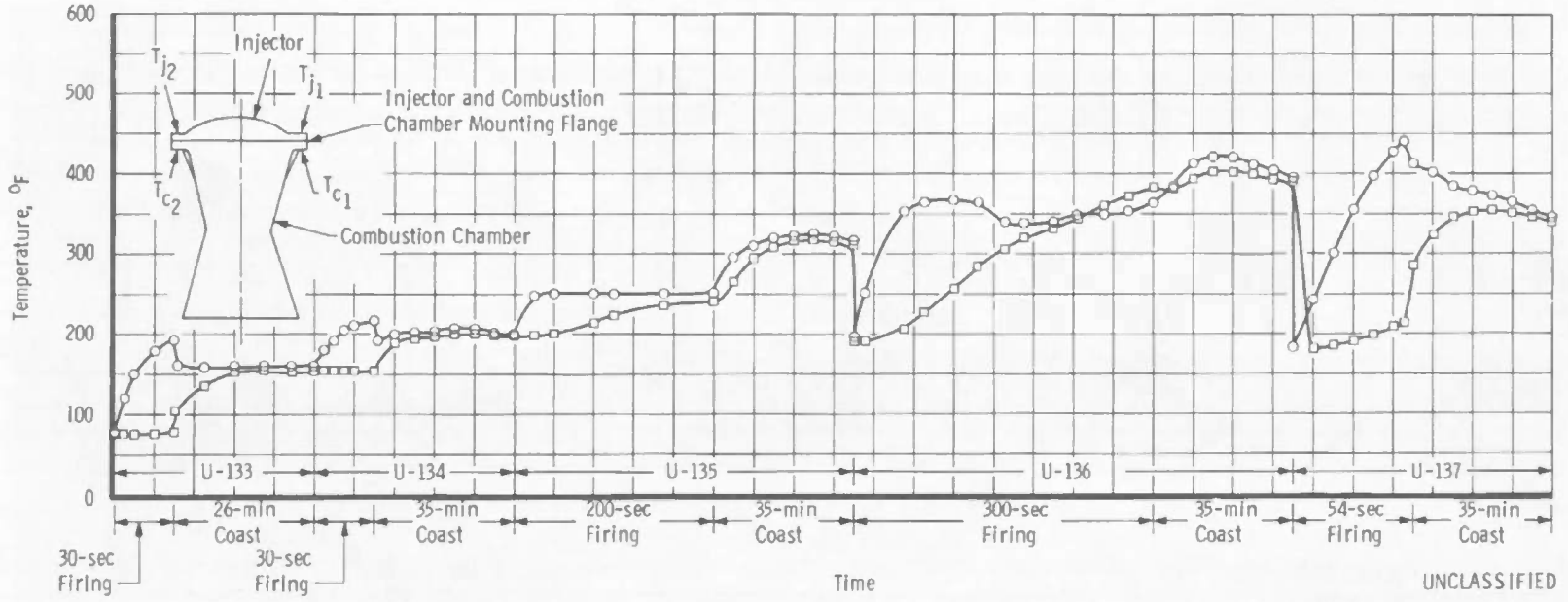

b. Final Firings

Fig. 29 Injector and Chamber Flange Temperature History Engine S/N 11C

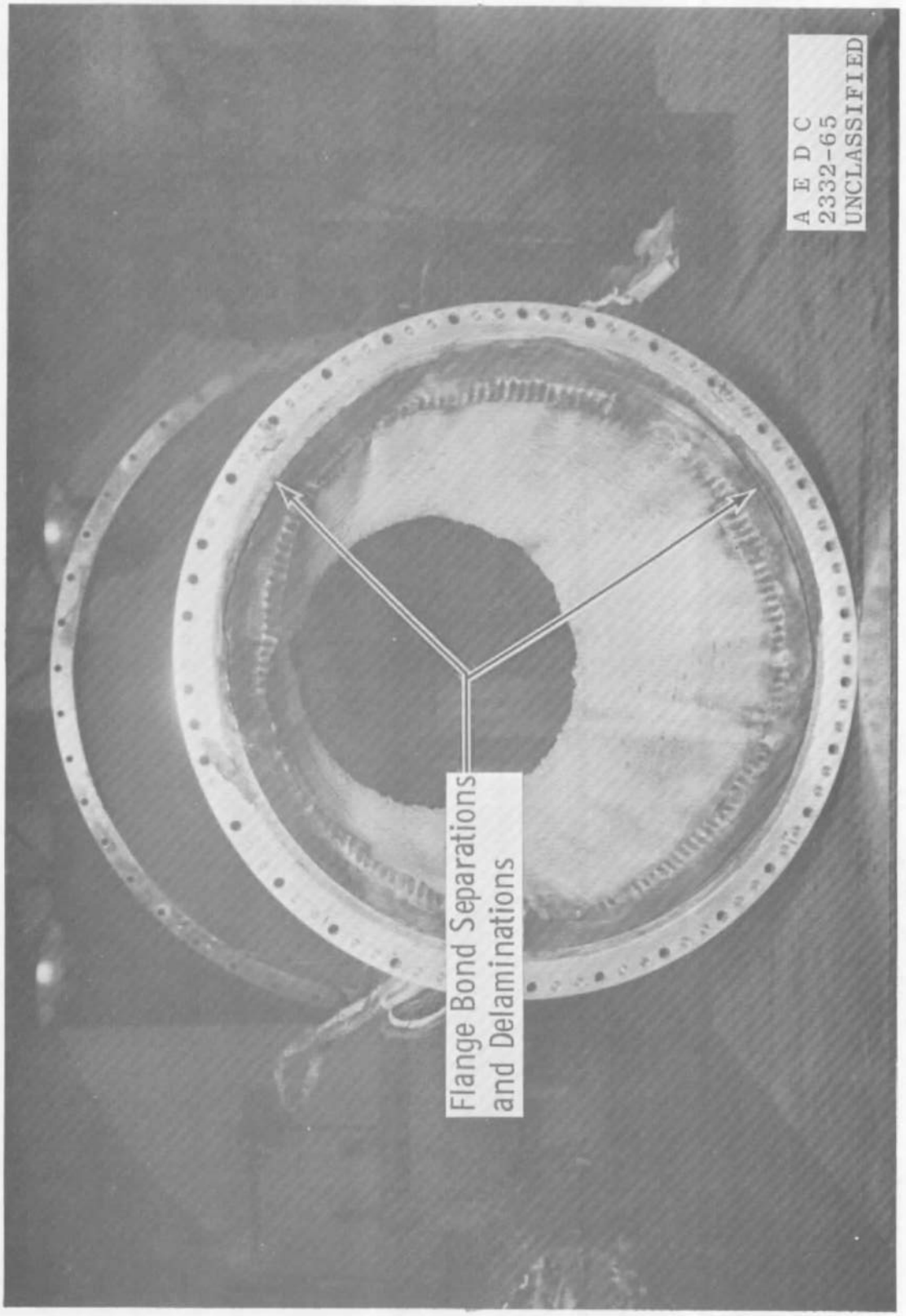

Fig. 30 Engine S/N 11C Chamber, Post-Fire, Injector End

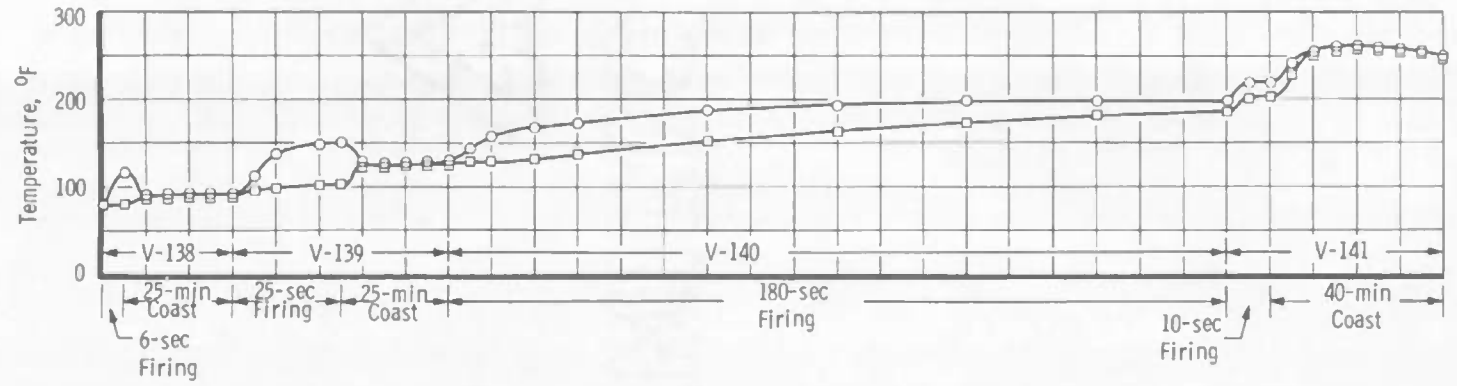

a. Initial Firings

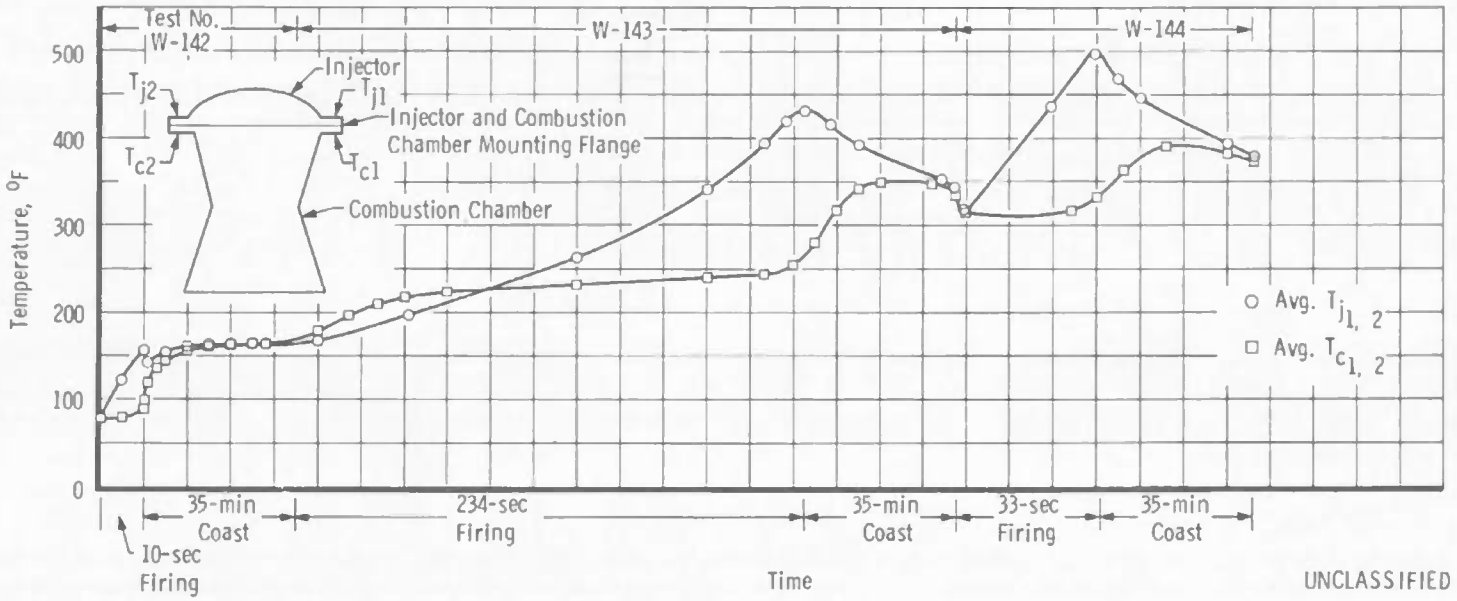

b. Final Firings

Fig. 31 Engine S/N 11D Injector and Chamber Flange Temperature History

UNCLASSIFIED

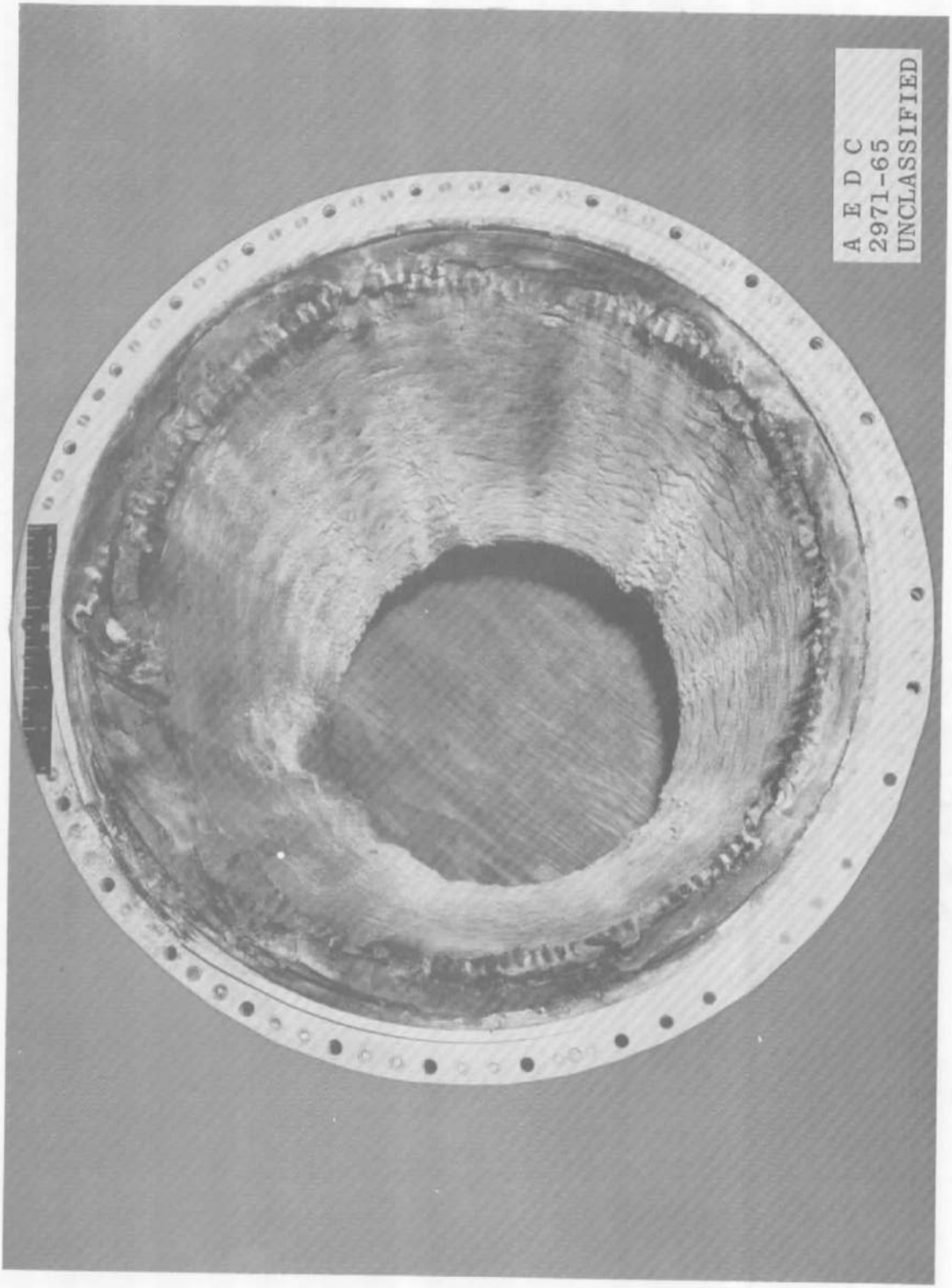

Fig. 32 Engine S/N 11D Chamber Post-Fire, Injector End

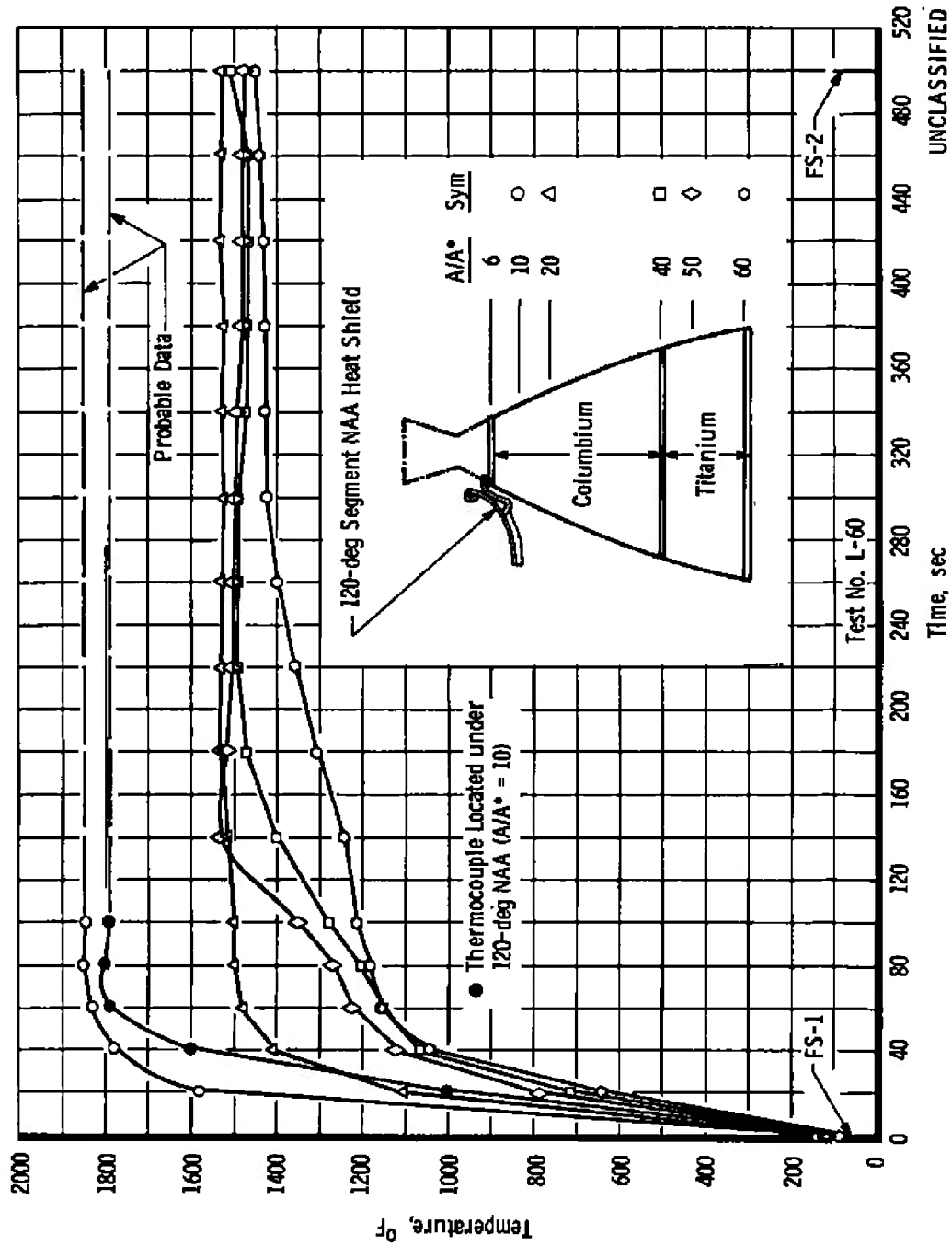

a. Engine S/N 9A, 500-sec Test

Fig. 33 Nozzle Extension Outer Surface Skin Temperature History

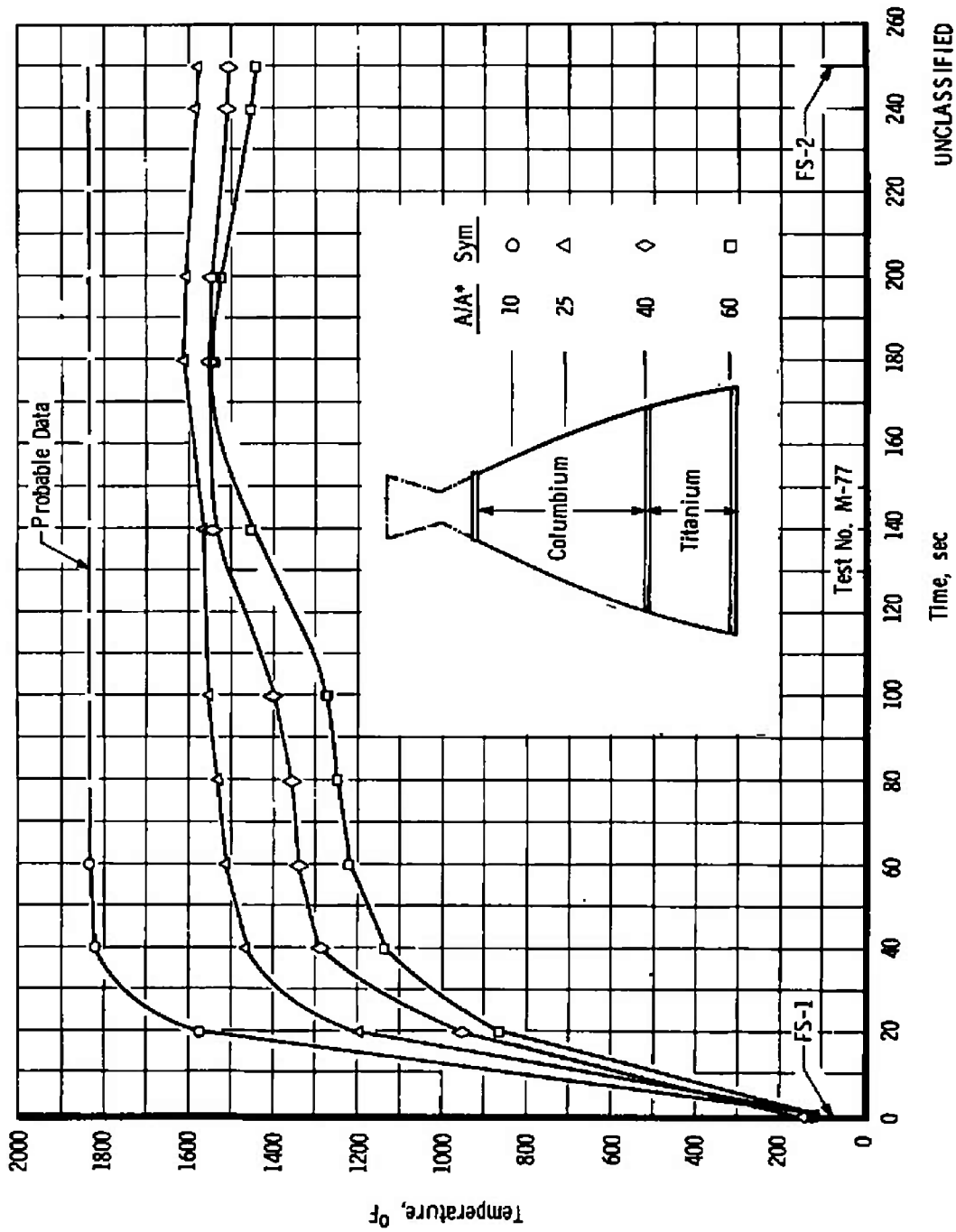

b. Engine S/N 11A, 250-sec Test

Fig. 33 Continued

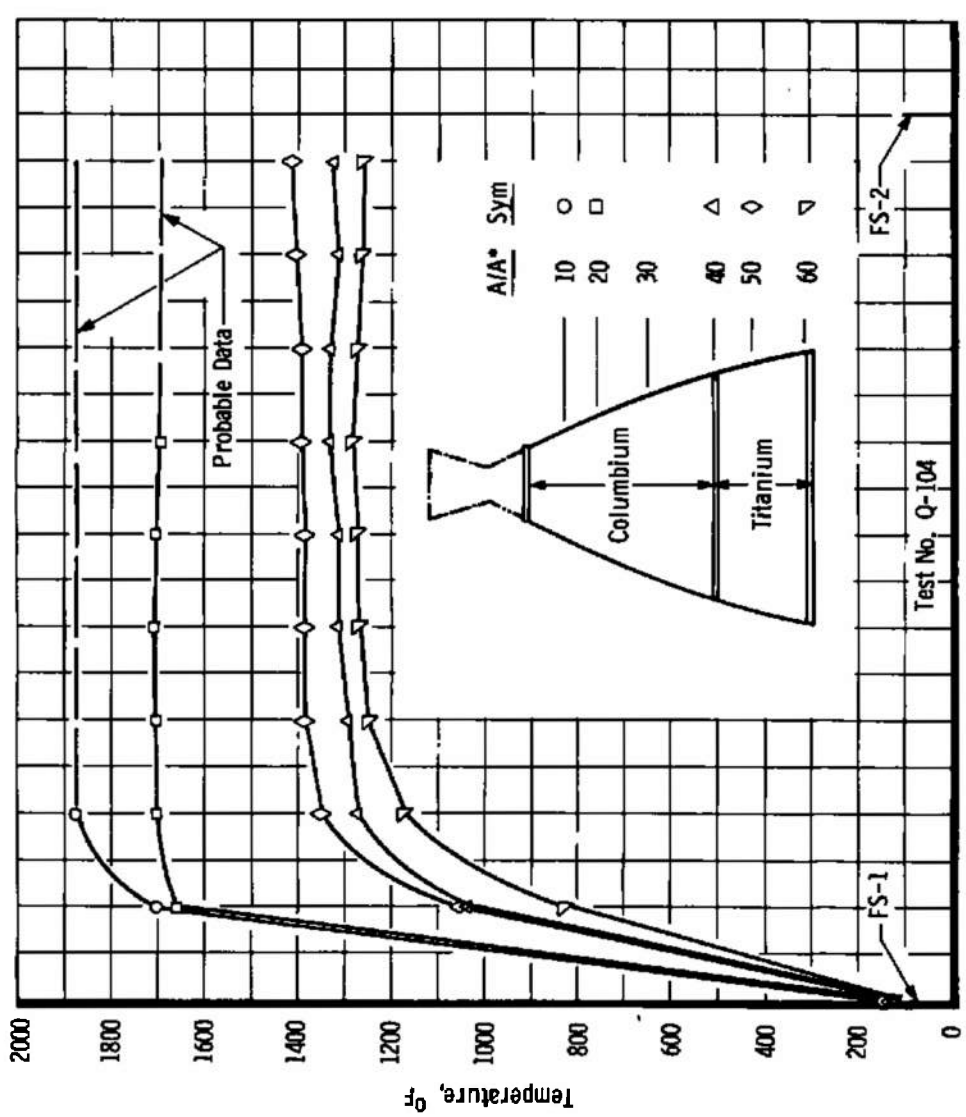

c. Engine S/N 9B, 193-sec Test

Fig. 33 Continued

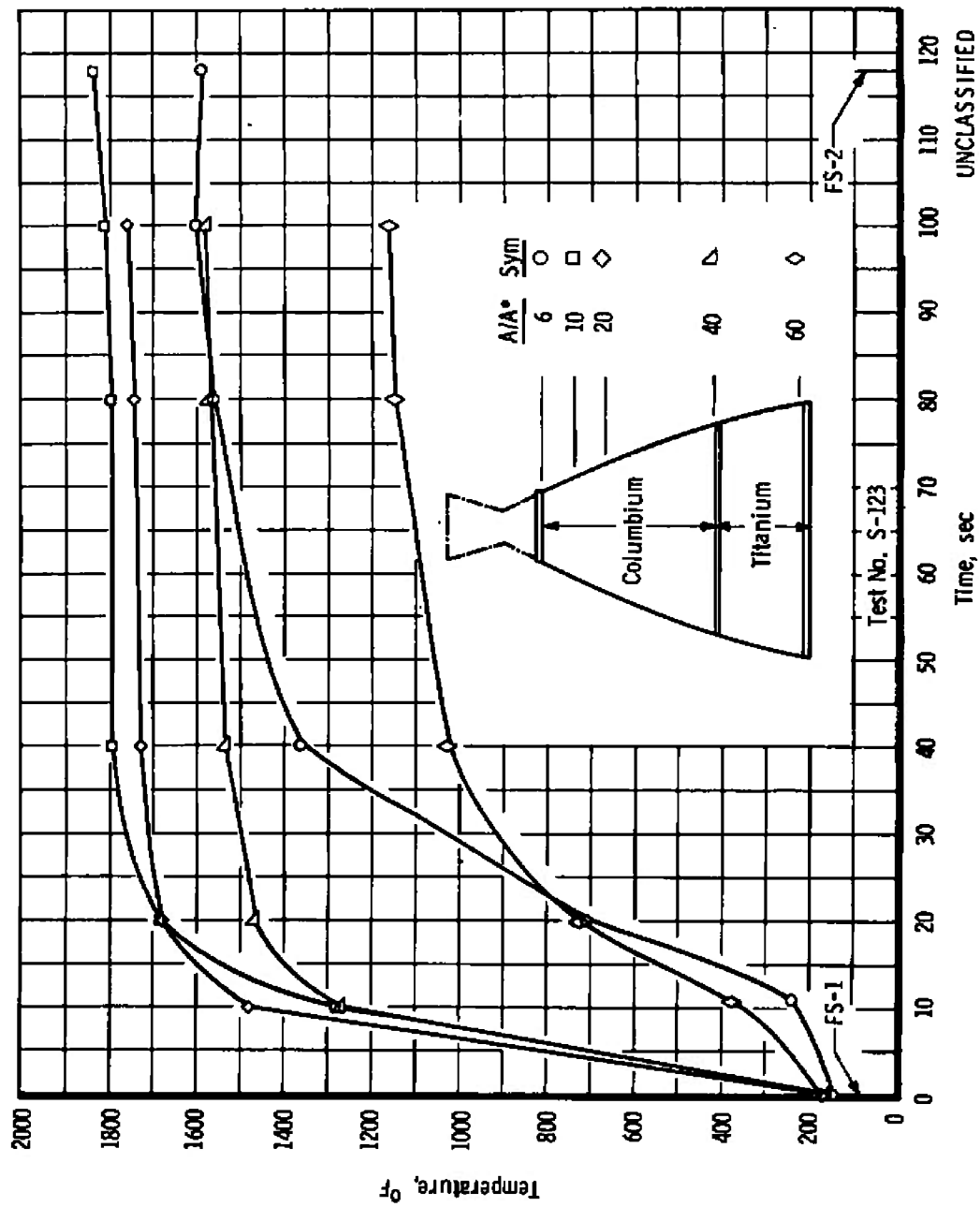

d. Engine S/N 11B, 118-sec Test

Fig. 33 Continued

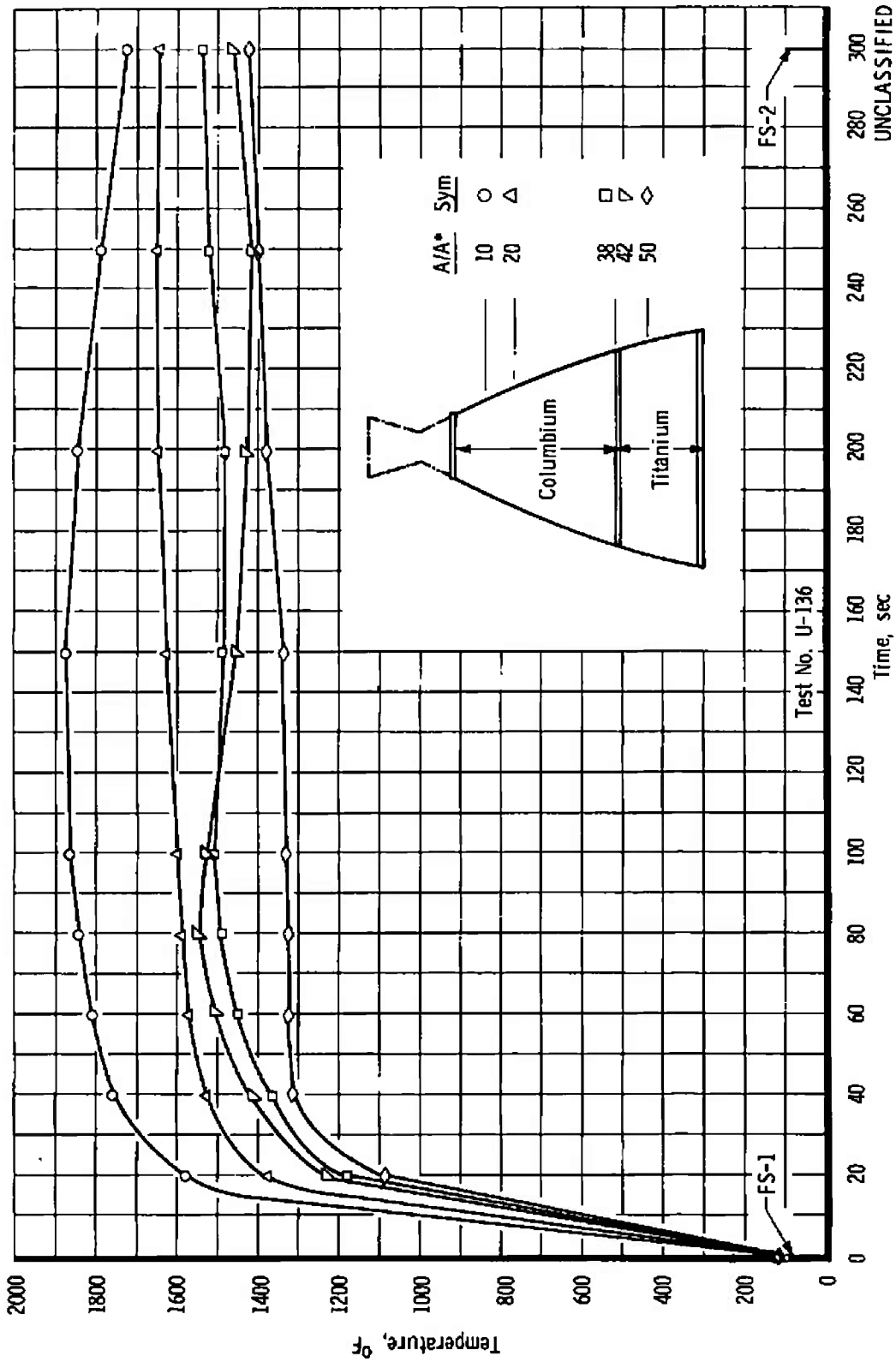

e. Engine S/N 11C, 300-sec Test

Fig. 33 Concluded

UNCLASSIFIED

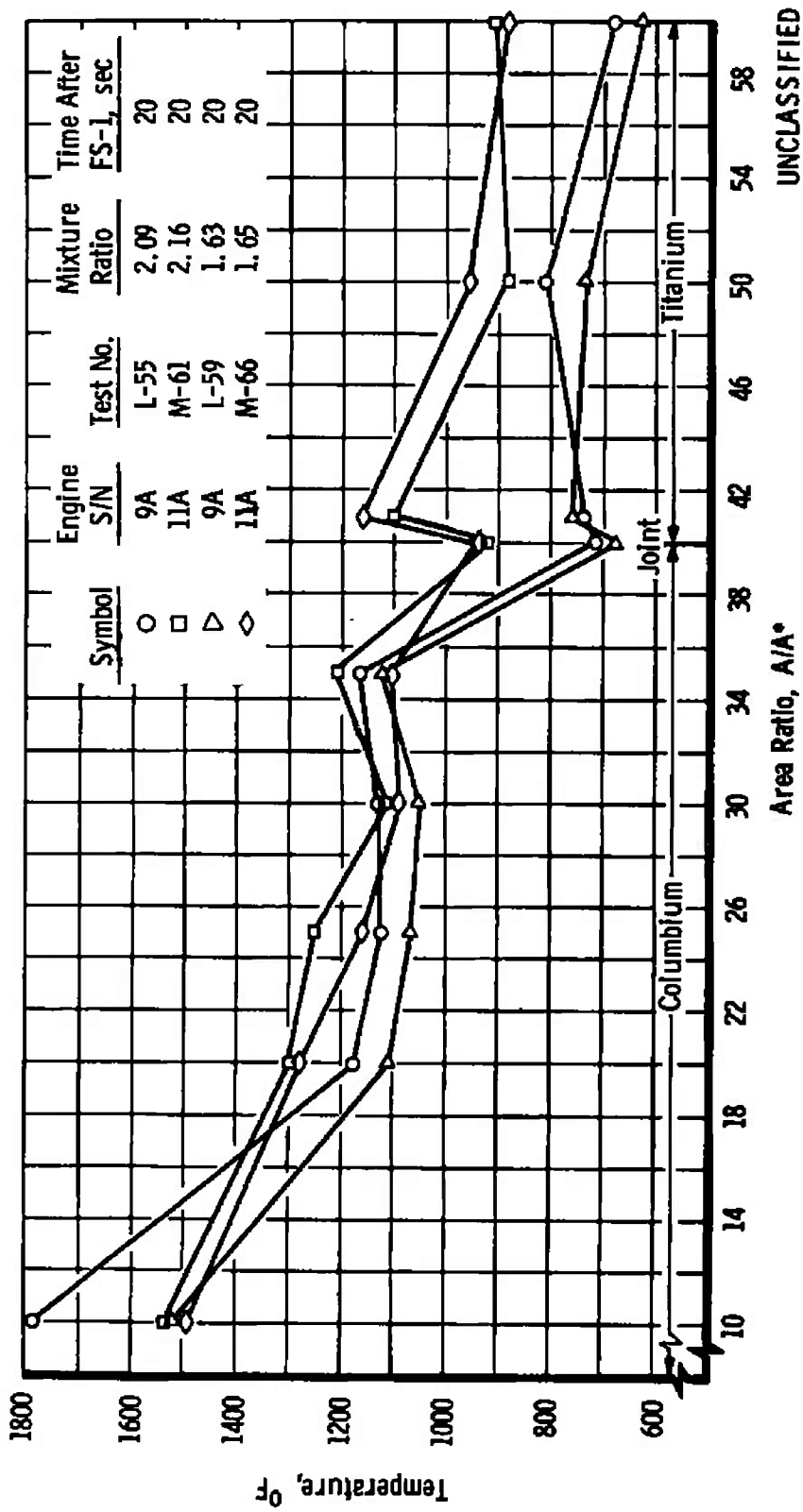

a. Effect of Mixture Ratio

Fig. 34 Nozzle Extension Temperature Profile

UNCLASSIFIED

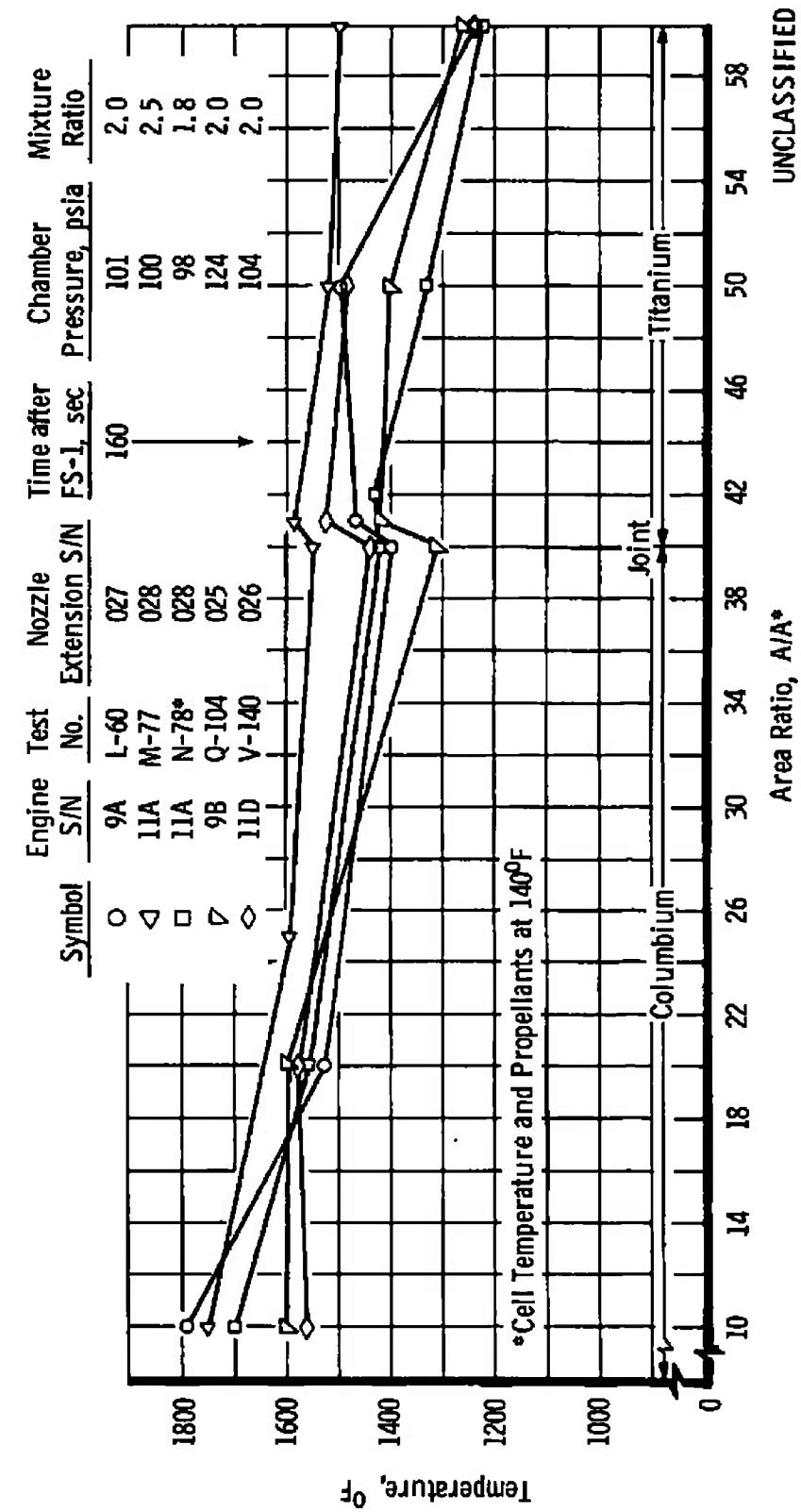

b. Effect of Mixture Ratio on Equilibrium Temperatures

Fig. 34 Concluded

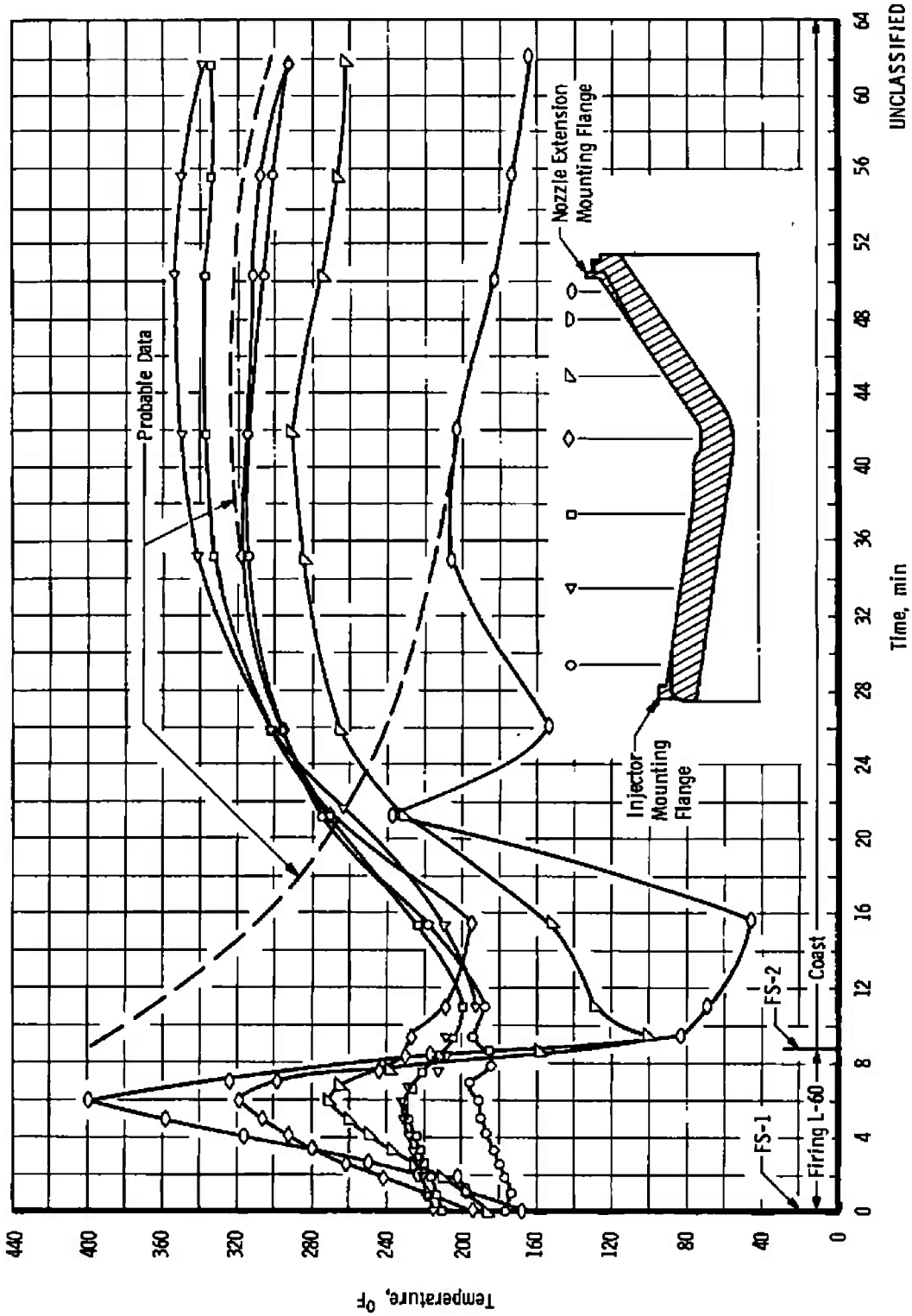

a. Engine S/N 9A, Test L-60

Fig. 35 Combustion Chamber Surface Temperature versus Time

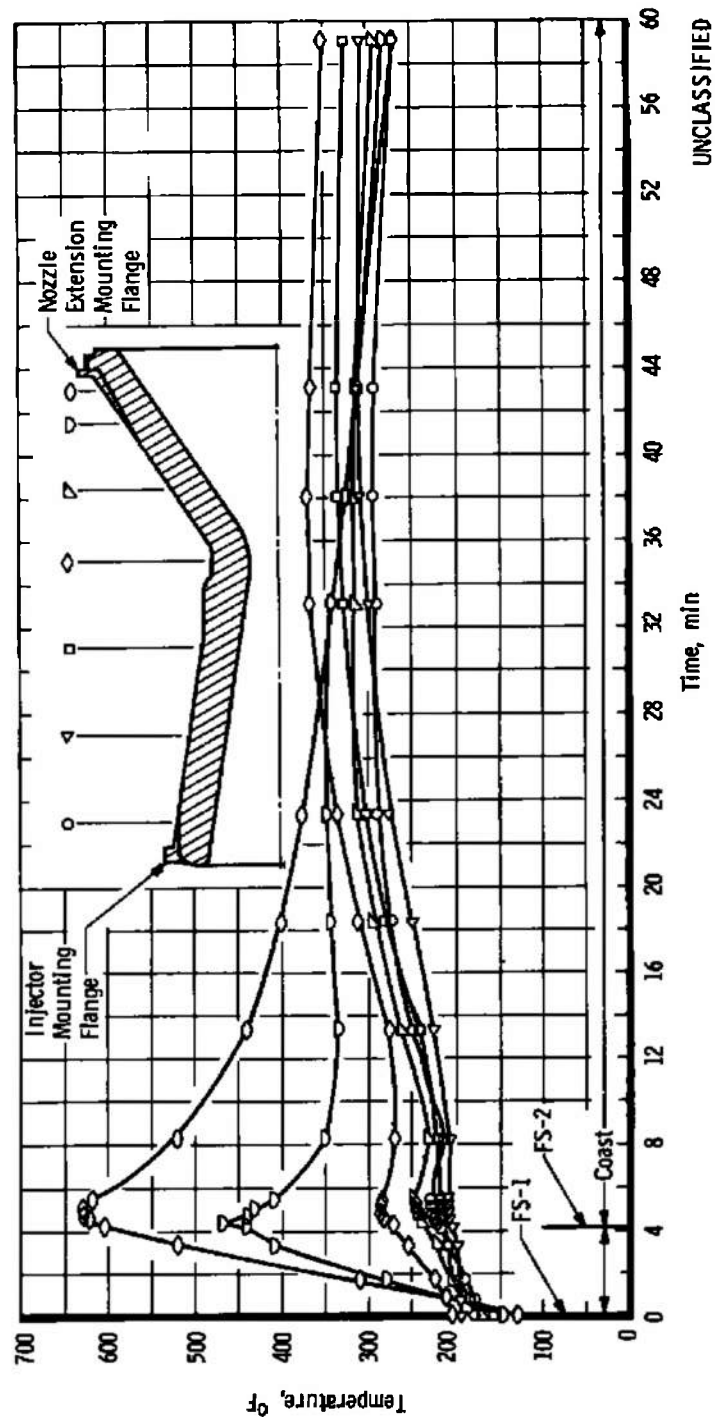

b. Engine S/N 11A, Test M-77

Fig. 35 Continued

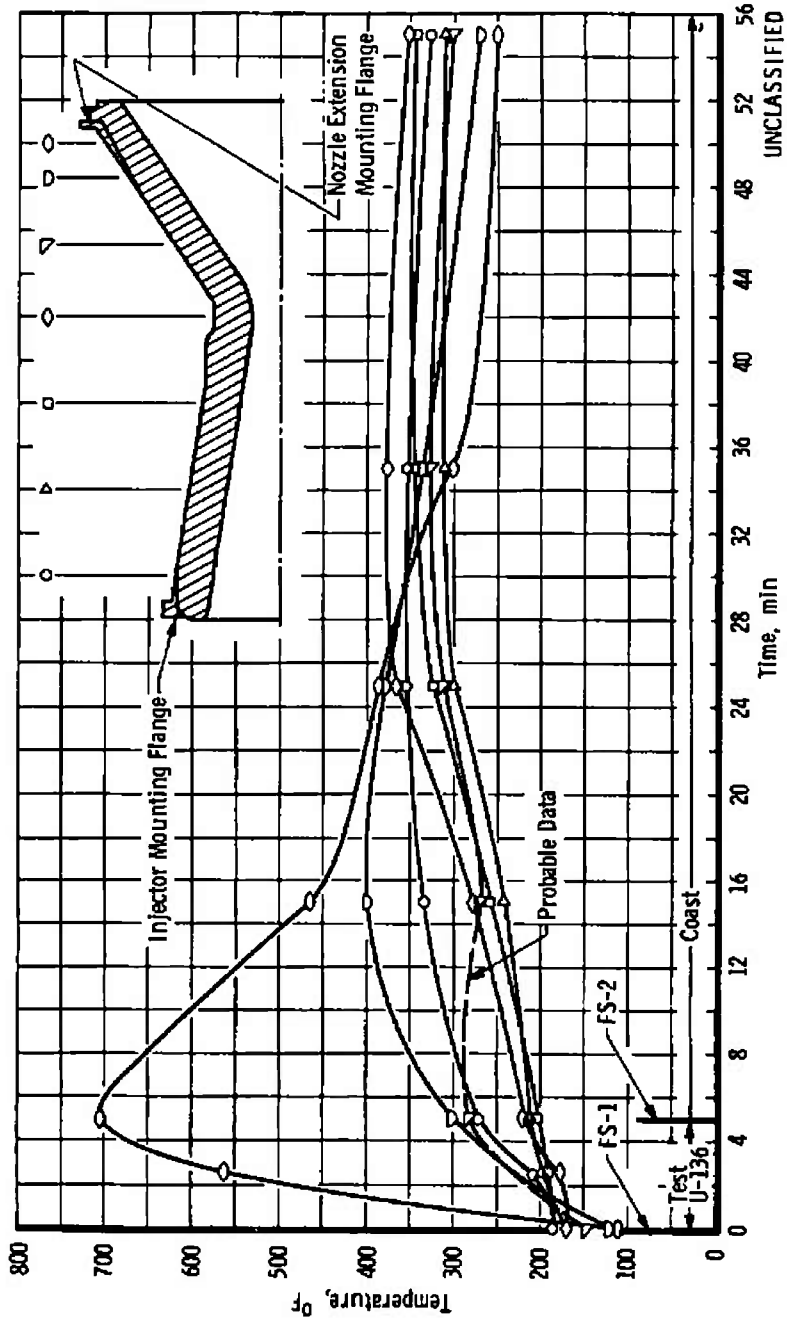

c. Engine S/N 11C, Test U-136

Fig. 35 Continued

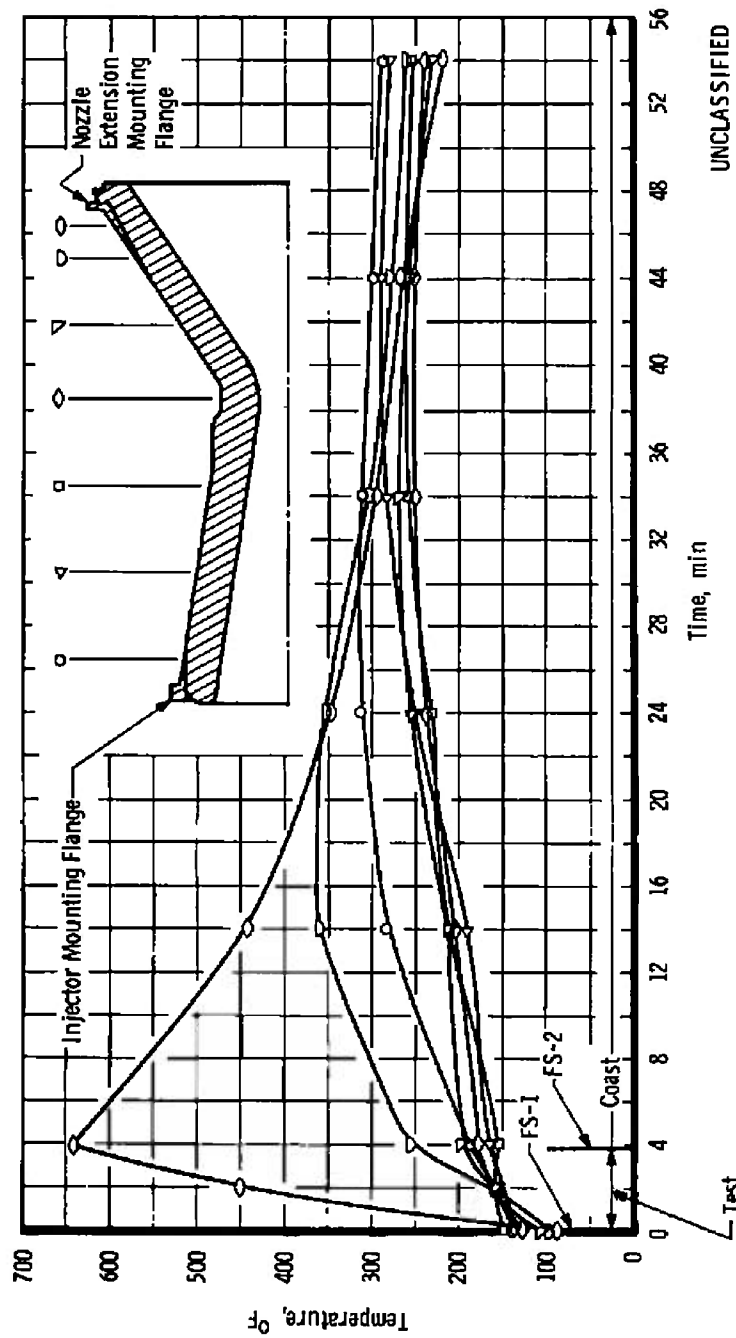

d. Engine S/N 11D, Test W-143

Fig. 35 Concluded

UNCLASSIFIED

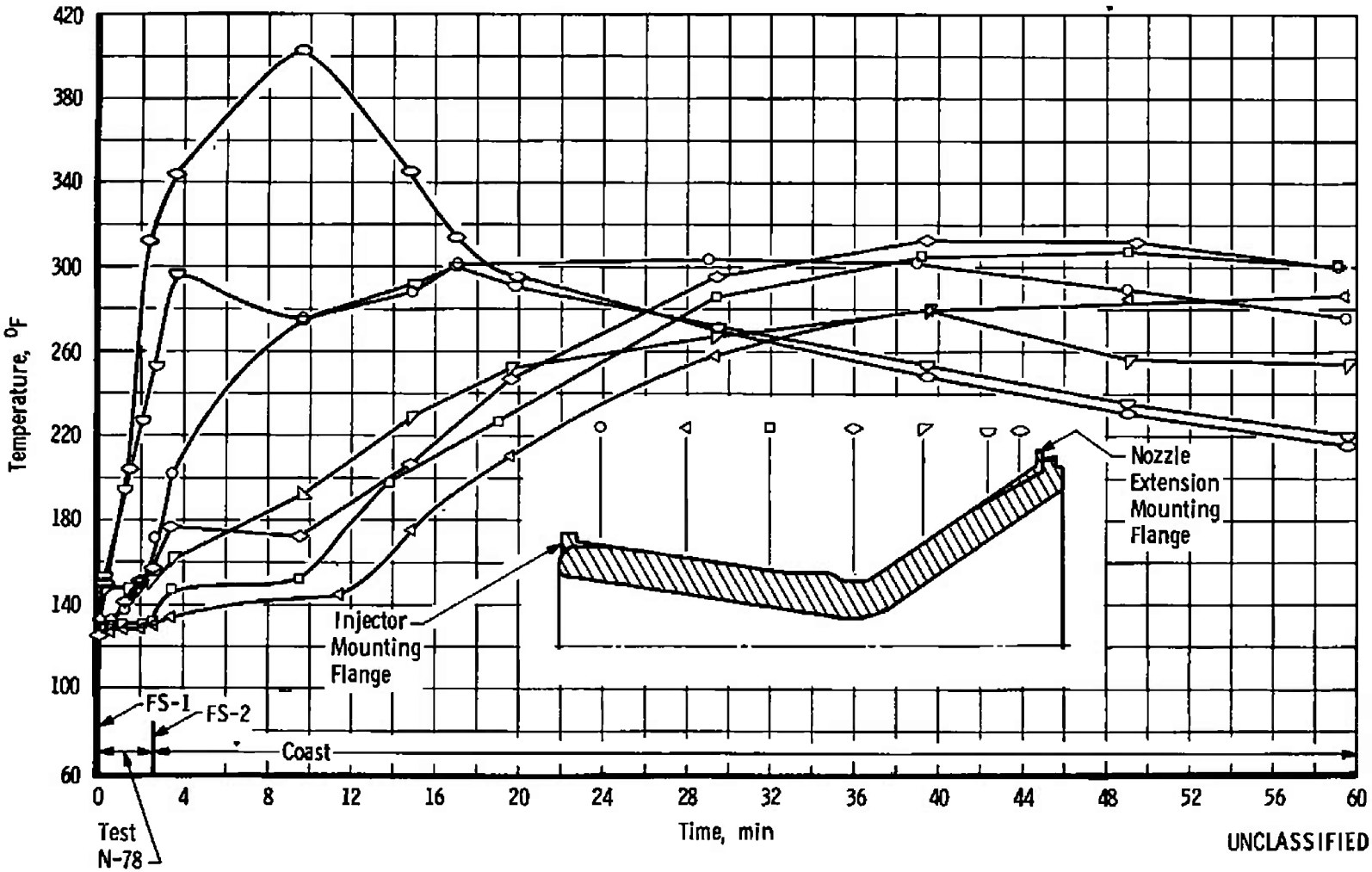

a. High Temperature Propellants, Test N-78, Engine S/N 11A

Fig. 36 Combustion Chamber Surface Temperature versus Time

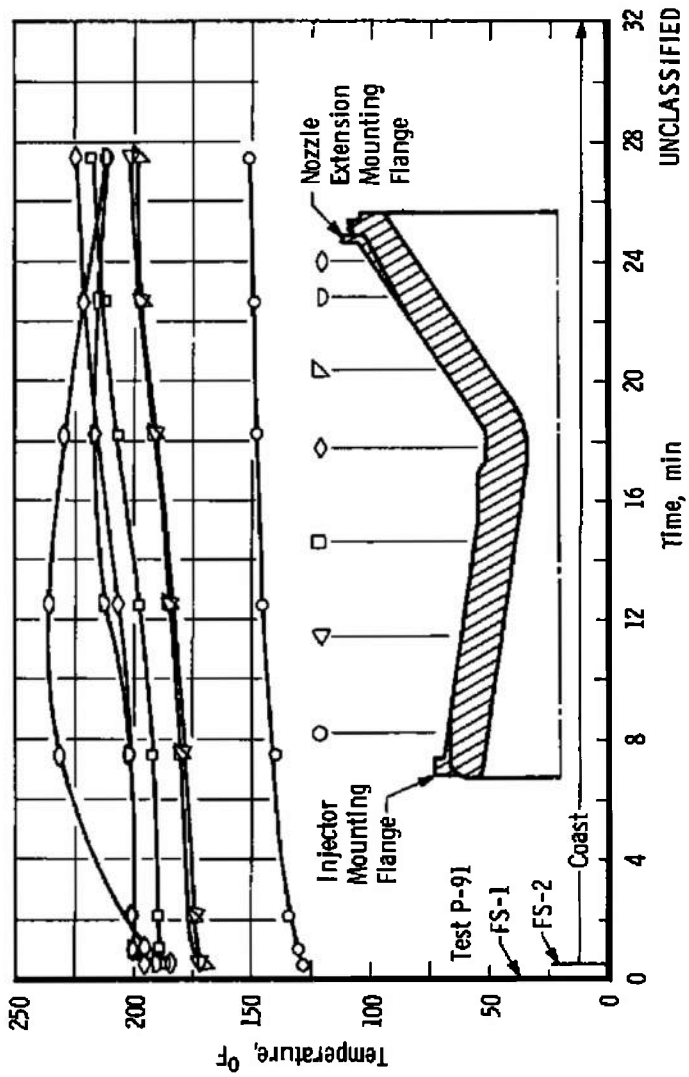

b. Low Temperature Propellants, Test P-91, Engine S/N 9B

Fig. 36 Concluded

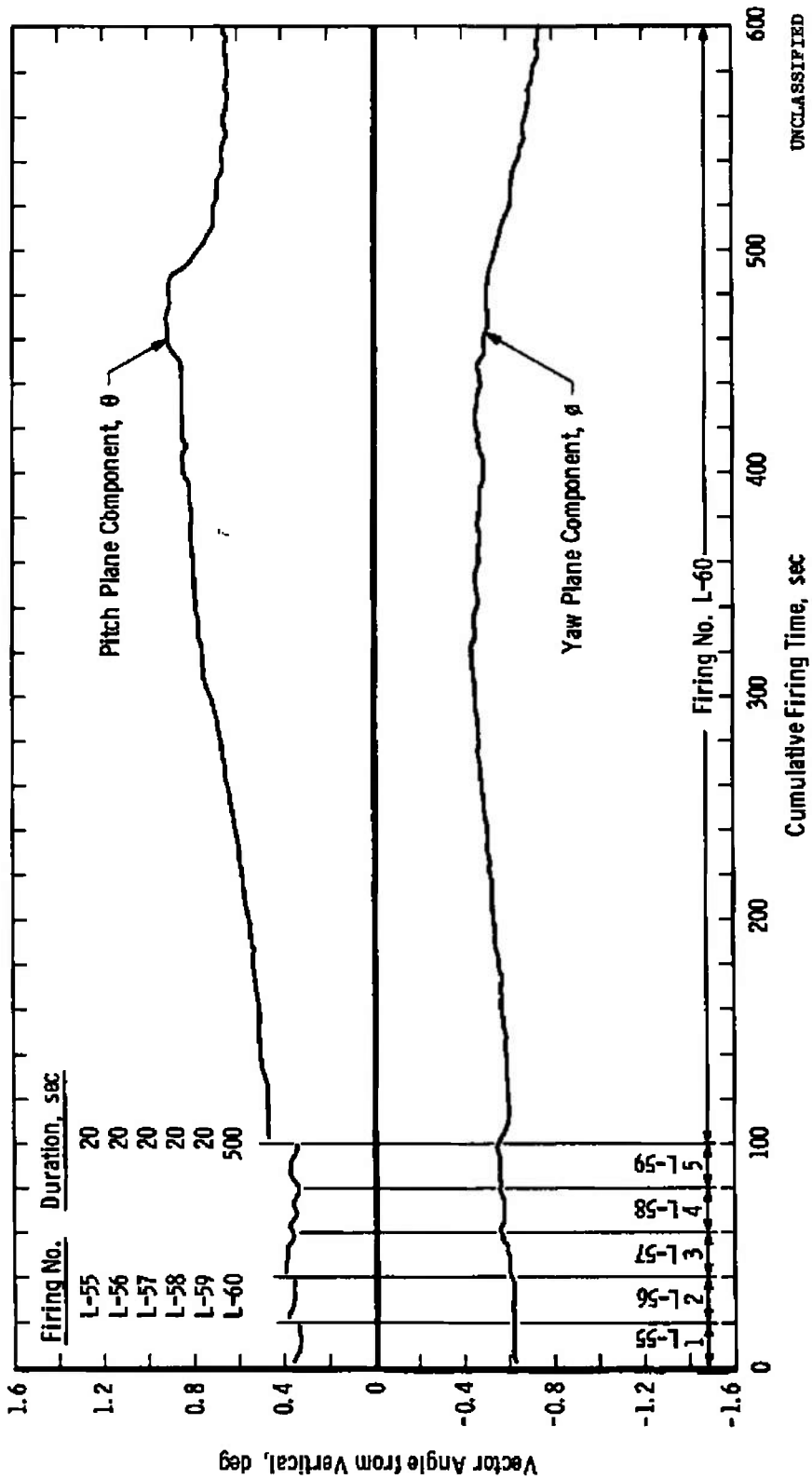

Fig. 37 Angular Variation of Thrust Vector Components of Engine S/N 9B

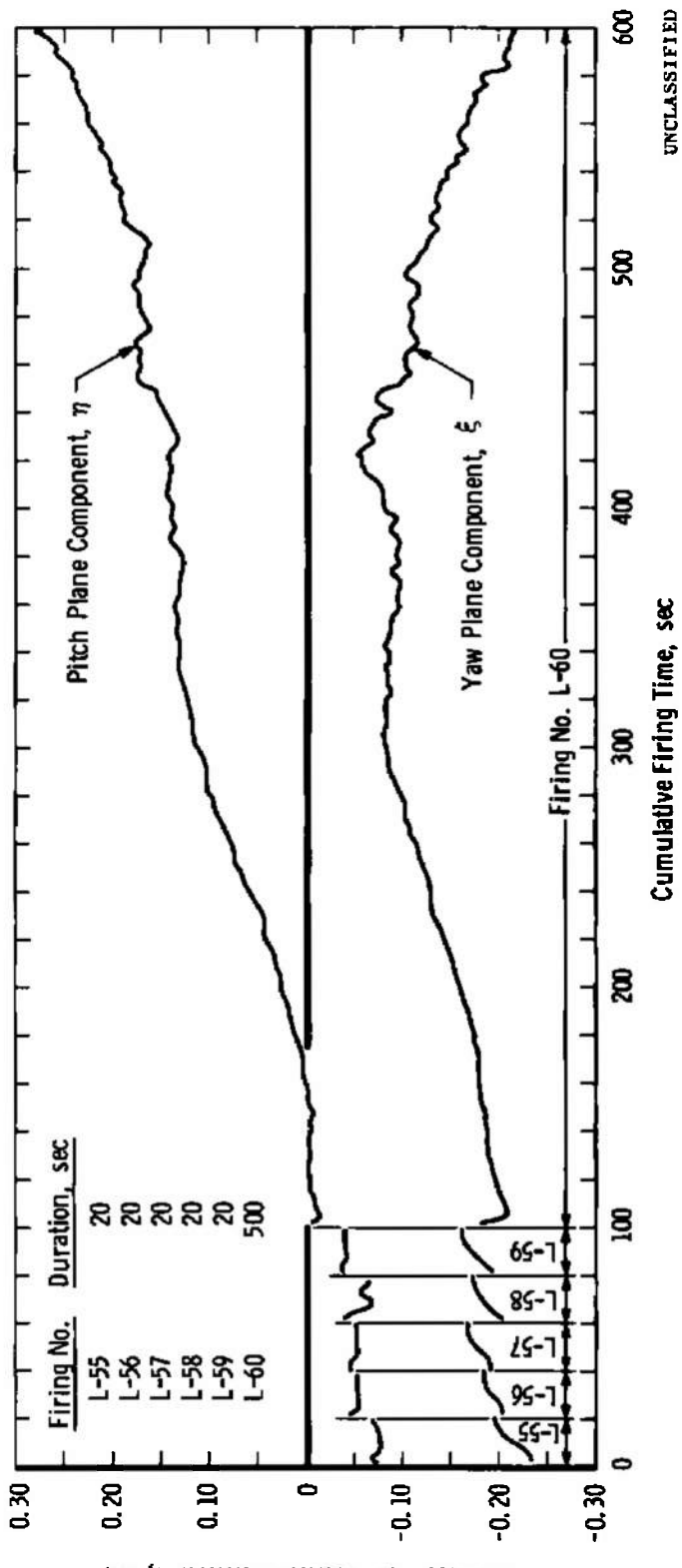

Fig. 38 Variation of Thrust Vector Intercept Components in the Chamber Throat Plane of Engine S/N 9A

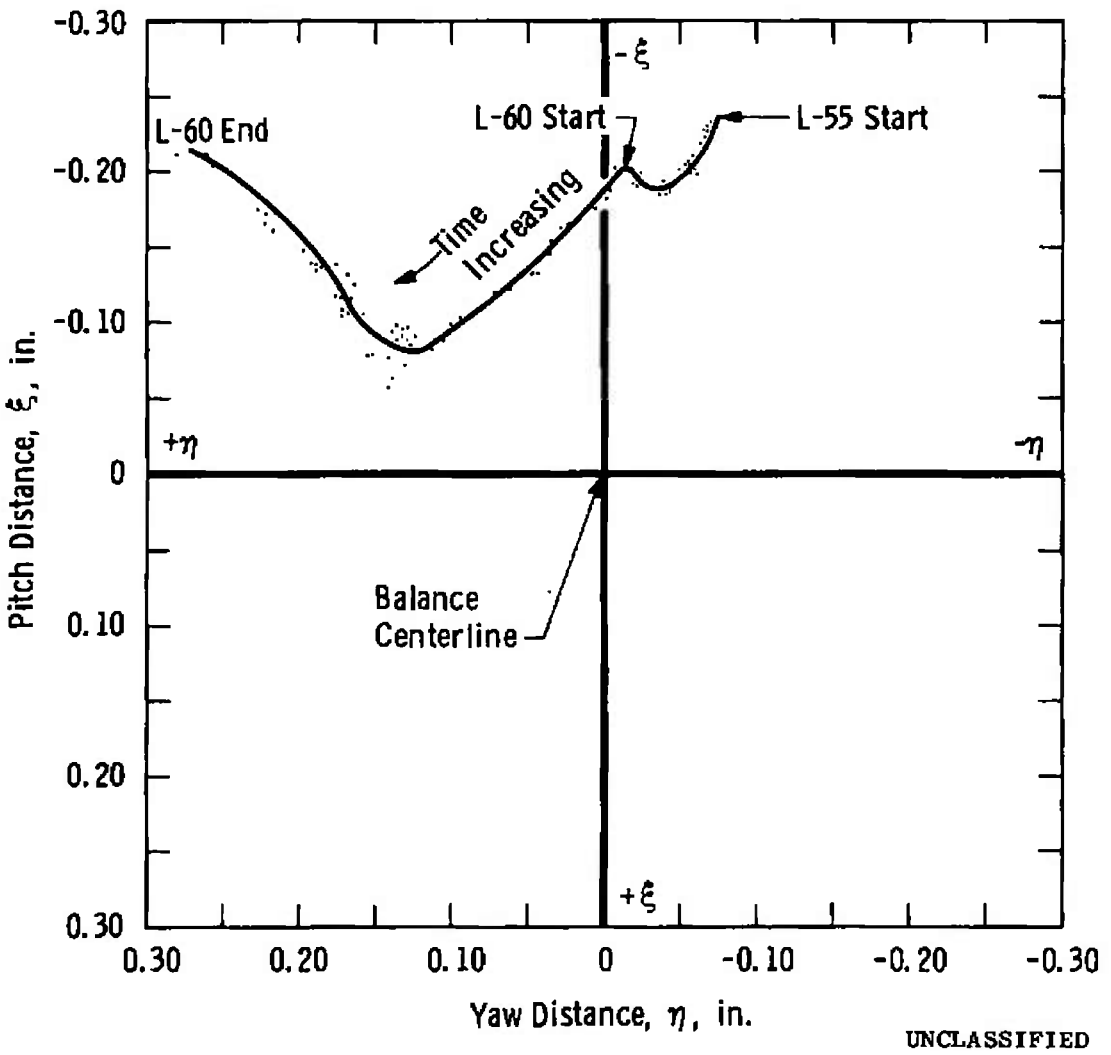

Fig. 39 Variation of Thrust Vector Intercept in the Chamber Throat Plane of Engine S/N 9A

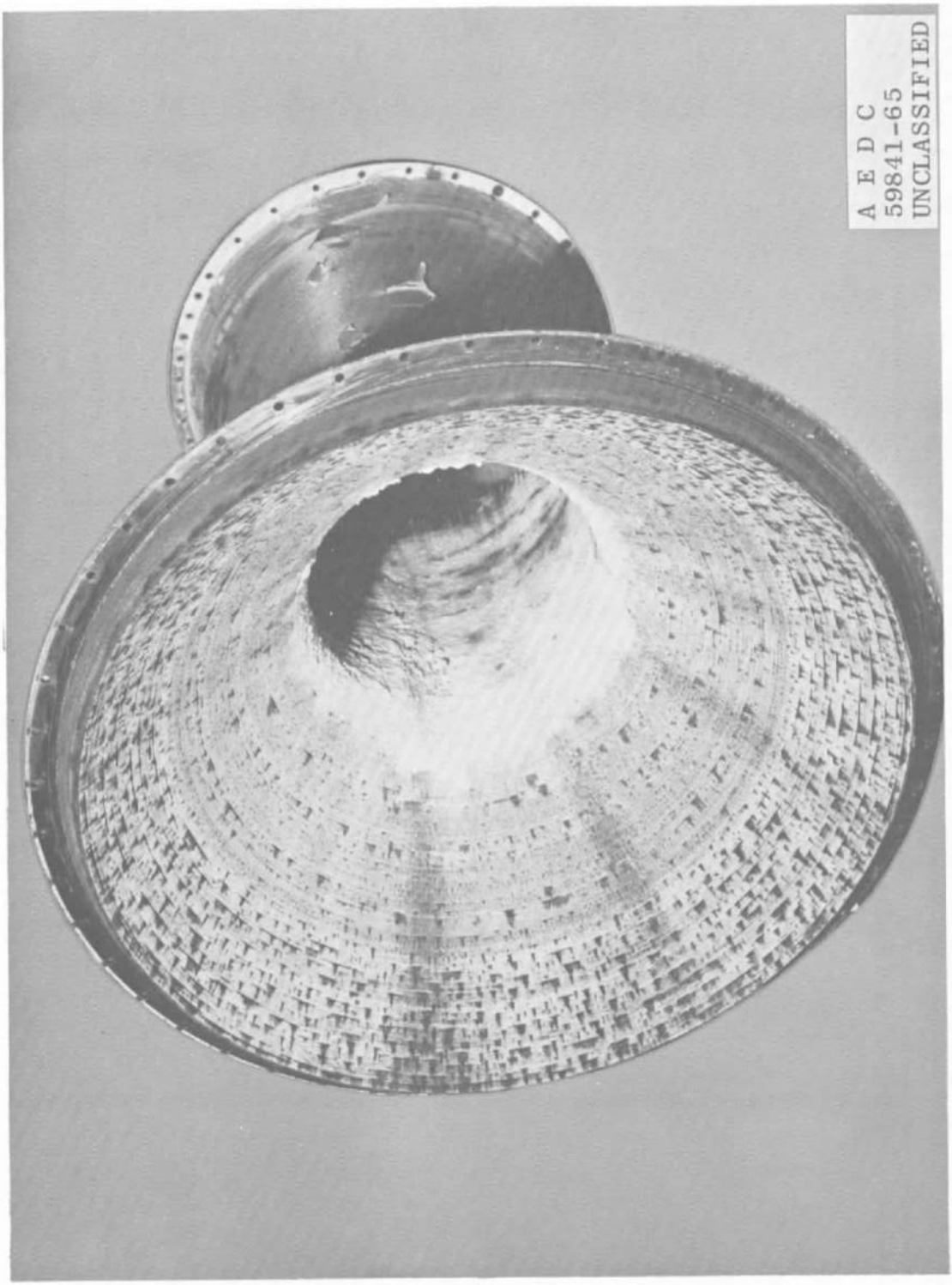

Fig. 40 Engine S/N 11A Chamber, Post-Fire, Nozzle End

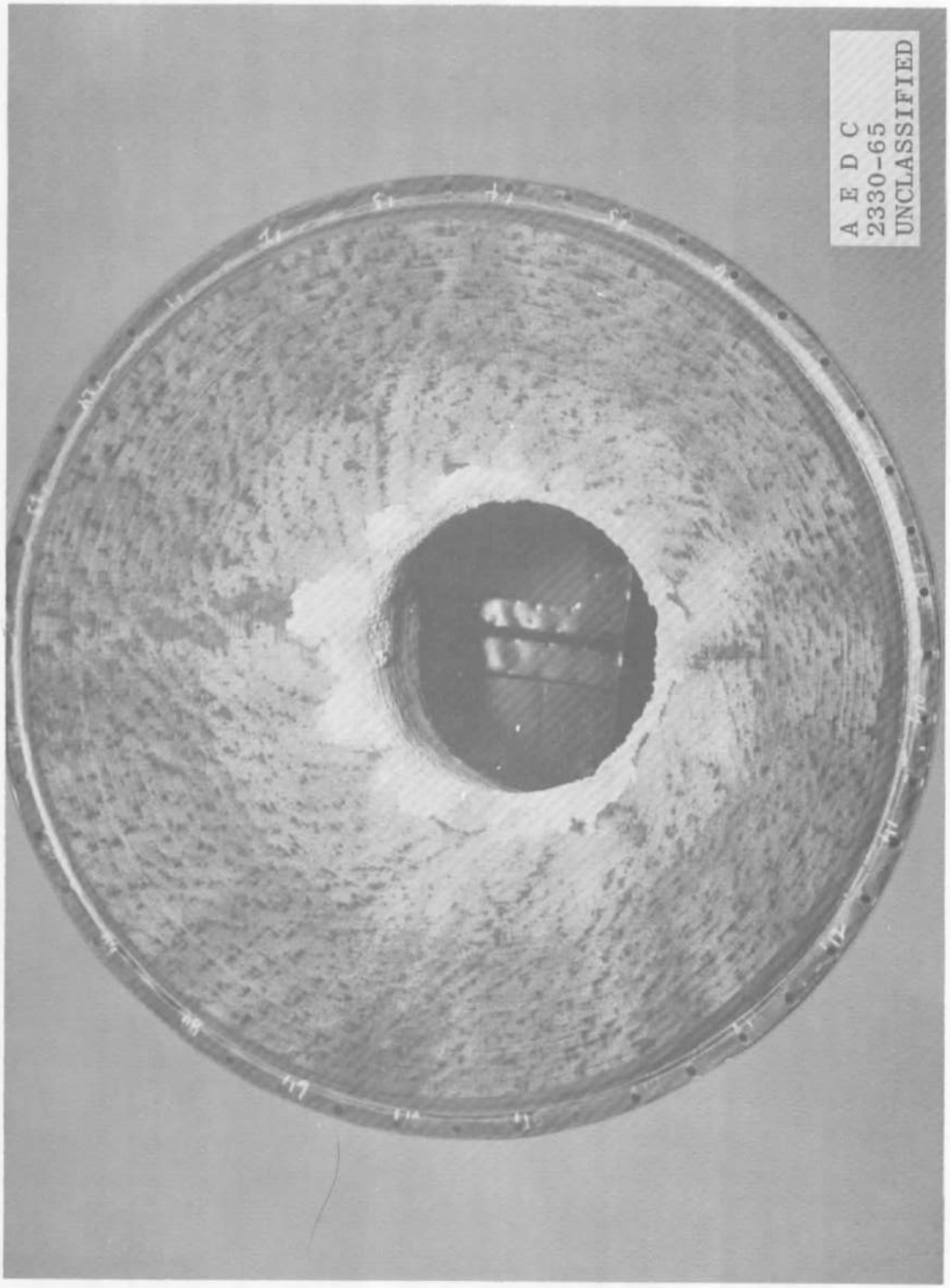

Fig. 41 Engine S/N 11C Chamber, Post-Fire, Nozzle End

TABLE I
GENERAL SUMMARY

Test No.	Test Date	Duration, sec	Engine S/N	Thrust Chamber Valve Bank	Test Objectives
L-55	4/27/65	20.3	9A	A	Performance at various mixture ratios and to prove endurance during steady-state operation.
L-56		20.7			
L-57		20.1			
L-58		20.9			
L-59		20.2			
L-60		500.1			
*M-61	5/14/65	20.4	11A	A and B	Simulated acceptance and pre-launch tests, gimbal operation, and performance at various mixture ratios. Gimbal during extended operation at high mixture ratios. TCV bank balance at high mixture ratios.
*M-62		20.3			
*M-63		20.4			
*M-64		20.6			
*M-65		20.3			
*M-66		20.4			
M-67		5.7		A	
M-68		5.1			
M-69		5.2			
M-70		5.1		B	
M-71		5.3			
M-72		5.3			
M-73		5.7		A and B	
M-74		4.8			
M-75		5.5			
M-76		4.6			
*M-77		250.1			
*N-78	5/20/65	159.9	11A	A and B	Performance during simulated mission duty cycle with propellants and cell environment at high temperatures. Gimbal data.
*N-79		15.6			
*N-80		15.0			
*N-81		15.1			
*N-82		15.1			
*N-83		15.2			
N-84		5 tests 0.95, 0.94, 0.95, 0.94, 0.84			
*N-85		90.2			
*P-86	6/8/65	10.3	9B	A and B	Performance with propellant and test cell environment at low temperatures. Gimbal data.
*P-87		10.5			
*P-88		10.4			
*P-89		10.1			
*P-90		10.2			
*P-91		29.6			
*P-92		30.1			
Q-93	6/11/65	5.6	9B	A and B	Performance at low and high chamber pressures. Engine durability during extended operation at high chamber pressure.
Q-94		5.0			
*Q-95		10.6		A	
*Q-96		10.1			
*Q-97		10.6		B	
*Q-98		10.3			
*Q-99		10.6		A and B	
*Q-100		10.4			
Q-101		5 tests 0.95, 0.95, 0.95, 0.95, 0.96		A	
Q-102		5 tests 0.95, 0.95, 0.97, 0.95, 0.95		B	
*Q-103		20.3		A and B	
*Q-104		193.0			

*Gimbal Tests

TABLE I (Concluded)

Test No.	Test Date	Duration, sec	Engine S/N	Thrust Chamber Valve Bank	Test Objectives
*R-105	6/30/65	10.3	11B	A and B	Performance at low and high chamber pressure and prove engine durability.
*R-106		10.2			
*R-107		10.1			
*R-108		10.1			
*R-109		10.3			
*R-110		30.3			
*R-111		30.3			
R-112		5.5			
R-113		5.6			
*R-114		10.0			
*R-115		10.1			
*R-116		10.3		A	
*R-117		10.6			
*R-118		10.1		B	
*R-119		10.5			
S-120	7/1/65	5 tests 0.98, 0.97, 0.91, 1.1, 0.90		A	
S-121		5 tests 0.97, 0.97, 0.92, 0.98 0.98		B	
*S-122		20.5		A and B	
*S-123		118.4			
*T-124	9/1/65	10.7	11C	A and B	Combustion chamber and injector temperature data, and performance using a new design combustion chamber.
*T-125		10.0			
*T-126		10.1			
*T-127		10.8			
*T-128		10.5			
*T-129		29.5			
T-130		5 tests 0.94, 0.94, 0.94, 0.94, 0.94		A	
T-131		5 tests 0.94, 0.93, 0.94, 0.94, 0.94		B	
*T-132		60.3		A and B	
U-133	9/3/65	30.1		A and B	
U-134		30.1			
*U-135		200.1			
*U-136		300.0			
*U-137		54.7			
*V-138	9/22/65	6.6	11D	A and B	Combustion chamber and injector temperature data, and prove chamber durability during low and high chamber pressure.
*V-139		25.0			
*V-140		180.7			
*V-141		10.0			
W-142	10/1/65	10.5		A and B	
*W-143		234.3			
*W-144		33.5			

*Gimbal Tests

TABLE II
SUMMARY OF ENGINE PERFORMANCE DATA FOR TEST FIRINGS AT DESIGN AND OFF-DESIGN CHAMBER PRESSURE

Run No.	Test Duration, sec	F_a, lbf	P_c, psia	$\dot{W}_o$, lb_m/sec	$\dot{W}_f$, lb_m/sec	P_a, psia	F_v, lbf	A_t, $in.^2$	MR	Isp_v, lbf-sec/lb_m	c*, ft/sec	C_{F_v}
Engine S/N 9A												
L-55	20	20,577	99.95	46.63	22.18	0.085	21,232	121.16	2.103	308.59	5662.5	1.753
L-56	20	20,569	100.17	45.69	22.66	0.082	21,197	120.86	2.015	319.12	5698.6	1.751
L-57	20	20,603	100.57	44.51	23.38	0.079	21,208	120.41	1.904	312.41	5739.3	1.751
L-58	20	20,741	101.39	43.71	24.31	0.077	21,333	120.33	1.798	313.65	5771.2	1.749
L-59	20	20,643	101.45	41.87	25.56	0.077	21,238	119.99	1.638	314.93	5808.2	1.745
L-60	500	20,441	99.90	44.58	22.96	0.080	21,055	120.31	1.942	311.78	5726.2	1.752
Engine S/N 11A												
M-61	20	21,331	103.67	49.14	22.68	0.099	22,086	121.84	2.167	307.51	5658.5	1.749
M-62	20	21,500	104.63	48.03	23.58	0.094	22,215	121.58	2.037	310.25	5716.0	1.746
M-63	20	21,141	103.13	46.25	23.78	0.093	21,848	121.39	1.945	311.97	5751.0	1.745
M-64	20	21,083	102.94	45.24	24.21	0.092	21,764	121.14	1.868	313.36	5776.7	1.745
M-65	20	21,390	105.34	43.68	26.34	0.093	22,097	120.44	1.658	315.61	5830.6	1.742
M-66	20	21,244	104.22	46.90	23.61	0.093	21,951	120.60	1.986	311.34	5735.9	1.746
M-77	250	20,632	102.01	50.58	20.64	0.090	21,319	119.38	2.450	299.32	5501.5	1.751
N-78	160	19,010	98.32	41.45	23.92	0.082	20,534	120.15	1.733	314.13	5814.1	1.738
N-79	15	21,164	103.37	46.72	23.40	0.080	21,776	120.85	1.997	310.53	5732.0	1.743
N-80	15	21,218	103.29	47.14	23.14	0.083	21,847	120.88	2.038	310.85	5715.8	1.750
N-81	15	21,166	103.11	46.63	23.40	0.083	21,797	121.03	1.993	311.26	5733.5	1.747
N-82	15	21,200	103.37	46.82	23.37	0.085	21,843	120.91	2.003	311.20	5729.5	1.748
N-83	15	21,319	103.68	46.95	23.46	0.081	21,933	120.96	2.001	311.48	5730.2	1.749
N-85	90	21,178	103.13	46.57	23.53	0.087	21,841	121.22	1.979	311.60	5738.5	1.747
Engine S/N 9B												
P-86	10	20,839	99.81	45.90	22.27	0.077	21,428	121.35	2.106	309.77	5633.1	1.769
P-87	10	21,046	100.94	47.31	22.54	0.077	21,629	121.21	2.099	309.67	5635.9	1.768
P-88	10	21,065	101.00	47.35	22.45	0.073	21,622	120.97	2.109	309.75	5631.5	1.770
P-89	10	21,045	101.12	47.30	22.52	0.077	21,630	120.93	2.100	309.82	5635.4	1.769
P-90	10	21,063	101.23	46.51	23.00	0.078	21,655	120.98	2.022	311.50	5668.0	1.768
P-92	30	20,711	100.08	46.54	22.18	0.075	21,279	120.28	2.098	309.66	5636.4	1.768
Engine S/N 11B												
R-105	10	20,473	98.45	44.37	22.88	0.071	21,013	121.76	1.940	312.47	5735.1	1.753
R-106	10	21,387	103.27	47.57	23.11	0.073	21,947	121.02	2.059	310.54	5689.5	1.756
R-107	10	20,949	101.37	45.46	23.31	0.071	21,486	120.85	1.950	312.42	5731.4	1.754
R-108	10	20,954	101.75	45.66	23.24	0.074	21,511	120.51	1.964	312.21	5726.3	1.754
R-109	10	20,954	101.99	45.75	23.16	0.074	21,511	120.17	1.976	312.14	5722.2	1.755
R-110	30	20,894	101.80	45.70	23.05	0.073	21,443	120.05	1.983	311.88	5719.5	1.754
R-111	30	20,838	101.82	45.19	23.28	0.072	21,382	119.85	1.941	312.30	5734.6	1.752
Engine S/N 11C												
T-124	10	-	103.42	46.10	24.10	0.093	-	121.64	1.903	-	5740.7	-
T-125	10	-	101.82	46.34	23.24	0.087	-	121.23	1.994	-	5708.3	-
T-126	10	-	102.63	47.14	23.14	0.085	-	121.14	2.037	-	5691.5	-
T-127	10	-	102.87	47.24	23.14	0.083	-	120.98	2.041	-	5689.8	-
T-128	10	-	103.18	47.38	23.19	0.082	-	120.95	2.043	-	5689.3	-
T-129	30	-	103.22	47.37	23.26	0.081	-	121.05	2.036	-	5691.9	-

TABLE II (Concluded)

Run No.	Test Duration, sec	F_a, lbf	P_c, psia	$\dot{W}_o$, lb_m/sec	$\dot{W}_f$, lb_m/sec	P_a, psia	F_v, lbf	A_t, in.^{2}	MR	Isp_v, lbf-sec/lb_m	c^*, ft/sec	C_{F_v}
Engine S/N 11D												
V-138	7	-	103.38	48.97	22.86	0.092	-	121.80	2.142	-	5639.5	-
V-139	25	-	102.19	47.59	23.04	0.092	-	121.86	2.066	-	5673.2	-
V-140	180	-	105.43	48.73	23.77	0.098	-	121.38	2.051	-	5679.4	-
V-141	10	-	107.74	49.23	24.10	0.115	-	120.22	2.043	-	5682.7	-
Engine S/N 9B												
Q-95	10	15,829	78.28	36.22	17.34	0.064	15,418	119.94	2.089	306.57	5640.2	1.749
Q-96	10	16,279	80.29	38.88	16.84	0.069	16,805	119.49	2.314	301.02	5529.5	1.752
Q-97	10	16,954	83.36	37.67	18.94	0.070	17,484	119.83	1.889	308.82	5680.9	1.749
Q-98	10	16,570	81.50	36.86	18.51	0.068	17,087	119.03	1.892	308.60	5670.6	1.748
Q-99	10	16,772	82.43	37.61	18.51	0.068	17,290	119.85	2.033	308.10	5663.8	1.750
Q-100	10	16,822	82.66	38.01	18.38	0.068	17,340	110.80	2.068	307.48	5649.3	1.751
Q-103	20	25,440	122.50	55.72	27.77	0.082	26,062	120.21	2.006	312.12	5674.1	1.770
Q-104	192	25,711	124.23	55.74	27.87	0.085	26,354	119.87	2.036	311.49	5652.5	1.770
Engine S/N 11B												
R-114	10	16,767	82.97	36.85	18.90	0.067	17,274	119.68	1.950	309.87	5731.5	1.739
R-115	10	16,519	81.74	36.39	18.60	0.066	17,021	119.78	1.057	309.55	5729.0	1.738
R-116	10	16,406	81.59	36.49	18.43	0.067	17,001	119.68	1.980	309.55	5720.6	1.741
R-117	10	16,494	81.58	36.54	18.45	0.067	17,001	118.82	1.981	309.20	5720.1	1.739
R-118	10	16,779	82.90	37.23	18.73	0.068	17,290	119.96	1.988	308.94	5717.5	1.739
R-119	10	16,787	83.06	37.23	18.81	0.071	17,305	110.97	1.979	308.78	5720.8	1.737
S-122	20	25,093	122.27	53.55	28.05	0.075	25,656	119.20	1.910	314.36	5745.5	1.760
S-123	118	24,949	121.45	55.26	26.73	0.077	25,531	119.29	2.068	311.43	5685.7	1.762
Engine S/N 11C												
T-132	60	-	125.51	58.53	27.53	0.098	-	120.49	2.125	-	5653.3	-
U-133	30	-	102.25	48.04	22.29	0.081	-	120.56	2.158	-	5639.7	-
U-134	30	-	102.84	48.20	22.37	0.082	-	120.40	2.150	-	5638.1	-
U-135	200	-	125.45	58.94	27.67	0.095	-	120.31	2.130	-	5651.5	-
U-136	200	-	113.44	53.46	24.50	0.087	-	121.64	2.182	-	5627.2	-
U-137	55	-	115.25	52.98	25.93	0.085	-	121.06	2.044	-	5688.9	-
Engine S/N 11D												
W-142	10	-	128.02	57.72	29.04	0.082	-	120.16	1.988	-	5704.3	-
W-143	234	-	125.29	55.76	28.87	0.091	-	120.18	1.932	-	5724.5	-
W-144	34	-	132.04	61.02	30.09	0.097	-	122.00	2.030	-	5688.6	-

TABLE III
SUMMARY OF TRANSIENT IMPULSE DATA

a. Ignition

Engine S/N	Test Number	Thrust Chamber Valve Bank	Chamber Pressure, psia	Rise Time to 100 percent, sec	Start Impulse, lb-sec
11A	M-67	A	104	0.59	3284
	M-68		104	0.60	3259
	M-69		105	0.60	3341
	M-70	B	106	0.58	3556
	M-71			0.58	3382
	M-72			0.59	3470
	M-73	A and B		0.55	3197
	M-74			0.54	3251
	M-75			0.55	3182
	M-76		105	0.57	3447
9B	P-86		101	0.65	6120
	P-87		102	0.50	3509
	P-88		102	0.50	3595
	P-89		103	0.51	3611
	P-90		103	0.51	3596
9B	Q-94		101	0.52	3740
	Q-95	A	80	0.54	2401
	Q-96	A	84	0.62	3650
	Q-97	B	84	0.57	2968
	Q-98	B	82	0.55	2756
	Q-99	A and B	83	0.57	3079
	Q-100		84	0.53	2994
11B	R-105		100	0.33	479
	R-106		105	0.29	251
	R-108		104		250
	R-109		104		206
	R-112		100		178
	R-113		100		158
	R-114		85	0.59	4019
	R-115		83	0.61	4216
	R-116	A		0.59	4019
	R-117	A		0.57	3924
	R-118	B	84	0.30	229
	R-119	B	84	0.30	199
11C	T-124	A and B	105	0.46	185
	T-125		104	0.42	193
	T-126		104	0.42	170
	T-127		105	0.41	167
	T-128		105	0.41	205
11D	V-138		103	0.49	226
	V-141		108	0.43	232
	W-142		131	0.47	307

TABLE III

b. Shutdown

Engine S/N	Test Number	Thrust Chamber Valve Bank	Chamber Pressure, psia	Shutdown Time to 1 percent, sec	Shutdown Impulse, lb-sec
11A	M-67	A	104	1.3	6,906
	M-68		104	1.5	6,831
	M-69		105	1.2	6,456
	M-70	B	106	1.3	6,782
	M-71				6,650
	M-72				6,574
	M-73	A and B			7,679
	M-74			1.6	7,642
	M-75			1.3	7,809
	M-76		105	1.3	6,626
9B	P-86		101	2.5	10,434
	P-87		102	1.9	10,244
	P-88		102	1.8	10,438
	P-89		103	1.6	10,369
	P-90		103		10,401
	Q-94		101		9,790
	Q-95	A	80	1.5	7,408
	Q-96	A	84		7,561
	Q-97	B	84		7,621
	Q-98	B	82	1.6	8,038
	Q-99	A and B	83		7,927
	Q-100		84		8,487
11B	R-105		100	2.8	10,437
	R-106		105	1.6	10,126
	R-107				
	R-108		104	1.9	9,983
	R-109		104	1.8	9,980
	R-112		100	1.5	9,864
	R-113		100	2.6	10,352
	R-114		85	2.7	7,764
	R-115		83	2.6	7,612
	R-116	A		2.7	8,227
	R-117	A		2.7	8,268
	R-118	B	84	2.8	8,680
	R-119	B	84	2.7	8,802
11C	T-124	A and B	105	2.8	11,839
	T-125		104	2.3	11,349
	T-126		104	2.7	11,597
	T-127		105	2.7	11,723
	T-128		105	2.6	11,576
11D	V-138		103	1.5	11,310
	V-141		108	1.4	11,160
	W-142		131	1.2	13,313

TABLE IV
MINIMUM IMPULSE DATA SUMMARY

Engine S/N	Test No.	Thrust Chamber Valve Bank	Chamber Pressure, psia	Test Duration, sec	Impulse, lb-sec
9B	Q-101A	A	125	0.95	22,426
	B			0.96	21,215
	C			0.95	22,061
	D			0.95	21,580
	E			0.96	22,547
	Q-102A	B	125	0.95	23,314
	B			0.95	22,667
	C			0.97	22,545
	D			0.95	23,168
	E			0.95	22,054
11B	S-120A	A	125	0.98	22,812
	B			0.97	25,731
	C			0.91	22,692
	D			1.05	26,019
	E			0.90	26,381
	S-121A	B	125	0.97	26,289
	B			0.97	26,121
	C			0.92	22,961
	D			0.98	26,437
	E			0.98	26,172
11C	T-130A	A	128	0.94	23,332
	B			0.94	23,612
	C			0.94	23,654
	D			0.94	24,823
	E			0.94	23,430
	T-131A	B		0.94	24,101
	B			0.93	26,154
	C			0.94	25,259
	D			0.94	24,291
	E			0.94	25,725

DOCUMENT CONTROL DATA - R&D

(Security classification of title, body of abstract and indexing annotation must be entered when the overall report is classified)

1 ORIGINATING ACTIVITY (Corporate author)
Arnold Engineering Development Center
ARO, Inc., Operating Contractor
Arnold AF Station, Tennessee

2a REPORT SECURITY CLASSIFICATION
[redacted]

2b GROUP
[redacted] Unclassified

3 REPORT TITLE
SIMULATED ALTITUDE TESTING OF THE APOLLO SERVICE MODULE PROPULSION SYSTEM (REPORT II, PHASE II DEVELOPMENT TEST)

4 DESCRIPTIVE NOTES (Type of report and inclusive dates)
Report II, Phase II Development Test

5. AUTHOR(S) (Last name, first name, initial)
Schulz, G. H. and DeFord, J. F., ARO, Inc.

This document has been approved for public release, its distribution is unlimited. By AF Letter Dated 27 June 1973

6. REPORT DATE	7a. TOTAL NO. OF PAGES	7b. NO. OF REFS
February 1966	116	4

8a. CONTRACT OR GRANT NO.	9a. ORIGINATOR'S REPORT NUMBER(S)
AF 40(600)-1200	AEDC-TR-66-17
b. ~~XXXXXXX~~ System 921E	
c	9b. OTHER REPORT NO(S) (Any other numbers that may be assigned this report)
d.	N/A

10 AVAILABILITY/LIMITATION NOTICES
Qualified users may obtain copies of this report from DDC. ~~Release to foreign governments or foreign nationals must have prior approval of NASA-MSC.~~

11 SUPPLEMENTARY NOTES	12. SPONSORING MILITARY ACTIVITY
N/A	National Aeronautics and Space Administration, Manned Spacecraft Center, Houston, Texas

13 ABSTRACT The Apollo Service Module (S/M) propulsion system, tested at Arnold Engineering Development Center (AEDC), consisted of the Aerojet-General Corporation AJ10-137 flight-type rocket engine and a North American Aviation ground test version of the Apollo S/M propellant system and was subjected to simulated altitudes above 100,000 ft during engine firing operations. This testing was conducted with the last six engine assemblies of the AEDC Phase II development program and included test firings with an accumulated duration of 3367.1 sec. The primary objectives of the test were to check out system operation, define propulsion system altitude performance, and prove engine structural endurance over ranges of propellant mixture ratio and combustion chamber pressure. Engine gimbaling operations were performed during certain firings. Ballistic performance of the six engine assemblies tested is presented in this report. Engine temperature data, the effect of ablation on the thrust vector, and a discussion of engine gimbal operation are also presented. (U)

This document has been approved for public release, its distribution is unlimited. By AF Letter Dated 27 June 1973

DD FORM 1 JAN 64 1473

DECLASSIFIED / UNCLASSIFIED

14. KEY WORDS	LINK A		LINK B		LINK C	
	ROLE	WT	ROLE	WT	ROLE	WT
Apollo Service Module rocket engines liquid propellants simulated altitude testing performance evaluation structural reliability gimbaling						

INSTRUCTIONS

1. ORIGINATING ACTIVITY: Enter the name and address of the contractor, subcontractor, grantee, Department of Defense activity or other organization *(corporate author)* issuing the report.

2a. REPORT SECURITY CLASSIFICATION: Enter the overall security classification of the report. Indicate whether "Restricted Data" is included. Marking is to be in accordance with appropriate security regulations.

2b. GROUP: Automatic downgrading is specified in DoD Directive 5200.10 and Armed Forces Industrial Manual. Enter the group number. Also, when applicable, show that optional markings have been used for Group 3 and Group 4 as authorized.

3. REPORT TITLE: Enter the complete report title in all capital letters. Titles in all cases should be unclassified. If a meaningful title cannot be selected without classification, show title classification in all capitals in parenthesis immediately following the title.

4. DESCRIPTIVE NOTES: If appropriate, enter the type of report, e.g., interim, progress, summary, annual, or final. Give the inclusive dates when a specific reporting period is covered.

5. AUTHOR(S): Enter the name(s) of author(s) as shown on or in the report. Enter last name, first name, middle initial. If military, show rank and branch of service. The name of the principal author is an absolute minimum requirement.

6. REPORT DATE: Enter the date of the report as day, month, year, or month, year. If more than one date appears on the report, use date of publication.

7a. TOTAL NUMBER OF PAGES: The total page count should follow normal pagination procedures, i.e., enter the number of pages containing information.

7b. NUMBER OF REFERENCES: Enter the total number of references cited in the report.

8a. CONTRACT OR GRANT NUMBER: If appropriate, enter the applicable number of the contract or grant under which the report was written.

8b, 8c, & 8d. PROJECT NUMBER: Enter the appropriate military department identification, such as project number, subproject number, system numbers, task number, etc.

9a. ORIGINATOR'S REPORT NUMBER(S): Enter the official report number by which the document will be identified and controlled by the originating activity. This number must be unique to this report.

9b. OTHER REPORT NUMBER(S): If the report has been assigned any other report numbers *(either by the originator or by the sponsor)*, also enter this number(s).

10. AVAILABILITY/LIMITATION NOTICES: Enter any limitations on further dissemination of the report, other than those imposed by security classification, using standard statements such as:

(1) "Qualified requesters may obtain copies of this report from DDC."

(2) "Foreign announcement and dissemination of this report by DDC is not authorized."

(3) "U. S. Government agencies may obtain copies of this report directly from DDC. Other qualified DDC users shall request through _____."

(4) "U. S. military agencies may obtain copies of this report directly from DDC. Other qualified users shall request through _____."

(5) "All distribution of this report is controlled. Qualified DDC users shall request through _____."

If the report has been furnished to the Office of Technical Services, Department of Commerce, for sale to the public, indicate this fact and enter the price, if known.

11. SUPPLEMENTARY NOTES: Use for additional explanatory notes.

12. SPONSORING MILITARY ACTIVITY: Enter the name of the departmental project office or laboratory sponsoring *(paying for)* the research and development. Include address.

13. ABSTRACT: Enter an abstract giving a brief and factual summary of the document indicative of the report, even though it may also appear elsewhere in the body of the technical report. If additional space is required, a continuation sheet shall be attached.

It is highly desirable that the abstract of classified reports be unclassified. Each paragraph of the abstract shall end with an indication of the military security classification of the information in the paragraph, represented as *(TS), (S), (C), or (U)*

There is no limitation on the length of the abstract. However, the suggested length is from 150 to 225 words.

14. KEY WORDS: Key words are technically meaningful terms or short phrases that characterize a report and may be used as index entries for cataloging the report. Key words must be selected so that no security classification is required. Identifiers, such as equipment model designation, trade name, military project code name, geographic location, may be used as key words but will be followed by an indication of technical context. The assignment of links, rules, and weights is optional.